

INFORMATION TO USERS

This manuscript has been reproduced from the microfilm master. UMI films the text directly from the original or copy submitted. Thus, some thesis and dissertation copies are in typewriter face, while others may be from any type of computer printer.

The quality of this reproduction is dependent upon the quality of the copy submitted. Broken or indistinct print, colored or poor quality illustrations and photographs, print bleedthrough, substandard margins, and improper alignment can adversely affect reproduction.

In the unlikely event that the author did not send UMI a complete manuscript and there are missing pages, these will be noted. Also, if unauthorized copyright material had to be removed, a note will indicate the deletion.

Oversize materials (e.g., maps, drawings, charts) are reproduced by sectioning the original, beginning at the upper left-hand corner and continuing from left to right in equal sections with small overlaps. Each original is also photographed in one exposure and is included in reduced form at the back of the book.

Photographs included in the original manuscript have been reproduced xerographically in this copy. Higher quality 6" x 9" black and white photographic prints are available for any photographs or illustrations appearing in this copy for an additional charge. Contact UMI directly to order.

U·M·I

University Microfilms International
A Bell & Howell Information Company
300 North Zeeb Road, Ann Arbor, MI 48106-1346 USA
313/761-4700 800/521-0600

Order Number 1355108

**Semi-analytical partial n 'th collision source correction for
multi-dimensional S_N photon transport calculations**

Winarno, Eko Yuli, M.S.

The University of Arizona, 1993

U·M·I
300 N. Zeeb Rd.
Ann Arbor, MI 48106



SEMI-ANALYTICAL PARTIAL N'TH COLLISION SOURCE
CORRECTION FOR MULTI-DIMENSIONAL S_N PHOTON
TRANSPORT CALCULATIONS

by
Eko Yuli Winarno

A Thesis Submitted to the Faculty of the
DEPARTMENT OF NUCLEAR AND ENERGY ENGINEERING
In Partial Fulfillment of the Requirements
For the Degree of
MASTER OF SCIENCE
WITH A MAJOR IN NUCLEAR ENGINEERING
In the Graduate College
THE UNIVERSITY OF ARIZONA

1993

STATEMENT BY AUTHOR

This thesis has been submitted in partial fulfillment of requirements for an advanced degree at the University of Arizona and is deposited in the University Library to be made available to borrowers under rules of the Library.

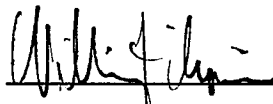
Brief quotations from this thesis are allowable without special permission, provided that accurate acknowledgment of source is made. Requests for permission for extended quotation from or reproduction of this manuscript in whole or in part may be granted by the head of the major department or the Dean of the Graduate College when in his or her judgment the proposed use of the material is in the interests of scholarship. In all other instances, however, permission must be obtained from the author.

Signed: _____



APPROVAL BY THESIS DIRECTOR

This thesis has been approved on the date shown below:



Dr. William L. Filippone

Professor of Nuclear and Energy Engineering

10/1/93

Date



Dr. David Hetrick

Professor of Nuclear and Energy Engineering

10/15/93

Date

ACKNOWLEDGEMENT

I wish to thank Dr. William L. Filippone for the opportunity he gave me to conduct this research. I'd like to acknowledge his continuous encouragement and assistance during this study.

I also gratefully thank Dr. David L. Hetrick for his assistance and helpful suggestions. The valuable comments and suggestions from Dr. Robert L. Seale and Dr. Phillip A. Secker are deeply appreciated. I am indebted to Bruce R. Ward for reading and commenting on the manuscript.

DEDICATION

*To my lovely parents who always share their wisdom and
to Mr. and Mrs. T. N. Machmud whom I admire most.*

TABLE OF CONTENTS

	Page
LIST OF FIGURES	7
ABSTRACT	10
1. INTRODUCTION	11
2. METHOD OF DEVELOPMENT	17
2.1 Procedure	23
3. ALGORITHM	25
4. COMPUTATIONAL RESULTS	35
4.1 Overall Structure of The Test Problems	35
4.2 Test Problem One	37
4.2.1 Description of Problem	37
4.2.2 Objective	38
4.2.3 Test One	38
4.2.4 Test Two	38
4.2.5 Test Three	38
4.2.6 Test Four	39
4.2.7 Test Five	39
4.3 Test Problem Two	51
4.3.1 Description of Problem	51
4.3.2 Objective	52
4.3.3 Test Group One	52
4.3.4 Test Group Two	53
4.3.5 Test Group Three	53
4.3.6 Test Group Four	54
4.4 Test Problem Three	69
4.4.1 Description of Problem	69
4.4.2 Objective	70
4.4.3 Discrete Ordinates S_N Method	71
4.4.4 SAPCS Method	71
4.4.5 Test Group One	72
4.4.6 Test Group Two	73
4.4.7 Test Group Three	74
4.5 Test Problem Four	91
4.5.1 Description of Problem	91
4.5.2 Objective	91
4.5.3 Test Group One	92
4.5.4 Test Group Two	93
4.5.5 Test Group Three	93

TABLE OF CONTENTS - Continued

	Page
4.6 Test Problem Five	103
4.6.1 Description of Problem	103
4.6.2 Objective	103
4.6.3 Test Group One	104
4.6.4 Test Group Two	104
4.6.5 Comparison Between the Two Group	105
5. CONCLUSION	116
REFERENCES	118

LIST OF FIGURES

Figure	Page
3.1 Three-dimensional spatial discretization showing mesh cell $A_{i,j,k}$	26
4.1a Individual mesh cell	35
4.1b General geometric scheme of tests	36
4.2 Geometric scheme for test problem one	37
4.2.1 Flux distribution from S_2	40
4.2.1a Flux distribution from SAP_1CS coupled with S_2	41
4.2.1b Flux distribution from SAP_2CS coupled with S_2	42
4.2.2 Flux distribution from S_4	43
4.2.2a Flux distribution from SAP_1CS coupled with S_4	44
4.2.3 Flux distribution from S_8	45
4.2.3a Flux distribution from SAP_1CS coupled with S_8	46
4.2.4 Flux distribution from S_{12}	47
4.2.4a Flux distribution from SAP_1CS coupled with S_{12}	48
4.2.5 Flux distribution from S_{16}	49
4.2.5a Flux distribution from SAP_1CS coupled with S_{16}	50
4.3 Geometric scheme for test problem two	51
4.3.1a Flux distribution from S_2 when “artificial multiplying” cells are present at the ripples	55
4.3.1b Flux distribution from SAP_1CS coupled with S_2 when “artificial multiplying” cells are present at the ripples	56
4.3.1c Flux distribution from SAP_2CS coupled with S_2 when “artificial multiplying” cells are present at the ripples	57
4.3.1d Flux distribution from SAP_3CS coupled with S_2 when “artificial multiplying” cells are present at the ripples	58
4.3.1e Flux distribution from SAP_4CS coupled with S_2 when “artificial multiplying” cells are present at the ripples	59
4.3.2a Flux distribution from S_4 when “artificial multiplying” cells are present at the ripple	60
4.3.2b Flux distribution from SAP_1CS coupled with S_4 when “artificial multiplying” cells are present at the ripples	61
4.3.2c Flux distribution from SAP_2CS coupled with S_4 when “artificial multiplying” cells are present at the ripples	62
4.3.3a Flux distribution from S_8 when “artificial multiplying” cells are present at the ripple	63
4.3.3b Flux distribution from SAP_1CS coupled with S_8 when “artificial multiplying” cells are present at the ripples	64
4.3.3c Flux distribution from SAP_2CS coupled with S_8 when “artificial multiplying” cells are present at the ripples	65

LIST OF FIGURES - Continued

Figure	Page
4.3.4a Flux distribution from S_{12} when “artificial multiplying” cells are present at the ripples	66
4.3.4b Flux distribution from SAP_1CS coupled with S_{12} when “artificial multiplying” cells are present at the ripples	67
4.3.4c Flux distribution from SAP_2CS coupled with S_{12} when “artificial multiplying” cells are present at the ripples	68
4.4 Geometric scheme for test problem three	69
4.4.1a Flux distribution from S_2 for a very hard transport problem.	76
4.4.1b Flux distribution from S_4 for a very hard transport problem.	77
4.4.1c Flux distribution from S_8 for a very hard transport problem.	78
4.4.1d Flux distribution from S_{12} for a very hard transport problem.	79
4.4.1e Flux distribution from S_{16} for a very hard transport problem.	80
4.4.2a1 Flux distribution from SAP_1CS coupled with S_2 for a very hard transport problem	81
4.4.2a2 Flux distribution from SAP_1CS coupled with S_2 for a very hard transport problem	82
4.4.2a3 Flux distribution from SAP_2CS coupled with S_2 for a very hard transport problem	83
4.4.2a4 Flux distribution from SAP_4CS coupled with S_2 for a very hard transport problem	84
4.4.2a5 Flux distribution from SAP_4CS coupled with S_2 for a very hard transport problem	85
4.4.3a1 Flux distribution from SAP_1CS coupled with S_4 for a very hard transport problem	86
4.4.3a2 Flux distribution from SAP_2CS coupled with S_4 for a very hard transport problem	87
4.4.3a3 Flux distribution from SAP_3CS coupled with S_4 for a very hard transport problem	88
4.4.3a4 Flux distribution from SAP_4CS coupled with S_4 for a very hard transport problem	89
4.4.3a5 Flux distribution from SAP_5CS coupled with S_4 for a very hard transport problem	90
4.5 Geometric scheme for test problem four	91
4.5.1a Flux distribution from S_8 for a very hard transport problem with “artificial multiplying” material at target cells	94
4.5.1b Flux distribution from S_{12} for a very hard transport problem with “artificial multiplying” material at target cells	95
4.5.1c Flux distribution from S_{16} for a very hard transport problem with “artificial multiplying” material at target cells	96

LIST OF FIGURES - Continued

Figure	Page
4.5.2a Flux distribution from SAP ₃ CS coupled with S ₂ for a very hard transport problem, with "artificial multiplying" material at target cells	97
4.5.2b Flux distribution from SAP ₄ CS coupled with S ₂ for a very hard transport problem, with "artificial multiplying" material at target cells	98
4.5.2c Flux distribution from SAP ₅ CS coupled with S ₂ for a very hard transport problem, with "artificial multiplying" material at target cells	99
4.5.3a Flux distribution from SAP ₃ CS coupled with S ₄ for a very hard transport problem, with "artificial multiplying" material at target cells	100
4.5.3b Flux distribution from SAP ₄ CS coupled with S ₄ for a very hard transport problem, with "artificial multiplying" material at target cells	101
4.5.3c Flux distribution from SAP ₅ CS coupled with S ₄ for a very hard transport problem, with "artificial multiplying" material at target cells	102
4.6 Geometric scheme for test problem five	103
4.6.1a Flux distribution from Monte Carlo-like technique on homogeneous cell test for total cross section = 0.1 cm ⁻¹	107
4.6.1b Flux distribution from S ₁₆ on homogeneous cell test for total cross section = 0.1 cm ⁻¹	108
4.6.1c Flux distribution from SAP ₁ CS coupled with S ₂ on homogeneous cell test for total cross section = 0.1 cm ⁻¹	109
4.6.1d Flux distribution from SAP ₁ CS coupled with S ₄ on homogeneous cell test for total cross section = 0.1 cm ⁻¹	110
4.6.1e Flux distribution from SAP ₁ CS coupled with S ₈ on homogeneous cell test for total cross section = 0.1 cm ⁻¹	111
4.6.2a Flux distribution from Monte Carlo-like technique on homogeneous cell test for total cross section = 0.0001 cm ⁻¹	112
4.6.2b Flux distribution from S ₁₆ on homogeneous cell test for total cross section = 0.0001 cm ⁻¹	113
4.6.2c Flux distribution from SAP ₁ CS coupled with S ₂ on homogeneous cell test for total cross section = 0.0001 cm ⁻¹	114
4.6.2d Flux distribution from SAP ₁ CS coupled with S ₄ on homogeneous cell test for total cross section = 0.0001 cm ⁻¹	115

ABSTRACT

A Semi-Analytical Partial n'th Collision Source (SAPNCS) method that is fully compatible with the standard three-dimensional S_N has been developed. The method generates a matrix operator that calculates scattering source for particles that have suffered n collisions in a selected number of mesh cells. Adopting this scattering source as distributed source, the standard three-dimensional S_N method then calculates the remaining contribution to the flux. The sum of uncollided and collided fluxes yields total flux. Several tests for photon transport calculation in x-y-z geometry have been fully conducted and the illustrative results demonstrating the capability of the method to mitigate and eliminate the observable ray effects are presented.

CHAPTER 1

INTRODUCTION

Most errors in the S_N method are caused by numerical diffusion and ray effects. The numerical diffusion arises from spatial discretization of the streaming term of the transport equation. The differencing approximations tend to “smear” the streaming photons into spatial regions that are, in reality, physically inaccessible.

Some efforts to eliminate the numerical diffusion and ray effect problems have been developed. The method of streaming rays^{1,2} reduces drastically the numerical diffusion. However, it does not mitigate the ray effects.

Ray effects are anomalous ripples that arise from the angular discretization of the streaming term of the transport equation. The ripples can be severe in problems with isolated sources and little scattering.

Since the ray effects were reported for the first time, a lot of methods have been proposed and developed to mitigate or to eliminate the ray effects. Increasing the number of discrete directions has been proposed³ as the first remedy. Even though the larger number of directions were applied, effects are remarkably persistent.⁴

The approach of alteration of the angular coupling in the streaming operator of the transport equation by applying a space-angle synthetics method was developed⁵. This method creates discrete ordinates-like equations with spatially varying direction in interval of solid angle. Unfortunately, no material result was provided.

Trial functions were also used to create discrete ordinate-like equation. First of all, piecewise constant trial functions in angle over an octant of the unit sphere were applied⁶ in the second order even-parity form of the transport equation. Secondly, piecewise bilinear trial functions in the angular variable were used⁷ in the finite element method. Both methods approximated the hyperbolic transport equation by an elliptic set of partial differential equation. After being tested at the same condition⁸, both were successful to mitigate the ray effect, but were slow to converge.

The conversion of discrete ordinates equations into spherical harmonics or spherical harmonics-like equation have been proposed. The method of converting S_N into a P_{N-1} solution in x-y geometry without an additional fictitious source was developed⁹. A conversion of S_N into P_L for $L < N - 1$ with an additional fictitious source was also developed¹⁰, even though it was not recommended¹¹. Moreover, the $S_N - P_{N-1}$ technique was extended¹² to curvilinear geometry and a fictitious source was added into this solution. These approaches are time consuming because convergence rates are slow.

A first collision source method¹³ has been developed to mitigate the ray effects in discrete ordinates calculations. The method analytically calculates the uncollided flux. The uncollided flux is used to create a first collision source. The source is then applied in the standard S_N method to produce the collided flux. The sum of the uncollided and collided fluxes is finally considered as the total flux distribution. Unfortunately, the first collision source method can not reduce the ray effects and numerical diffusion that come from the multi-scattered particles.

An extended first collision source combined with effective cross sections has been proposed for electron transport¹⁴. This method considers that the transport equation has fewer collisions but larger deflections per collision. Electrons that remain within a small solid angle centered about the same direction are considered to be extended uncollided particles. The effective uncollided flux is used to generate an extended first collision source.

The use of a super computer in conventional discrete ordinates (S_N) calculation has been proposed¹⁵. This method uses a new discrete ordinates method that is particularly created for large-memory computers. It calculates combinations of elements of multiple collisions, integral, and conventional S_N and produces a matrix operator. Source iteration is then calculated directly from this matrix. This method is able to reduce the ray effects and the numerical dispersion as well.

An integral discrete ordinates method¹⁶ designed to take advantage of super computer capabilities has been developed. This method uses the same technique as the conventional S_N method. The medium is divided into spacial mesh cells and the discrete directions are used. However, a nearly exact matrix representation of the streaming operator is used instead of an approximation differencing scheme. This matrix is then stored on large memory computers for repeated use in the source iteration. The integral method is capable of eliminating the ray effects and reducing the numerical dispersion. However, the promising method requires large memory computers to store the matrix and a large number of time consuming multiplications within the source iteration. For comparison, the conventional S_N computation time

varies as the number of mesh cells, but the time for integral computation may vary as the number of mesh cells cubed.

A new semi-analytic partial n 'th collision source (SAPNCS) correction is described here as a method to eliminate both the ray effect and numerical diffusion problem coming from original source and multi-scattered photons. As with the S_N technique, the medium is divided into two regions. Each region contains a number of spacial mesh cells. Region A covers SAPNCS cells that have high scattering and low absorption cross section, while region B has low scattering with moderate absorption. The first uncollided flux is analytically calculated. The analytic result for the first uncollided flux is then employed to create the first scattering source. The first scattering source at region A is used to calculate the second uncollided flux. These steps are used until the n 'th uncollided flux and n 'th scattering source are found. Furthermore, the n 'th scattering source at region A and total scattering source in region B are applied as a distributed source for a standard three-dimensional S_N method to calculate the collided flux. Finally, the sum of these two fluxes is the total flux that represents the overall solution of the problem and should be void of significant ray effects and numerical dispersion.

When the medium is homogeneous, region A only, and n is close to infinity, the SAPNCS method is essentially an integral method. However, the SAPNCS technique assigns a small fraction of the mesh cells to region A and considers the number of collisions only up to 5. Therefore, the SAPNCS method is integral- S_N hybrid method at same time, when it uses integrals for only a selected number of cells (region A) and

it uses integral for only a finite number of collision, n . Consequently, the SAPNCS technique has two advantages :

1. It should be much faster than the integral method on scalar machines.
2. It is easily implemented into standard three-dimensional S_N codes. (no multi-dimensional integral code exist).

Numerical tests for four different geometric problems have been conducted. The first problem is an ordinary three-dimensional slab geometry with two different materials. The first material sitting at and around the source is called region A or SAPNCS region, and the other is region B. When conventional S_N is used, ray effects will arise, even for S_{16} . However, a combination of SAPNCS method and the conventional S_N could eliminate the effects.

The second geometric problem is the same as the first one, but “artificial multiplying” material, material with relatively large scattering cross section, is inserted into cells in which the ripples would be passing through. Secondary ray effects arising from scattering sources could not be eliminated by first collision source correction alone. Higher collision source corrections are absolutely needed.

The third test is geometrically different from the last two tests. A source and targets are placed across from each other. Huge blocks of “black-absorber” material, with a large absorption capability, are placed between them. No particles can go directly from the source to the Targets, because the “black-absorber” will absorb them completely. This very hard transport problem could not be solved easily by

either Monte Carlo or the conventional S_N method. The Monte Carlo method needs a huge number of histories and the S_N method requires a very fine angular mesh. That means both methods need large computing time. However, the SAPNCS method will show how the particles reach the targets easily and fast.

The fourth test is similar to the third, except targets are filled in with “artificial multiplying” material. The secondary source is expected to rise at the targets, and the higher flux distribution at and around the target is expected to occur.

Geometric problem for the last test contents only the SAPNCS material. Monte Carlo-like method is one of the methods used. The others are S_N and SAPNCS methods. The methods are used to calculate flux distribution for two different cross sections. The results from those methods for the same cross section are visually compared. The results from the Monte Carlo-like and SAPNCS methods are similar but the result from the S_N method is lower than those from the previous methods. All those tests are visually presented.

CHAPTER 2

METHOD OF DEVELOPMENT

The transport equation can be written as :

$$[\hat{\Omega} \cdot \vec{\nabla} + \sigma(\vec{r}, E)] \Phi(\vec{r}, \hat{\Omega}, E) = \int d\Omega' dE' \sigma_s(\vec{r}, E' \rightarrow E, \hat{\Omega}' \rightarrow \hat{\Omega}) \Phi(\vec{r}, \hat{\Omega}', E') + q \quad (2.1)$$

This equation can be symbolically written

$$L\Phi = F\Phi + q \quad (2.2)$$

where

$$L = \hat{\Omega} \cdot \vec{\nabla} + \sigma(\vec{r}, E) \quad (2.3)$$

$$F = \int d\Omega' dE' \sigma_s(\vec{r}, E' \rightarrow E, \hat{\Omega}' \rightarrow \hat{\Omega}) \quad (2.4)$$

$\Phi(\vec{r}, \hat{\Omega}, E)$ = flux at position \vec{r} , direction $\hat{\Omega}$, and energy E

q = the extraneous source

$\sigma(\vec{r}, E)$ = the total cross section

$\sigma_s(\vec{r}, E' \rightarrow E, \hat{\Omega}' \rightarrow \hat{\Omega})$ = the differential scattering cross section.

When the medium is divided into two regions, A and B, the operator F presumably consists of two parts :

$$F = F_a + F_b, \quad (2.5)$$

superscript a and b refer to region A and B, respectively. This assumption should meet certain conditions in which :

$$F_a = \begin{cases} F & \text{if } \vec{r} \in \text{region A} \\ 0 & \text{otherwise} \end{cases} \quad (2.6)$$

Similar as above, the flux Φ can also be separated into two parts :

$$\Phi = \Phi_a + \Phi_b \quad (2.7)$$

Φ_a is the solution of the transport equation as:

$$L\Phi_a = F_a \Phi_a + q \quad (2.8)$$

where q is always inside region A. By combining eqs. (2.2), (2.5), (2.7), and (2.8),

$$L\Phi_b = F \Phi_b + F_b \Phi_a \quad (2.9)$$

The solution to eq. (2.8) can be expressed as :

$$\Phi_a = \sum_{\ell=0}^{\infty} \Phi_a^\ell \quad (2.10)$$

where

$$L \Phi_a^0 = q \quad (2.11)$$

and

$$L \Phi_a^{\ell+1} = F_a \Phi_a^\ell \quad (2.12)$$

All fluxes carrying the superscript 0 are called an uncollided flux, while those carrying the superscript ℓ are identified as collided fluxes. Φ_a can further be separated into two parts

$$\Phi_a = \Phi_a^{n-} + \Phi_a^{n+} \quad (2.13)$$

where

$$\Phi_a^{n-} = \sum_{\ell=0}^n \Phi_a^{\ell} \quad (2.14)$$

and

$$\Phi_a^{n+} = \sum_{\ell=n+1}^{\infty} \Phi_a^{\ell} \quad (2.15)$$

Φ_a^{n-} is the flux of particles that have not collided in region B and have collided less than $n+1$ times in region A, while Φ_a^{n+} is the flux of particles that have scattered more than n times in region A but have not collided in region B. When eqs. (2.10), (2.13), (2.14), and (2.15) are inserted into eq. (2.12) the result is

$$L \Phi_a^{n+} = F_a \Phi_a^{n+} + F_a \Phi_a^n \quad (2.16)$$

By inserting eq. (2.13) into eq. (2.7), the latter may be written as :

$$\Phi = \Phi_a^{n-} + \Phi_{S_N} \quad (2.17)$$

where

$$\Phi_{S_N} = \Phi_b + \Phi_a^{n+} \quad (2.18)$$

Φ_{S_N} is the flux of particles that have at least one collision in region B and/or at least n collision in region A. By adding eqs. (2.9) and (2.16) and inserting eqs. (2.13) and (2.18) into them it will be found

$$L \Phi_{S_N} = F \Phi_{S_N} + q^{n+1} \quad (2.19)$$

where

$$q^{n+1} = F_b \Phi_a^{n-} + F_a \Phi_a^n \quad (2.20)$$

q^{n+1} are defined as distributed sources that entirely cover all the cells.

Φ_a^{n-} and q^{n+1} have to be determined by using a semi-analytical method and eq.(2.19) is then solved by using a conventional S_N solver. The flux Φ_a^{n-} should be free of ray effects and numerical diffusion errors. By choosing n and A appropriately Φ_{S_N} can also be free of significant numerical errors. An appropriate choice of n and A would also minimize the computation time to calculate Φ_a^{n-} and q^{n+1} , while it is still maintaining the total flux Φ (eq.(2.18)) acceptably accurate. Two limiting choices of n and A are considered. First of all, with $n = 0$, for example, $\Phi_a^{n-} = \Phi_a^{0-} = \Phi_a^0$ is the uncollided flux, and $q^{n+1} = q^1 = F \Phi_a^0$ is the first collision source. Moreover eq.(2.18) and (2.20) result in the conventional first collision source correction¹³. If A is considered to be the entire medium and n equals infinity (∞), then $\Phi_{S_N} = \Phi_b = \Phi_a^{n+} = 0$, and finally $\Phi = \Phi_a^{n-}$ is the integral transport solution¹⁶. Therefore, the SAPNCS correction can range anywhere from a first collision source correction to a full integral transport solution.

To obtain Φ_a^{n-} and q^{n+1} , first of all, the Φ_a^ℓ have to be determined by solving eq.(2.11) and eq.(2.12). Those equations can be expressed as :

$$\Phi_a^\ell = L^{-1} q_a^\ell, \quad \ell = 0, 1, \dots, n \quad (2.21)$$

where

$$q_a^0 = q = \text{extraneous source} \quad (2.22)$$

$$q_a^\ell = F_a \Phi_a^{\ell-1} \quad (2.23)$$

and

$$\Phi_a^{\ell+1} = L^{-1} F_a \Phi_a^\ell \quad (2.24)$$

When expressed numerically, L^{-1} will be a $(I \times J \times K) \times (I \times J \times K)$ matrix, in which I , J , and K represent the number of spacial mesh cells for x , y , and z directions, respectively. For most cases, it is not feasible to solve this equation in its present form due to the large size of L^{-1} . Since $F_a \Phi_a^\ell$ is non zero only in region A, a $(I \times J \times K) \times (M)$ representation of L^{-1} denoted as L_a^{-1} is feasible, where M is the number of mesh cells in region A. Therefore, eq.(2.21) and eq.(2.24) become

$$\Phi_a^\ell = L_a^{-1} q_a^\ell, \quad \ell = 0, 1, \dots, n \quad (2.25)$$

and

$$\Phi_a^{\ell+1} = L_a^{-1} F_a \Phi_a^\ell \quad (2.26)$$

However, as we now demonstrate, most of the calculation for eq.(2.24) can be carried out using an even smaller $M \times M$ representation of L^{-1} denoted as L_{aa}^{-1} .

Let Φ_a^ℓ be separated into two parts

$$\Phi_a^\ell = \Phi_{aa}^\ell + \Phi_{ab}^\ell \quad (2.27)$$

where

Φ_{aa}^ℓ = fluxes inside region A coming from $(\ell - 1)^{th}$ collision sources in region A

Φ_{ab}^ℓ = fluxes inside region B coming from $(\ell - 1)^{th}$ collision sources in region A

When eq.(2.27) is inserted into eq.(2.26), the latter becomes

$$\Phi_a^{\ell+1} = L_a^{-1} F_a [\Phi_{aa}^\ell + \Phi_{ab}^\ell] \quad (2.28)$$

Yet $F_a \Phi_{ab}^\ell = 0$, because operator F_a is zero inside region B and eq.(2.28) will become

$$\Phi_a^{\ell+1} = L_a^{-1} F_a \Phi_{aa}^\ell \quad (2.29)$$

As mentioned above, Φ_{aa}^ℓ exists inside region A due to scattering sources in region A

and the Φ_{aa}^ℓ can then be calculated from

$$\Phi_{aa}^{\ell+1} = L_{aa}^{-1} F_a \Phi_{aa}^\ell, \quad \ell = 0, 1, \dots, n \quad (2.30)$$

where

$$\Phi_{aa}^0 = L_{aa}^{-1} q_a^0 \quad (2.31)$$

and L_{aa}^{-1} is the $(M \times M)$ matrix representation of L^{-1} .

When eq.(2.22), eq.(2.25), eq.(2.29), and eq.(2.30) are inserted into eq.(2.14),

we find

$$\Phi_a^{n-} = \sum_{\ell=0}^n \Phi_a^\ell \quad (2.32)$$

$$= \Phi_a^0 + \sum_{\ell=1}^n \Phi_a^\ell \quad (2.33)$$

$$= \Phi_a^0 + \sum_{\ell=0}^{n-1} \Phi_a^{\ell+1} \quad (2.34)$$

$$= \Phi_a^0 + \sum_{\ell=0}^{n-1} L_a^{-1} F_a \Phi_{aa}^\ell \quad (2.35)$$

$$= L_a^{-1} [q + F_a \sum_{\ell=0}^{n-1} \Phi_{aa}^\ell] \quad (2.36)$$

$$= L_a^{-1} [q + F_a \Phi_{aa}^{(n-1)-}] \quad (2.37)$$

where

$$\Phi_{aa}^{(n-1)-} = \sum_{\ell=0}^{n-1} \Phi_{aa}^{\ell} \quad (2.38)$$

From eq. (2.30), eq. (2.31), eq. (2.37), and eq. (2.38), we conclude that we can use L_{aa}^{-1} , an (M x M) matrix, ℓ times and L_a^{-1} , an (I x J x K x M) matrix, once, instead of using L^{-1} , an (I x J x K) x (I x J x K) matrix, ($\ell + 1$) times.

When eq. (2.27) is inserted into eq. (2.20), the latter becomes

$$q^{n+1} = F_b \Phi_{aa}^{n-} + F_b \Phi_{ab}^{n-} + F_a \Phi_a^n \quad (2.39)$$

$F_b \Phi_{aa}^{n-} = 0$, because F_b is zero inside region A. Consequently, eq. (2.39) above becomes

$$q^{n+1} = F_b \Phi_{ab}^{n-} + F_a \Phi_a^n \quad (2.40)$$

2.1 Computational Procedure

The computational procedure for the SAPNCS technique can be summarized as

1. The first uncollided flux, Φ_a^0 has to be calculated from eq. (2.31)

$$\Phi_a^0 = L_{aa}^{-1} q_a^0 \quad (2.31)$$

Next, we iteratively calculate eqs. (2.30) and eq. (2.38)

$$\Phi_{aa}^{\ell+1} = L_{aa}^{-1} F_a \Phi_{aa}^{\ell} \quad (2.30)$$

$$\Phi_{aa}^{(n-1)-} = \sum_{\ell=0}^{n-1} \Phi_{aa}^{\ell} \quad (2.38)$$

2. The flux Φ_a^{n-} , can be obtained from eq. (2.37):

$$\Phi_a^{n-} = L_a^{-1} (q + F_a \Phi_{aa}^{(n-1)-}) \quad (2.37)$$

3. The SAPNCS code then provides distributed sources, q^{n+1} , for standard discrete ordinates S_N code. The distributed sources will be obtained from eq. (2.40) :

$$q^{n+1} = F_b \Phi_{ab}^{n-} + F_a \Phi_a^n \quad (2.40)$$

Φ_{ab}^{n-} is part of Φ_a^{n-} inside cell B, so that eq. (2.40) can be rewritten as

$$q^{n+1} = F_b \Phi_a^{n-} + F_a \Phi_a^n \quad (2.20)$$

Φ_a^{n-} comes from eq. (2.37) while Φ_a^n is obtained from eq. (2.29) with $\ell + 1 = n$.

4. This distributed source is then used by the conventional discrete ordinates S_N code to solve eq. (2.19):

$$L \Phi_{S_N} = F \Phi_{S_N} + q^{n+1} \quad (2.19)$$

5. The total flux, Φ , is sum of the integral transport and S_N transport contributions as stated at eq. (2.17):

$$\Phi = \Phi_a^{n-} + \Phi_{S_N} \quad (2.17)$$

CHAPTER 3

ALGORITHM

We, first of all, analytically calculate the elements of operator L_a^{-1} which includes all elements of L_{aa}^{-1} . The main contributions to a matrix element $[L^{-1}]_{i,j,k}$ are the incoming and outgoing currents to a mesh cell $A_{i,j,k}$ located at coordinate (i, j, k) in region A. The incoming current at the surface area $A_{i-\frac{1}{2},j,k}$ of cell $A_{i,j,k}$ (figure 3.1) is, for example,

$$J_{i-\frac{1}{2},j,k} = \int_{y_{i-\frac{1}{2},j-\frac{1}{2},k}}^{y_{i-\frac{1}{2},j+\frac{1}{2},k}} \int_{z_{i-\frac{1}{2},j,k-\frac{1}{2}}}^{z_{i-\frac{1}{2},j,k+\frac{1}{2}}} \frac{q e^{-\sigma r_{i-\frac{1}{2}}(y,z)}}{4\pi r_{i-\frac{1}{2}}^2(y,z)} \mu_{i-\frac{1}{2},j,k} dy dz \quad (3.1)$$

where

$$r_{i-\frac{1}{2}}(y, z) = \sqrt{x_{i-\frac{1}{2}}^2 + y^2 + z^2} \quad (3.2)$$

$$\mu_{i-\frac{1}{2},j,k} = \cosine \theta = x_{i-\frac{1}{2}} / \sqrt{x_{i-\frac{1}{2}}^2 + y^2 + z^2} \quad (3.3)$$

and

σ = total cross section along the path of $r_{i-\frac{1}{2}}(y, z)$

$x_{i-\frac{1}{2}}$ = projection of $r_{i-\frac{1}{2}}(y, z)$ along x axis

$A_{i-\frac{1}{2},j,k}$ = surface area of cell $A_{i,j,k}$ perpendicular to x axis

$$= \Delta y \cdot \Delta z$$

Δy = the width of mesh cell $A_{i,j,k}$

Δz = the height of mesh cell $A_{i,j,k}$.

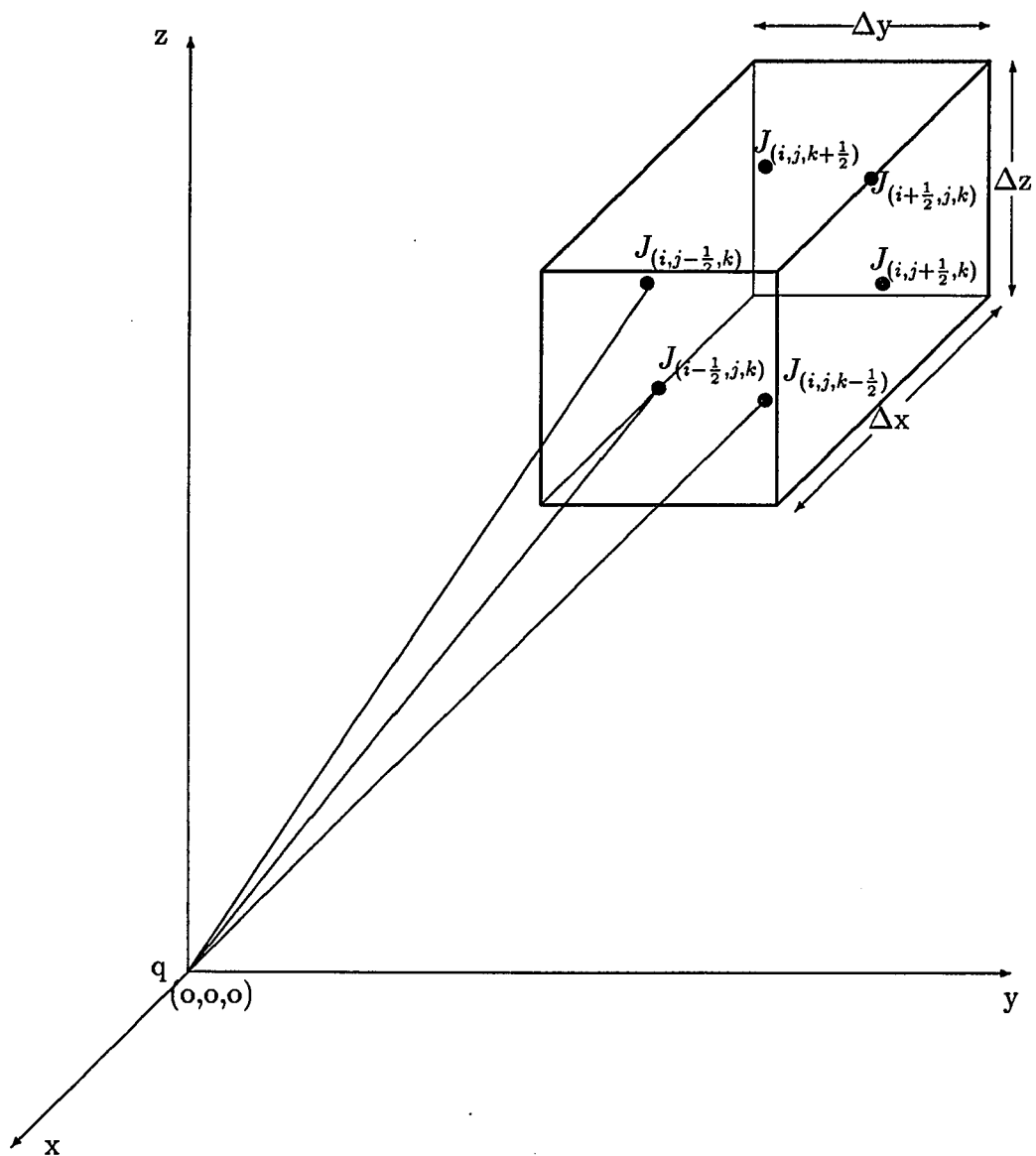


Figure 3.1 Three-dimensional spatial discretization showing mesh cell $A_{i,j,k}$

Using eq. (3.3), eq. (3.1) becomes

$$J_{i-\frac{1}{2},j,k} = \int_{y_{i-\frac{1}{2},j-\frac{1}{2},k}}^{y_{i-\frac{1}{2},j+\frac{1}{2},k}} \int_{z_{i-\frac{1}{2},j,k-\frac{1}{2}}}^{z_{i-\frac{1}{2},j,k+\frac{1}{2}}} \frac{qe^{-\sigma r_{i-\frac{1}{2}}(y,z)}}{4\pi} (x_{i-\frac{1}{2}}) \frac{1}{r_{i-\frac{1}{2}}^3(y,z)} dydz \quad (3.4)$$

This equation is so difficult to solve analytically that we assume that an approximate solution has to be taken into account. The solution we are applying for is a cell-averaged current coming perpendicular to surface area $A_{i-\frac{1}{2},j,k}$, $\bar{J}_{i-\frac{1}{2},j,k}$:

$$\bar{J}_{i-\frac{1}{2},j,k} = \frac{qe^{-\sigma \overline{r_{i-\frac{1}{2}}(y,z)}}}{4\pi} (x_{i-\frac{1}{2}}) A_{i-\frac{1}{2},j,k} \overline{\frac{1}{r_{i-\frac{1}{2}}^3(y,z)}} \quad (3.5)$$

where

$$\overline{r_{i-\frac{1}{2}}(y,z)} = \int_{y_{i-\frac{1}{2},j-\frac{1}{2},k}}^{y_{i-\frac{1}{2},j+\frac{1}{2},k}} \int_{z_{i-\frac{1}{2},j,k-\frac{1}{2}}}^{z_{i-\frac{1}{2},j,k+\frac{1}{2}}} \sqrt{x_{i-\frac{1}{2},j,k}^2 + y^2 + z^2} dy dz \quad (3.6)$$

and

$$\overline{\frac{1}{r_{i-\frac{1}{2}}^3(y,z)}} = \int_{y_{i-\frac{1}{2},j-\frac{1}{2},k}}^{y_{i-\frac{1}{2},j+\frac{1}{2},k}} \int_{z_{i-\frac{1}{2},j,k-\frac{1}{2}}}^{z_{i-\frac{1}{2},j,k+\frac{1}{2}}} \frac{1}{(\sqrt{x_{i-\frac{1}{2},j,k}^2 + y^2 + z^2})^3} dy dz \quad (3.7)$$

Both the average distance from source to surface area $A_{i-\frac{1}{2},j,k}$, $\overline{r_{i-\frac{1}{2}}(y,z)}$, and $\overline{\frac{1}{r_{i-\frac{1}{2}}^3(y,z)}}$ can be analytically calculated. Eq. (3.5) may be written equivalently as :

$$\bar{J}_{i-\frac{1}{2},j,k} = \bar{H}_{i-\frac{1}{2},j,k} q \quad (3.8)$$

in which

$$\bar{H}_{i-\frac{1}{2},j,k} = \frac{e^{-\sigma \overline{r_{i-\frac{1}{2}}(y,z)}}}{4\pi} (x_{i-\frac{1}{2}}) A_{i-\frac{1}{2},j,k} \overline{\frac{1}{r_{i-\frac{1}{2}}^3(y,z)}} \quad (3.9)$$

Using particle balance the average uncollided flux can be expressed in terms of the cell surface current as

$$\Phi_{i,j,k} = \frac{(\bar{J}_{i-\frac{1}{2},j,k} - \bar{J}_{i+\frac{1}{2},j,k}) + (\bar{J}_{i,j-\frac{1}{2},k} - \bar{J}_{i,j+\frac{1}{2},k}) + (\bar{J}_{i,j,k-\frac{1}{2}} - \bar{J}_{i,j,k+\frac{1}{2}})}{(\sigma_{i,j,k} V_{i,j,k})} \quad (3.10)$$

$\sigma_{i,j,k}$ = total cross section of mesh cell $A_{i,j,k}$

$V_{i,j,k}$ = volume of mesh cell $A_{i,j,k}$

Inserting eq.(3.8) into eq.(3.10) and using analogous expressions for the remaining currents allows eq.(3.10) to be written as:

$$\Phi_{i,j,k} = \frac{(\bar{H}_{i-\frac{1}{2},j,k} - \bar{H}_{i+\frac{1}{2},j,k}) + (\bar{H}_{i,j-\frac{1}{2},k} - \bar{H}_{i,j+\frac{1}{2},k}) + (\bar{H}_{i,j,k-\frac{1}{2}} - \bar{H}_{i,j,k+\frac{1}{2}})}{(\sigma_{i,j,k} V_{i,j,k})} q \quad (3.11)$$

and finally

$$\Phi_{i,j,k} = [L^{-1}]_{i,0,j,0,k,0} q_{0,0,0} \quad (3.12)$$

where

$$[L^{-1}]_{i,0,j,0,k,0} = \frac{(\bar{H}_{i-\frac{1}{2},j,k} - \bar{H}_{i+\frac{1}{2},j,k}) + (\bar{H}_{i,j-\frac{1}{2},k} - \bar{H}_{i,j+\frac{1}{2},k}) + (\bar{H}_{i,j,k-\frac{1}{2}} - \bar{H}_{i,j,k+\frac{1}{2}})}{(\sigma_{i,j,k} V_{i,j,k})} \quad (3.13)$$

$[L^{-1}]_{i,0,j,0,k,0}$ = one element of the operator L_a^{-1} for mesh cell $A_{i,j,k}$

when a source is placed at mesh cell $A_{0,0,0}$.

The L_a^{-1} matrix can be expressed as

$$L_a^{-1} = \left[\begin{array}{c} \left[\begin{array}{ccc} [[L^{-1}]]_{1,1} & \cdots & [[L^{-1}]]_{K'',1} \\ [[L^{-1}]]_{1,2} & \cdots & [[L^{-1}]]_{K'',2} \\ \vdots & \ddots & \vdots \\ [[L^{-1}]]_{1,K''} & \cdots & [[L^{-1}]]_{K'',K''} \end{array} \right] \cdots \left[\begin{array}{c} [[L^{-1}]]_{K,1} \\ [[L^{-1}]]_{K,2} \\ \vdots \\ [[L^{-1}]]_{K,K''} \end{array} \right] \end{array} \right] \quad (3.14)$$

The submatrix representation for the (k, k'') operator is defined as

$$[[L^{-1}]]_{k,k''} = \left[\begin{array}{c} \left[\begin{array}{ccc} [[L^{-1}]]_{1,1,k,k''} & \cdots & [[L^{-1}]]_{J'',1,k,k''} \\ [[L^{-1}]]_{1,2,k,k''} & \cdots & [[L^{-1}]]_{J'',2,k,k''} \\ \vdots & \ddots & \vdots \\ [[L^{-1}]]_{1,J'',k,k''} & \cdots & [[L^{-1}]]_{J'',J'',k,k''} \end{array} \right] \cdots \left[\begin{array}{c} [[L^{-1}]]_{J,1,k,k''} \\ [[L^{-1}]]_{J,2,k,k''} \\ \vdots \\ [[L^{-1}]]_{J,J'',k,k''} \end{array} \right] \end{array} \right] \quad (3.15)$$

The sub-submatrix $[[L^{-1}]]_{j,j'',k,k''}$ can be expressed as

$$[[L^{-1}]]_{j,j'',k,k''} = \left[\begin{array}{c} \left[\begin{array}{ccc} [L^{-1}]_{1,1,j,j'',k,k''} & \cdots & [L^{-1}]_{I'',1,j,j'',k,k''} \\ [L^{-1}]_{1,2,j,j'',k,k''} & \cdots & [L^{-1}]_{I'',2,j,j'',k,k''} \\ \vdots & \ddots & \vdots \\ [L^{-1}]_{1,I'',j,j'',k,k''} & \cdots & [L^{-1}]_{I'',I'',j,j'',k,k''} \end{array} \right] \cdots \left[\begin{array}{c} [L^{-1}]_{I,1,j,j'',k,k''} \\ [L^{-1}]_{I,2,j,j'',k,k''} \\ \vdots \\ [L^{-1}]_{I,I'',j,j'',k,k''} \end{array} \right] \end{array} \right] \quad (3.16)$$

where I'' , J'' , and K'' represent the number of spacial mesh cells of region A for x, y, and z directions, respectively and $I'' \times J'' \times K''$ equals m. The matrix inside L_a^{-1} is the

operator L_{aa}^{-1} . The operator L_a^{-1} represents uncollided transport between the cells in region A (call SAPNCS cells) and the whole cells. Thus, the L_a^{-1} is an $[m \times I \times J \times K]$ matrix. A matrix inside the operator L_a^{-1} is the operator L_{aa}^{-1} . The operator L_{aa}^{-1} represents uncollided transport between the cells in region A themselves and is an $[m \times m]$ matrix. Therefore, the matrix L_{aa}^{-1} can be expressed as

$$L_{aa}^{-1} = \begin{bmatrix} [[[L^{-1}]]]_{1,1} & [[[L^{-1}]]]_{2,1} & \cdots & [[[L^{-1}]]]_{K'',1} \\ [[[L^{-1}]]]_{1,2} & [[[L^{-1}]]]_{2,2} & \cdots & [[[L^{-1}]]]_{K'',2} \\ \vdots & \vdots & \ddots & \vdots \\ [[[L^{-1}]]]_{1,K''} & [[[L^{-1}]]]_{2,K''} & \cdots & [[[L^{-1}]]]_{K'',K''} \end{bmatrix} \quad (3.17)$$

The submatrix representation for the (k'', k''') operator is defined as

$$[[[L^{-1}]]]_{k'',k'''} = \begin{bmatrix} [[L^{-1}]]_{1,1,k'',k'''} & [[L^{-1}]]_{2,1,k'',k'''} & \cdots & [[L^{-1}]]_{J'',1,k'',k'''} \\ [[L^{-1}]]_{1,2,k'',k'''} & [[L^{-1}]]_{2,2,k'',k'''} & \cdots & [[L^{-1}]]_{J'',2,k'',k'''} \\ \vdots & \vdots & \ddots & \vdots \\ [[L^{-1}]]_{1,J'',k'',k'''} & [[L^{-1}]]_{2,J'',k'',k'''} & \cdots & [[L^{-1}]]_{J'',J'',k'',k'''} \end{bmatrix} \quad (3.18)$$

The sub-submatrix $[[L^{-1}]]_{j'',j''',k'',k'''}$ can be expressed as

$$[[L^{-1}]]_{j'',j''',k'',k'''} = \begin{bmatrix} [L^{-1}]_{1,1,j'',j''',k'',k'''} & [L^{-1}]_{2,1,j'',j''',k'',k'''} & \cdots & [L^{-1}]_{I'',1,j'',j''',k'',k'''} \\ [L^{-1}]_{1,2,j'',j''',k'',k'''} & [L^{-1}]_{2,2,j'',j''',k'',k'''} & \cdots & [L^{-1}]_{I'',2,j'',j''',k'',k'''} \\ \vdots & \vdots & \ddots & \vdots \\ [L^{-1}]_{1,I'',j'',j''',k'',k'''} & [L^{-1}]_{2,I'',j'',j''',k'',k'''} & \cdots & [L^{-1}]_{I'',I'',j'',j''',k'',k'''} \end{bmatrix} \quad (3.19)$$

The extraneous and scattering sources are exclusively located in the region A.

A vector displaying the distribution of sources may be expressed as

$$q_a^\ell = \begin{pmatrix} [[[q^\ell]]]_1 \\ [[[q^\ell]]]_2 \\ [[[q^\ell]]]_3 \\ \vdots \\ [[[q^\ell]]]_{K''} \end{pmatrix} \quad (3.20)$$

The subvector representation for the (k'') source is defined as

$$[[[q^\ell]]]_{k''} = \begin{pmatrix} [[q^\ell]]_{1,k''} \\ [[q^\ell]]_{2,k''} \\ [[q^\ell]]_{3,k''} \\ \vdots \\ [[q^\ell]]_{J'',k''} \end{pmatrix} \quad (3.21)$$

The sub-subvector $[[q^\ell]]_{j'',k''}$ can be expressed as

$$[[q^\ell]]_{j'',k''} = \begin{pmatrix} [q^\ell]_{1,j'',k''} \\ [q^\ell]_{2,j'',k''} \\ [q^\ell]_{3,j'',k''} \\ \vdots \\ [q^\ell]_{I'',j'',k''} \end{pmatrix} \quad (3.22)$$

The result of multiplying the matrix $L_{\alpha\alpha}^{-1}$ by the vector q_{α}^{ℓ} , the $\Phi_{\alpha\alpha}^{\ell}$, can be expressed as

$$\Phi_{\alpha\alpha}^{\ell} = \begin{pmatrix} [[[\Phi^{\ell}]]_1 \\ [[[\Phi^{\ell}]]_2 \\ [[[\Phi^{\ell}]]_3 \\ \vdots \\ [[[\Phi^{\ell}]]_{K''} \end{pmatrix} \quad (3.23)$$

The subvector representation for the (k'') source is defined as

$$[[[\Phi^{\ell}]]_{k''} = \begin{pmatrix} [[\Phi^{\ell}]_{1,k''} \\ [[\Phi^{\ell}]_{2,k''} \\ [[\Phi^{\ell}]_{3,k''} \\ \vdots \\ [[\Phi^{\ell}]_{J'',k''} \end{pmatrix} \quad (3.24)$$

The sub-subvector $[[\Phi^{\ell}]]_{j'',k''}$ can be expressed as

$$[[\Phi^{\ell}]]_{j'',k''} = \begin{pmatrix} [\Phi^{\ell}]_{1,j'',k''} \\ [\Phi^{\ell}]_{2,j'',k''} \\ [\Phi^{\ell}]_{3,j'',k''} \\ \vdots \\ [\Phi^{\ell}]_{I'',j'',k''} \end{pmatrix} \quad (3.25)$$

Unlike the Φ_{aa}^ℓ , the Φ_a^{n-} occupies the whole mesh cell. So the Φ_a^{n-} can be expressed as

$$\Phi_a^{n-} = \begin{pmatrix} [[[\Phi^{n-}]]_1 \\ [[[\Phi^{n-}]]_2 \\ [[[\Phi^{n-}]]_3 \\ \vdots \\ [[[\Phi^{n-}]]_K \end{pmatrix} \quad (3.26)$$

The subvector representation for the (k) flux is defined as

$$[[[\Phi^{n-}]]_k = \begin{pmatrix} [[\Phi^{n-}]_{1,k} \\ [[\Phi^{n-}]_{2,k} \\ [[\Phi^{n-}]_{3,k} \\ \vdots \\ [[\Phi^{n-}]_{J,k} \end{pmatrix} \quad (3.27)$$

The sub-submatrix $[[[\Phi^{n-}]]_{j,k}$ can be expressed as

$$[[[\Phi^{n-}]]_{j,k} = \begin{pmatrix} [\Phi^{n-}]_{1,j,k} \\ [\Phi^{n-}]_{2,j,k} \\ [\Phi^{n-}]_{3,j,k} \\ \vdots \\ [\Phi^{n-}]_{I,j,k} \end{pmatrix} \quad (3.28)$$

The q^{n+1} occupies the same mesh cell as the Φ_a^{n-} , so the q^{n+1} can be expressed as

$$q^{n+1} = \begin{pmatrix} [[[q^{n+1}]]_1 \\ [[q^{n+1}]]_2 \\ [[[q^{n+1}]]_3 \\ \vdots \\ [[[q^{n+1}]]_K \end{pmatrix} \quad (3.29)$$

The subvector of the k^{th} source can be expressed as

$$[[[q^{n+1}]]_k = \begin{pmatrix} [[q^{n+1}]_{1,k} \\ [[q^{n+1}]_{2,k} \\ [[q^{n+1}]_{3,k} \\ \vdots \\ [[q^{n+1}]_{J,k} \end{pmatrix} \quad (3.30)$$

The sub-subvector $[[q^{n+1}]_{j,k}$ can be expressed as

$$[[q^{n+1}]_{j,k} = \begin{pmatrix} [q^{n+1}]_{1,j,k} \\ [q^{n+1}]_{2,j,k} \\ [q^{n+1}]_{3,j,k} \\ \vdots \\ [q^{n+1}]_{I,j,k} \end{pmatrix} \quad (3.31)$$

CHAPTER 4

COMPUTATIONAL RESULTS

Chapter four gives our computational results using the S_N and the SAPNCS methods for four test problems. Both the S_N and the SAPNCS methods were tested under the same conditions for each problem. This chapter is composed of five sections. Section one describes the overall structure of the test problems. Section two explains test problem one, and sections three through six discuss test problems two through five, respectively.

4.1 Overall Structure of Test Problems

Each of our test problems uses 861 mesh cells that have the same dimension. The individual mesh cells have a width of one centimeter, a height of one centimeter, and a length of 31 centimeters. Figure 4.1 gives the dimensions of an individual mesh cells. Figure 4.2 shows the overall structure of the four test problems.

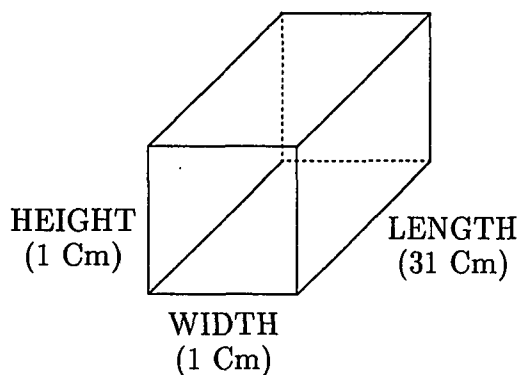


Figure 4.1a Individual mesh cell

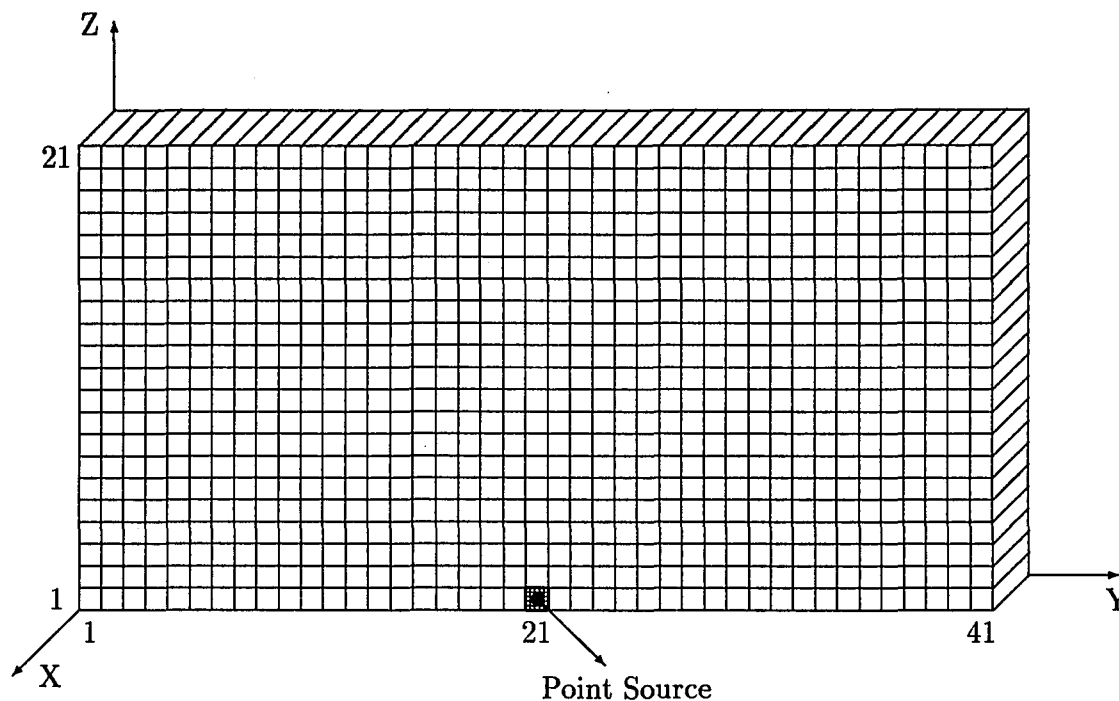


Figure 4.1b General geometric scheme of tests

Each of the test problems has 41 mesh cells along the y-axis and 21 mesh cells along the z-axis. This arrangement creates a matrix of mesh cells with a size of (41 x 21). For all test problems, an isotropic photon source is located at the center of mesh cell (21 x 1). Figure 4.1b shows the photon source as a dark circle. The source releases monoenergetic photons. The shaded cell is used to indicate the SAPNCS cell which is a high scatter and low absorption cell. The SAPNCS cell has a macroscopic total cross section of 0.1 cm^{-1} and a scattering cross section of 0.09 cm^{-1} . The unshaded or homogeneous cells are low scatter regions with moderate absorption. The homogeneous cells have a macroscopic total cross section of 0.06 cm^{-1} and a scattering cross section of 0.01 cm^{-1} .

The five test problems basically based on one general geometric scheme shown in Figure 4.1b will be performed.

4.2 Test Problem One

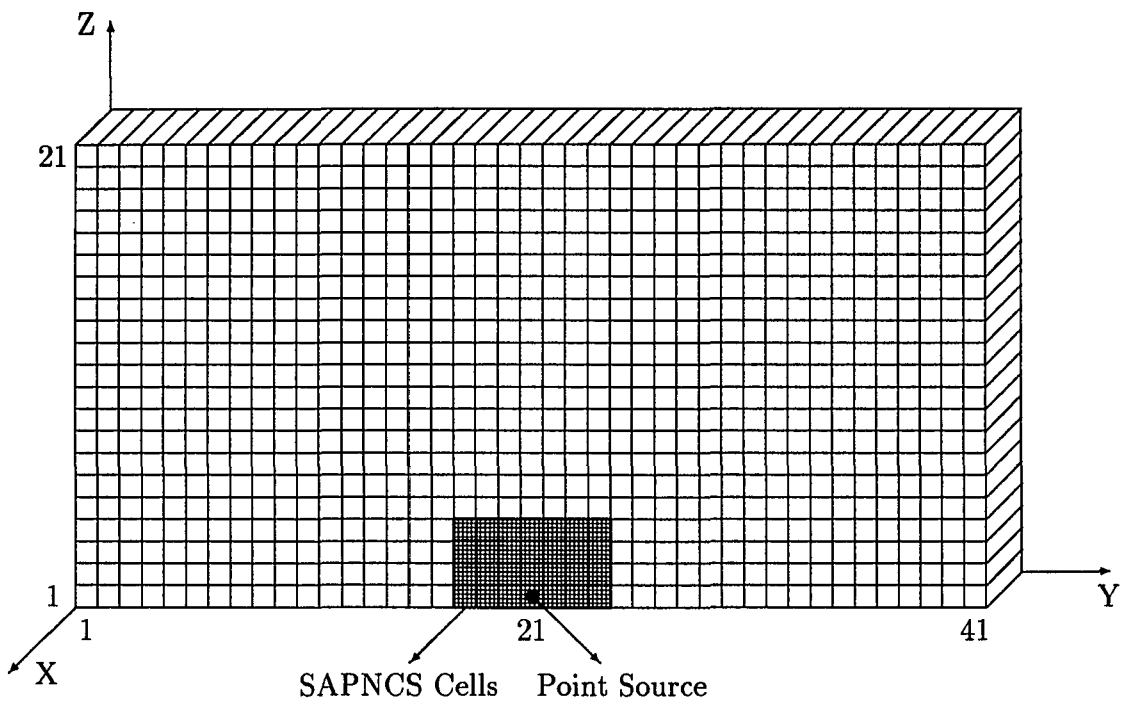


Figure 4.2 Geometric scheme for test problem one

4.2.1 Description of Problem

Figure 4.2 describes a geometric scheme for test problem one. The geometric scheme of test problem one is based on the general geometric scheme with the SAPNCS cells extending from mesh cell 18 to 24 in width and from mesh cell 1 to 4 in height, so that there are 28 SAPNCS cells including one cell where the source is located.

4.2.2 Objective

The objective of this test is to demonstrate the capability of the SAPNCS technique to eliminate the ray effects. Several tests were conducted using the conventional discrete ordinates for angular quadratures of 2 (S_2) to 16 (S_{16}).

4.2.3 Test One

The first test was performed using S_2 . Ray effects were very severe as shown in Figure 4.2.1. When Semi-Analytical Partial First Collision Source (SAP_1CS) was applied, the ray effects were considerably mitigated. Figure 4.2.1a shows barely noticeable effects that still exist. The effects were totally eliminated when Semi-Analytical Partial Second Collision Source (SAP_2CS) was used as illustrated in Figure 4.2.1b.

4.2.4 Test Two

The second test was conducted for S_4 . The ray effects were larger in number but less severe than the test for S_2 as indicated in Figure 4.2.2. Unlike the first test, the ray effects disappeared when SAP_1CS was applied. Figure 4.2.2a demonstrates the effectiveness of the SAPNCS method to eliminate the ray effects.

4.2.5 Test Three

S_8 was used to perform the third test. Figure 4.2.3 shows the present of the ray effects. The ray effects were much less noticeable than in test two. When SAP_1CS was used, the effects disappeared as illustrated in Figure 4.2.3a.

4.2.6 Test Four

An additional test for S_{12} was conducted. The ray effects were much less noticeable than in the previous three tests as illustrated in Figure 4.2.4. The ray effects were eliminated when SAP_1CS was applied as shown in Fig. 4.2.4a.

4.2.7 Test Five

The last test for test problem one was performed using S_{16} . The ray effects were barely noticeable, except on cells near the source. Figure 4.2.5 shows that the ray effects were also present even in high angular quadrature. SAP_1CS was used to eliminate the ray effects as demonstrated in Figure 4.2.5a.

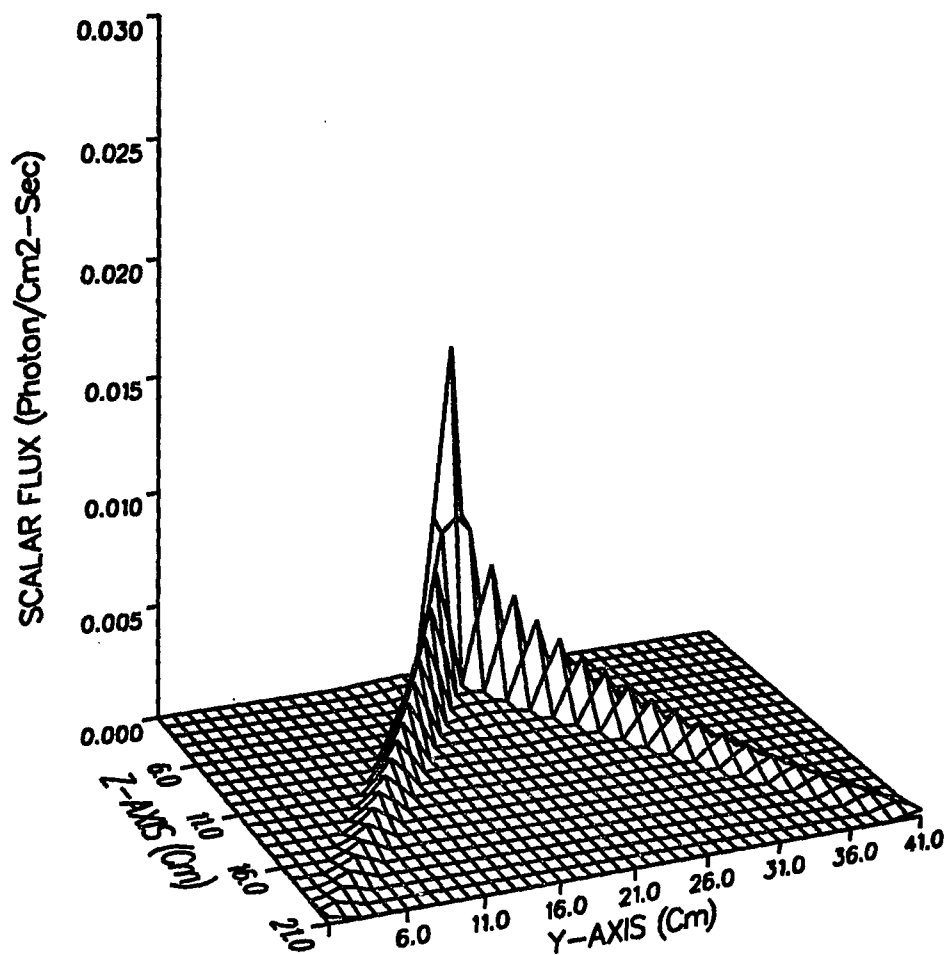


Figure 4.2.1 Flux distribution from S_2 .

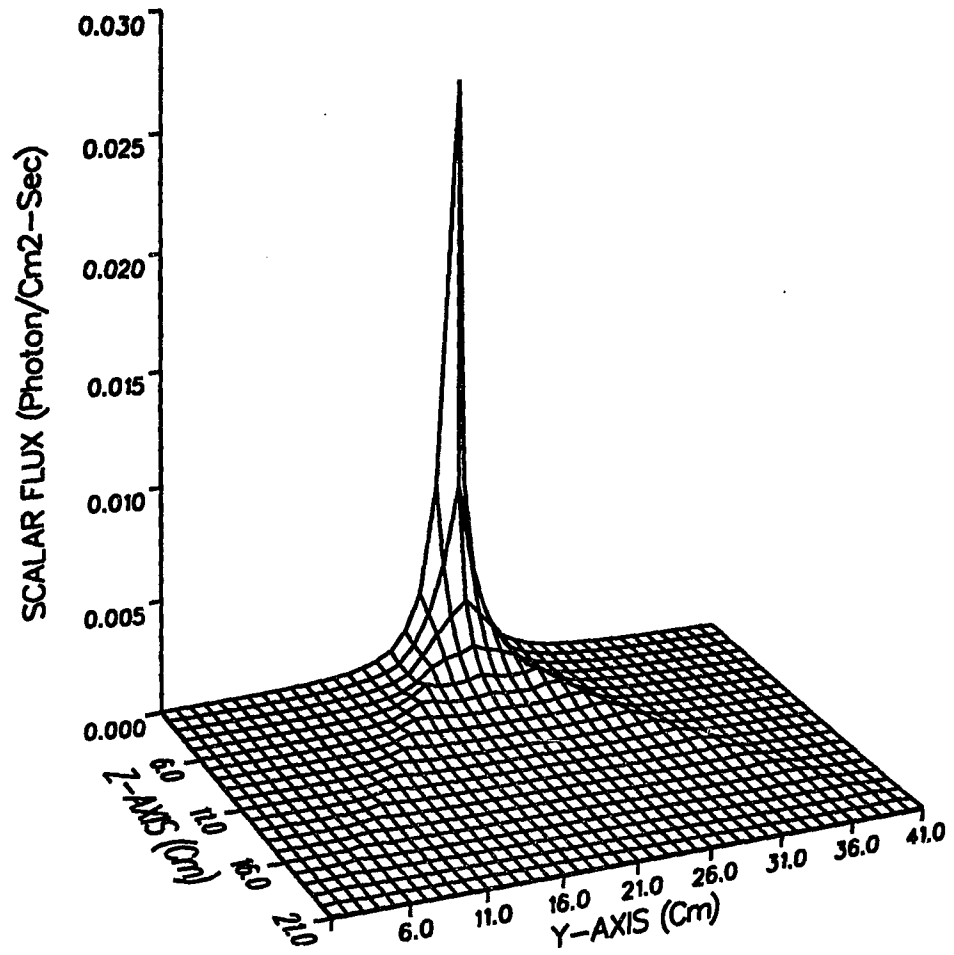


Figure 4.2.1a Flux distribution from SAP_1CS coupled with S_2 .

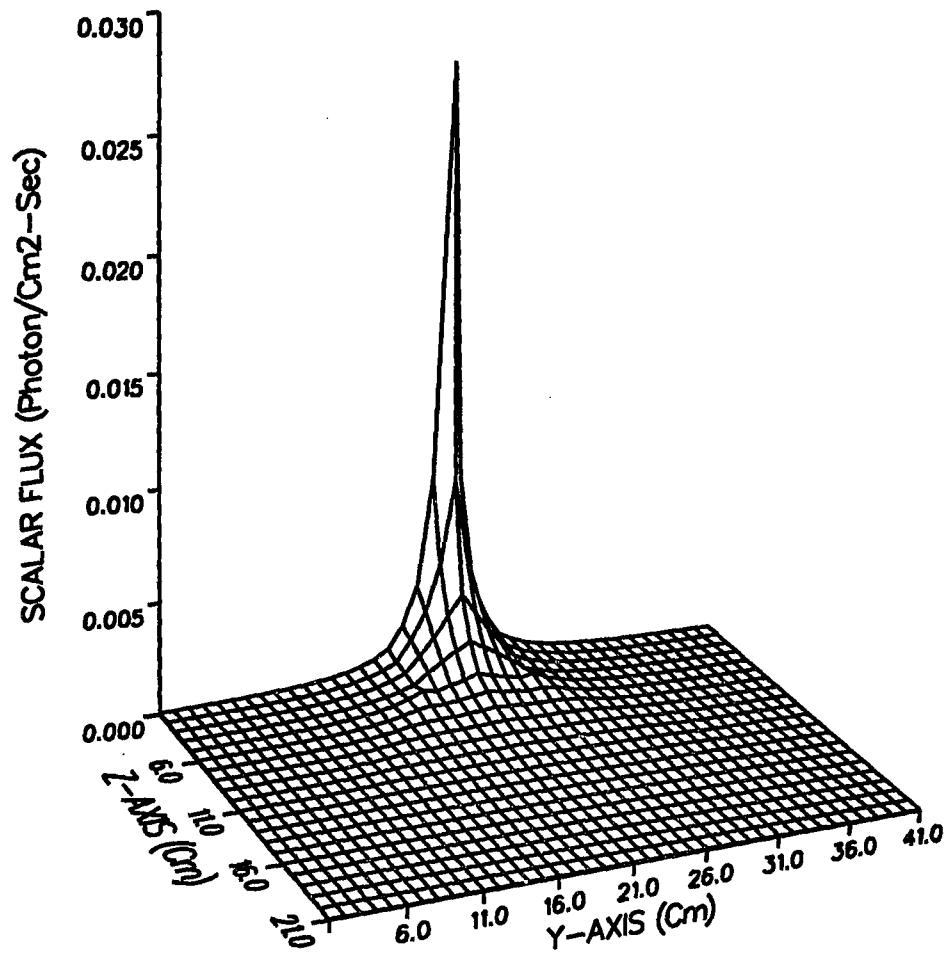


Figure 4.2.1b Flux distribution from SAP₂CS coupled with S₂.

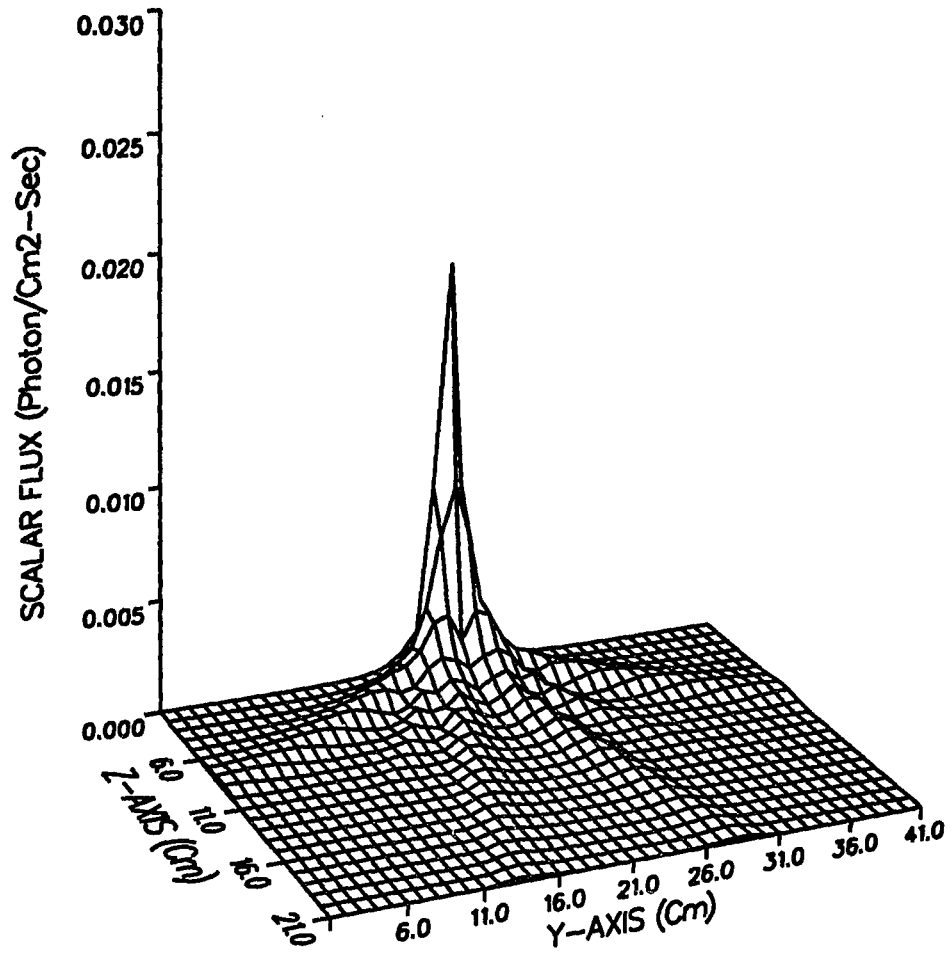


Figure 4.2.2 Flux distribution from S_4 .

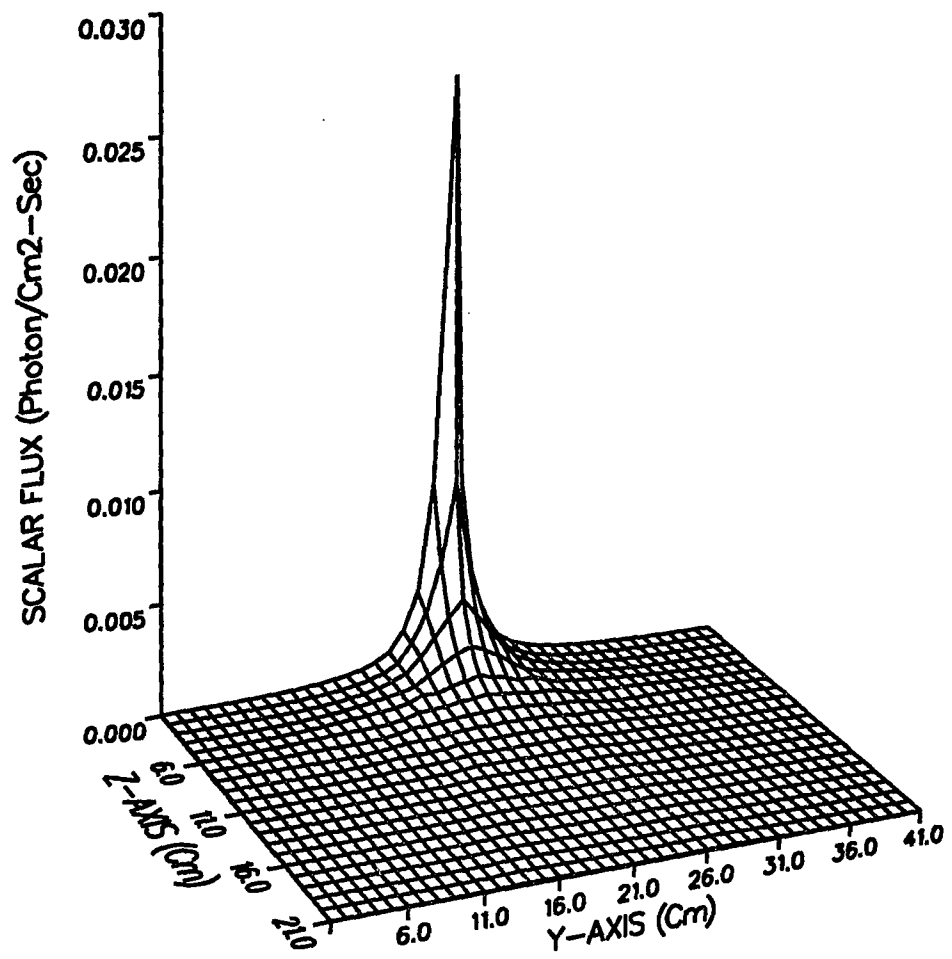


Figure 4.2.2a Flux distribution from SAP_1CS coupled with S_4 .

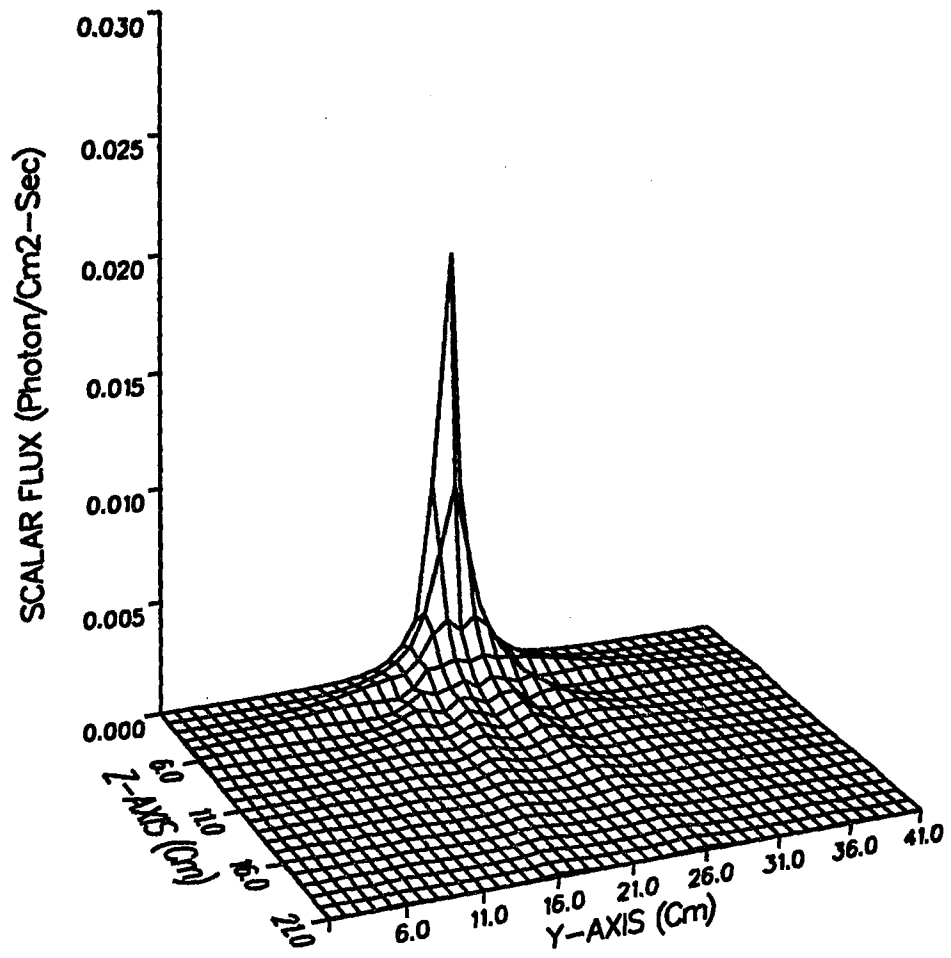


Figure 4.2.3 Flux distribution from S₈.

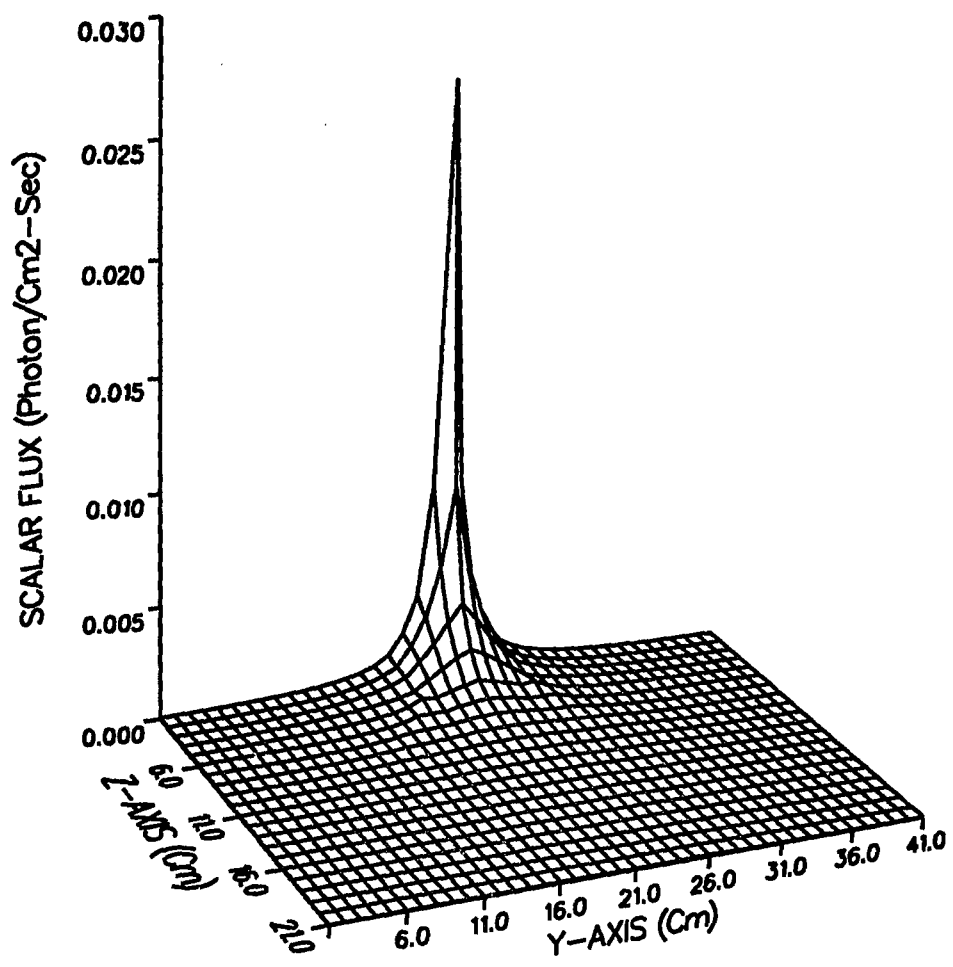


Figure 4.2.3a Flux distribution from SAP_1CS coupled with S_8 .

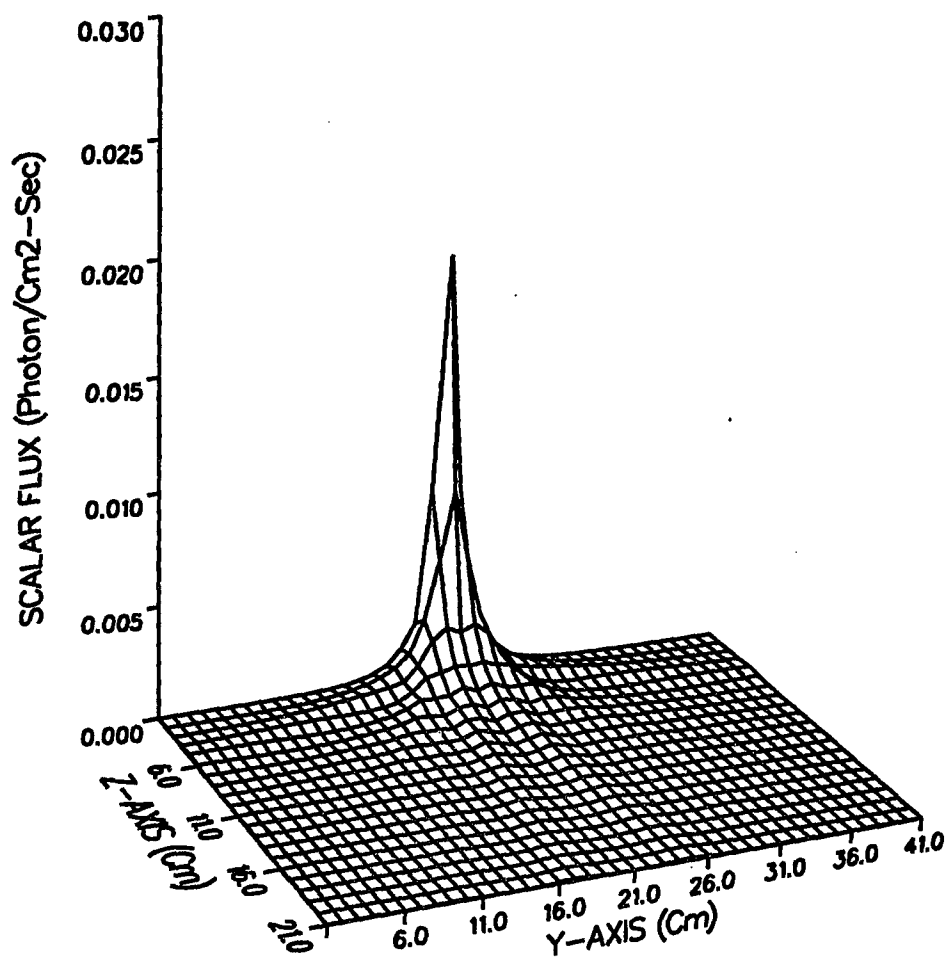


Figure 4.2.4 Flux distribution from S_{12} .

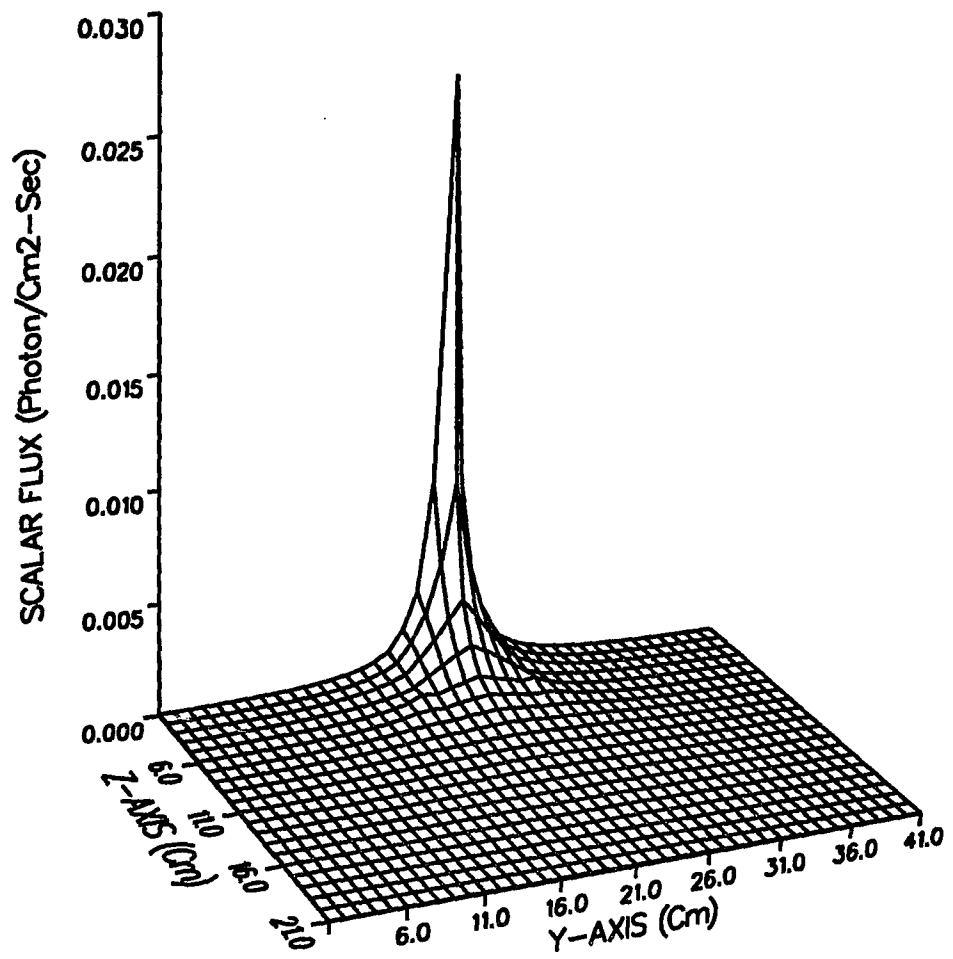


Figure 4.2.4a Flux distribution from SAP_1CS coupled with S_{12} .

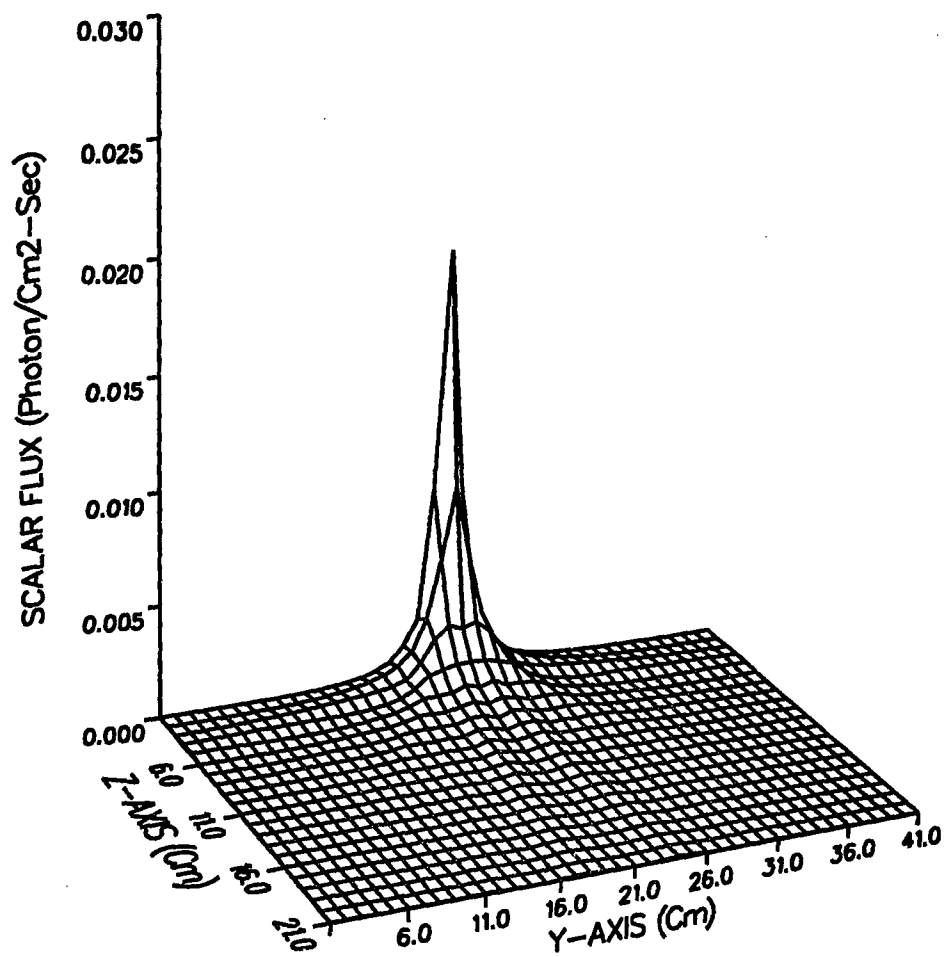


Figure 4.2.5 Flux distribution from S₁₆.

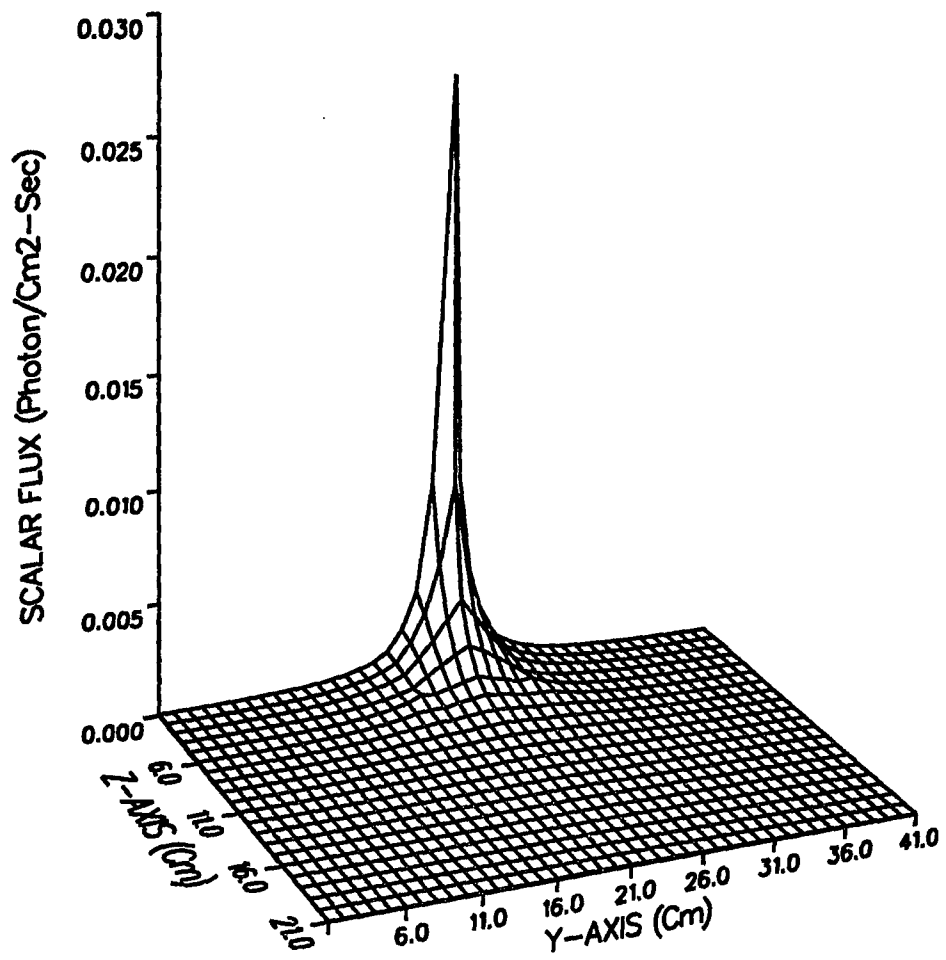


Figure 4.2.5a Flux distribution from SAP_1CS coupled with S_{16} .

4.3 Test Problem Two

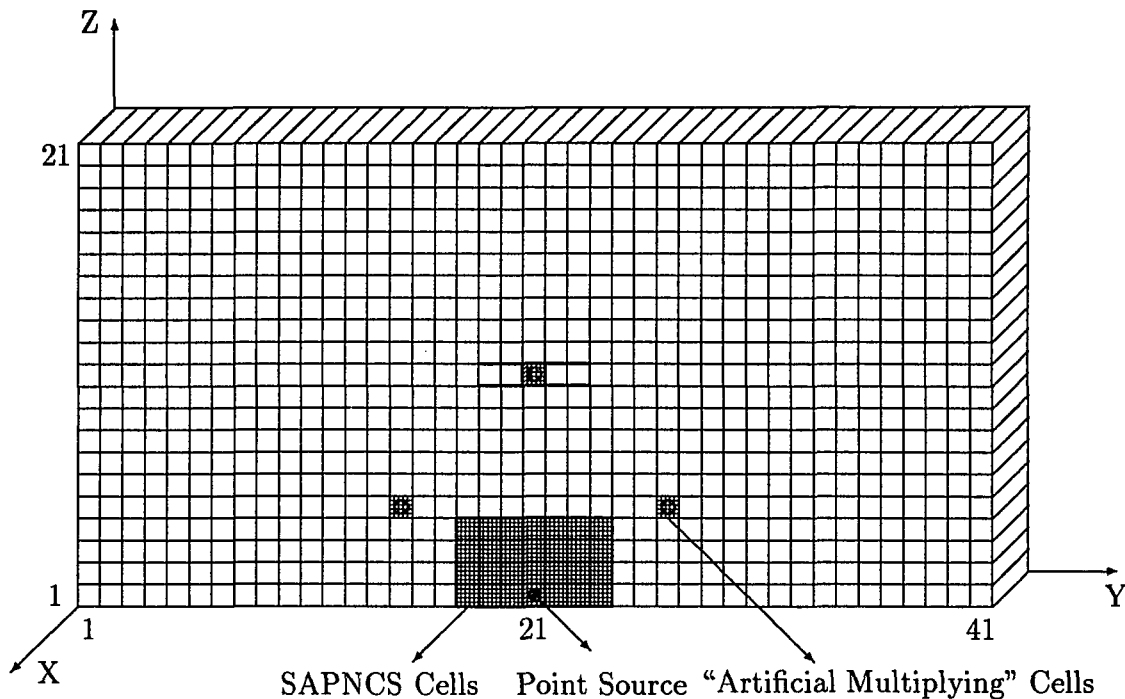


Figure 4.3 Geometric scheme for test problem two

Shaded cells are SAPNCS cells, high scatter and low absorption regions. Circles are “artificial multiplying” cells that have a large scattering cross section. The “artificial multiplying” cells are placed at the path in which the ripples occur, and the remaining cells are low scatter regions with moderate absorption. A disk, a circle with the center filled in, is an isotropic source.

4.3.1 Description of Problem

Figure 4.3 describes a geometric scheme for test problem two. The geometric scheme of problem test two is similar to test problem one, except large scattering cross section material was inserted into specific mesh cells. The scattering cross section of this material was 1.2 cm^{-1} which is thirteen times larger than that of SAPNCS material. The mesh cells with large scattering cross section material are

called “artificial multiplying” cells. The “artificial multiplying” cells are divided into three groups. Figure 4.3 indicates the position of the three “artificial multiplying” cells. The “artificial multiplying” cells were located in coordinates (1,15,5), (1,21,11), and (1,27,5). The first term in the bracket is the x-coordinate, the second term is the y-coordinate, and the last term is the z-coordinate. The “artificial multiplying” cells were placed on paths where the ray effects were suspected of occurring. When the ray effects hit the “artificial multiplying” cells, secondary sources were created. As a result, new or secondary ray effects arose and the initial ray effects became much more noticeable.

4.3.2 Objective

The objective of this test is to demonstrate the capability of the SAPNCS technique to eliminate first and secondary ray effects as well. There are four groups of tests were conducted. The first group of tests were performed by using S_2 and combination of SAP_1CS and S_2 , SAP_2CS and S_2 , SAP_3CS and S_2 , and SAP_4CS and S_2 . The second group of test applied S_4 , SAP_1CS combined with S_4 , and SAP_2CS coupled with S_4 . The third group used S_8 , SAP_1CS combined with S_8 and SAP_2CS combined with S_8 . The fourth group applied S_{12} , SAP_1CS combined with S_{12} , and SAP_2CS coupled with S_{12} .

4.3.3 Test Group One

The first test conducted using the “artificial multiplying” cells was S_2 . Both first and secondary ray effects were very severe, as shown in Figure 4.3.1a. When SAP_1CS was applied, both first and secondary ray effects were considerably reduced as seen in Figure 4.3.1b. The first and secondary ray effects were substantially reduced. SAP_2CS was then used to reduce further the ray effects. The SAP_2CS method worked very well to reduce the ray effects as illustrated in Figure 4.3.1c. This figure shows that the first ray effects were barely noticeable and that the secondary ones were even smaller. A SAP_3CS was then utilized to get the effects reduced even further. Figure 4.3.1d demonstrates that the first ray effects were totally gone and the secondary ones were less noticeable. Finally, the SAP_4CS was applied and both effects totally disappeared as shown in Figure 4.3.1e.

4.3.4 Test Group Two

A test for S_4 was performed under the same conditions as test one except the number and positions of the “artificial multiplying” cells. Four “artificial multiplying” cells were placed at coordinates (1,11,5), (1,17,10), (1,25,10), and (1,30,5).

In this test, the first and secondary ray effects were noticeable, but less severe than in test one as seen in Figure 4.3.2a. The secondary ray effects are minimal, because the secondary sources are also less powerful. When SAP_1CS was used, both the first and secondary effects were slightly reduced as shown in Figure 4.3.2.b. The effects were finally eliminated after SAP_2CS were applied as seen in Figure 4.3.2c.

4.3.5 Test Group Three

The third test was conducted for S_8 with four “artificial multiplying” cells. Locations of the “artificial multiplying” cells were slightly different with test group two. The cells were placed at coordinates (1,11,5), (1,17,10), (1,25,10), and (1,30,5).

The results were similar to test group two. The first and secondary ray effects were noticeable, but less severe, as illustrated in Figure 4.3.3a. However SAP_1CS alone could not eliminate the first and secondary effects as shown in Figure 4.3.3b. Consequently, the SAP_2CS had to be used to eliminate the effects totally as illustrated in Figure 4.3.3c.

4.3.6 Test Group Four

The fourth and final test was conducted using S_{12} with four “artificial multiplying” cells on coordinates (1,11,3), (1,19,9), (1,23,9), and (1,30,3).

The first and secondary ray effects were less noticeable than using S_2 , S_4 , and S_8 . Figure 4.3.4a shows the result for S_{12} . When the SAP_1CS were applied, the ray effects were still present as seen in Figure 4.3.4b. Therefore, the SAP_2CS was used to eliminate the effects as demonstrated in Figure 4.3.4c.

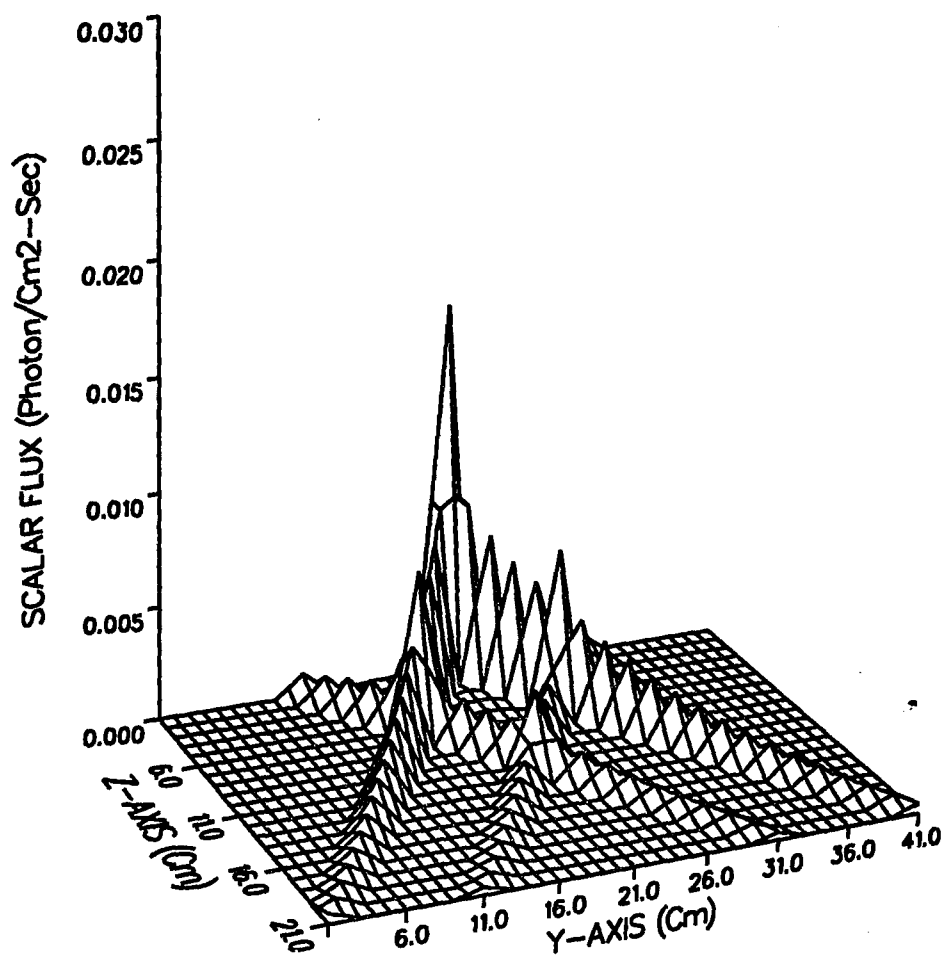


Figure 4.3.1a Flux distribution from S_2 when "artificial multiplying" cells are present at the ripples

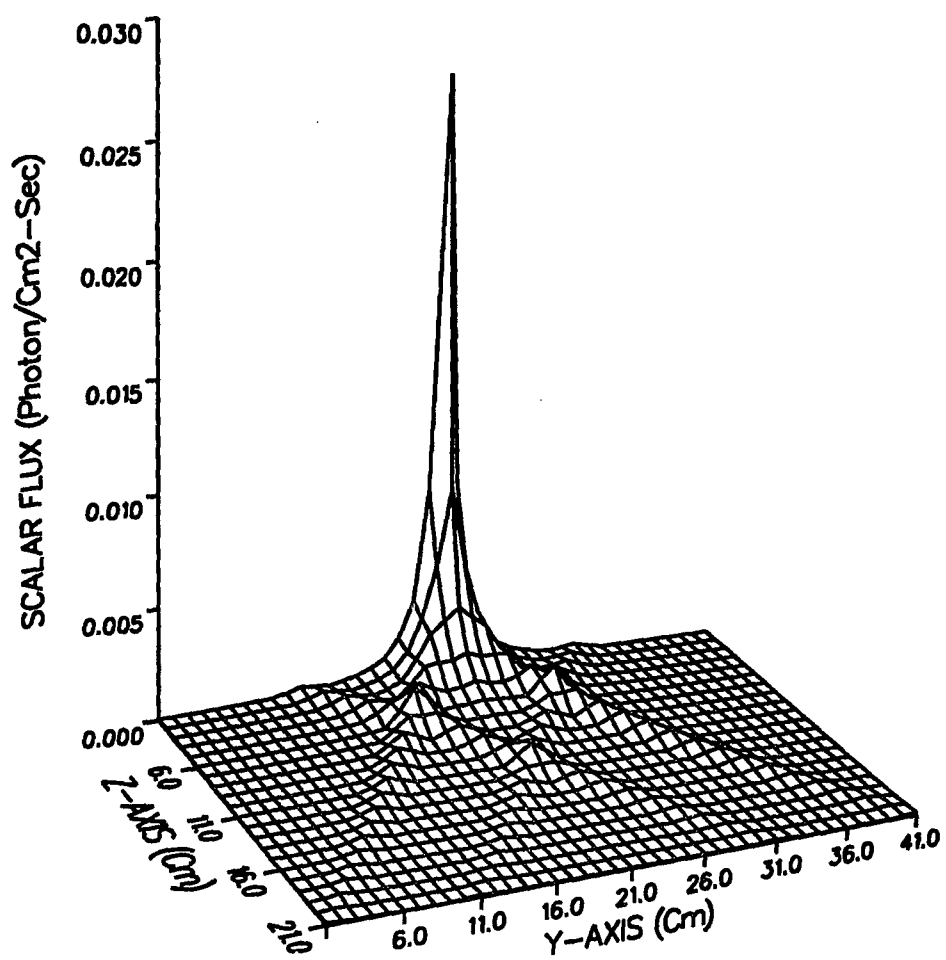


Figure 4.3.1b Flux distribution from SAP_1CS coupled with S_2 when "artificial multiplying" cells are present at the ripples

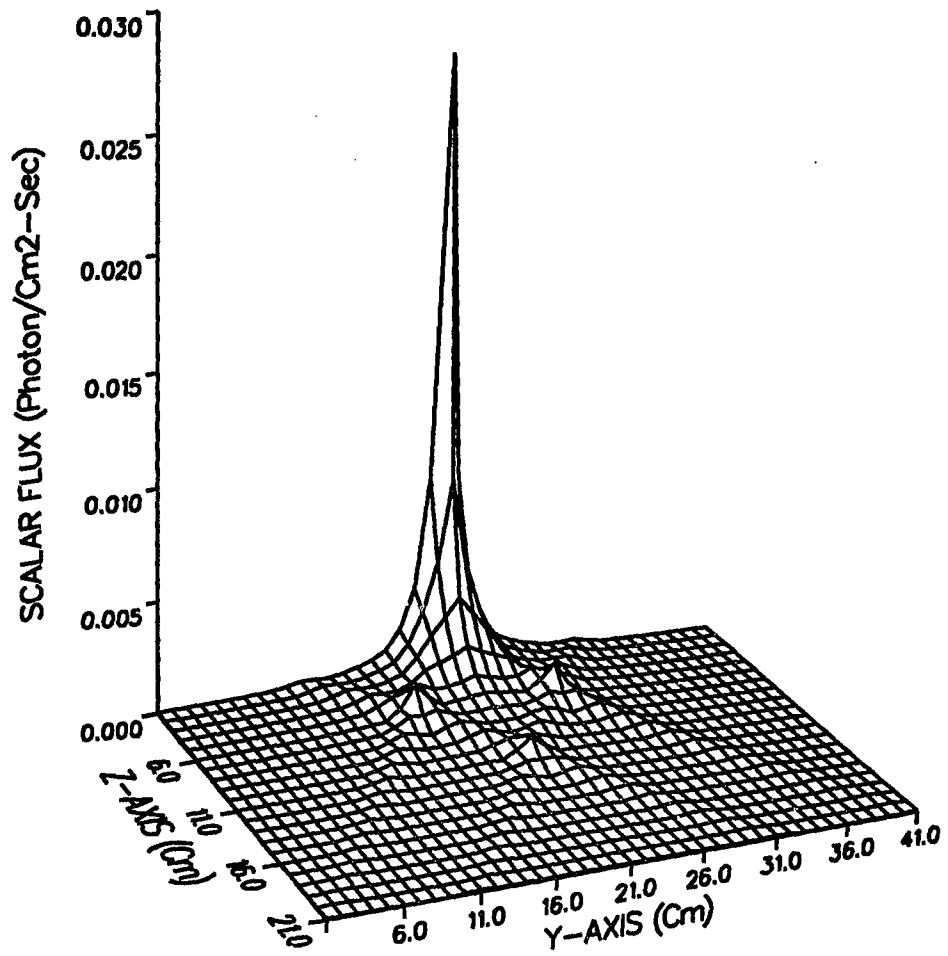


Figure 4.3.1c Flux distribution from SAP_2CS coupled with S_2 when "artificial multiplying" cells are present at the ripples

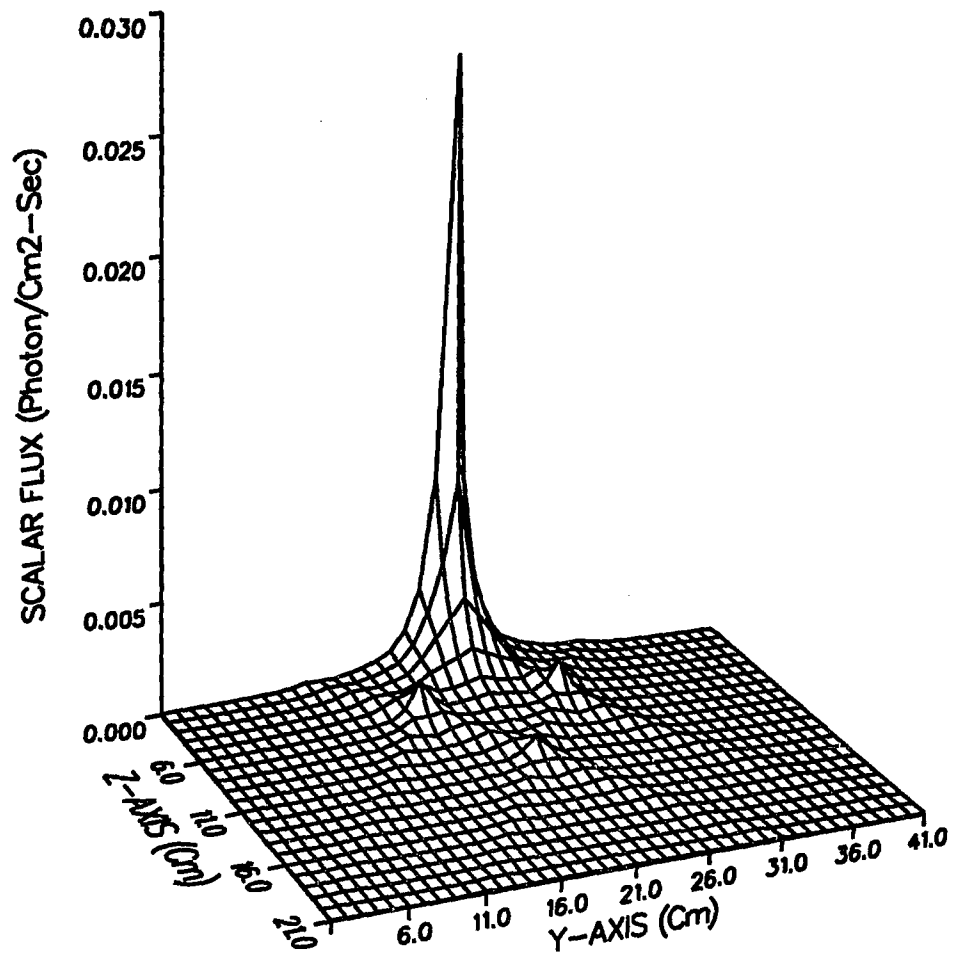


Figure 4.3.1d Flux distribution from SAP_3CS coupled with S_2 when "artificial multiplying" cells are present at the ripples

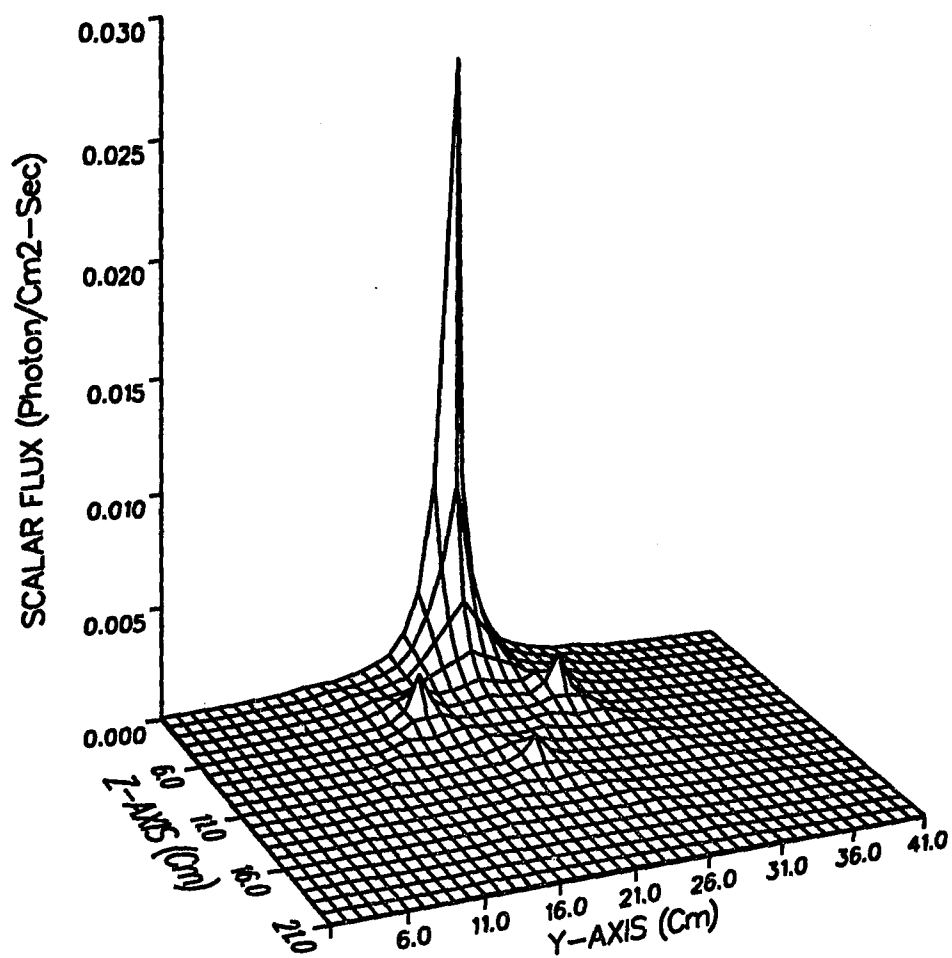


Figure 4.3.1e Flux distribution from SAP₄CS coupled with S₂ when "artificial multiplying" cells are present at the ripples

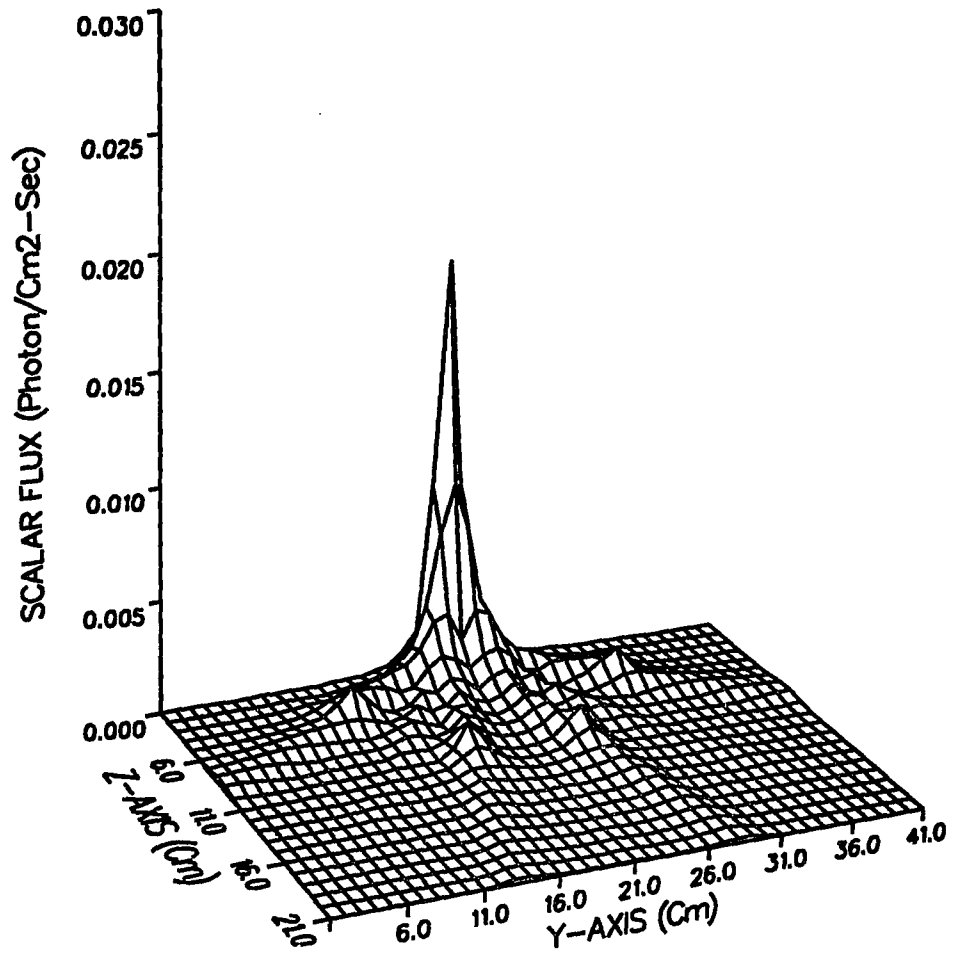


Figure 4.3.2a Flux distribution from S_4 when "artificial multiplying" cells are present at the ripples

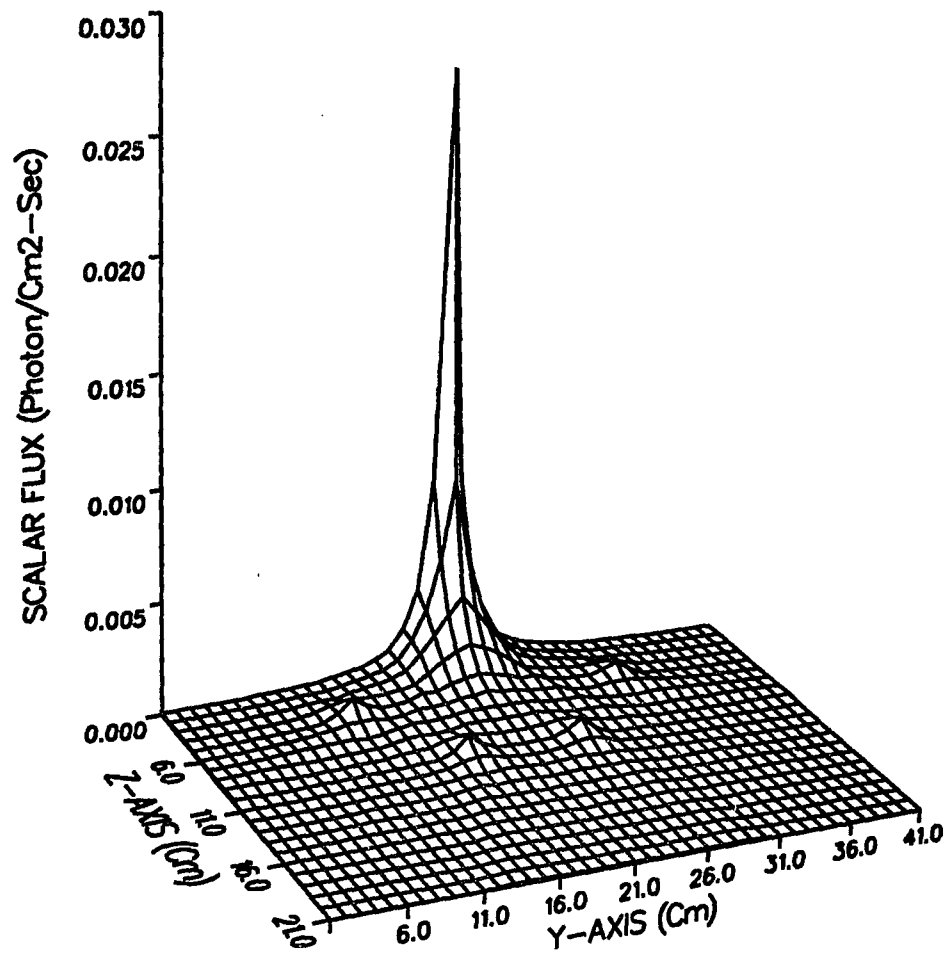


Figure 4.3.2b Flux distribution from SAP_1CS coupled with S_4 when "artificial multiplying" cells are present at the ripples

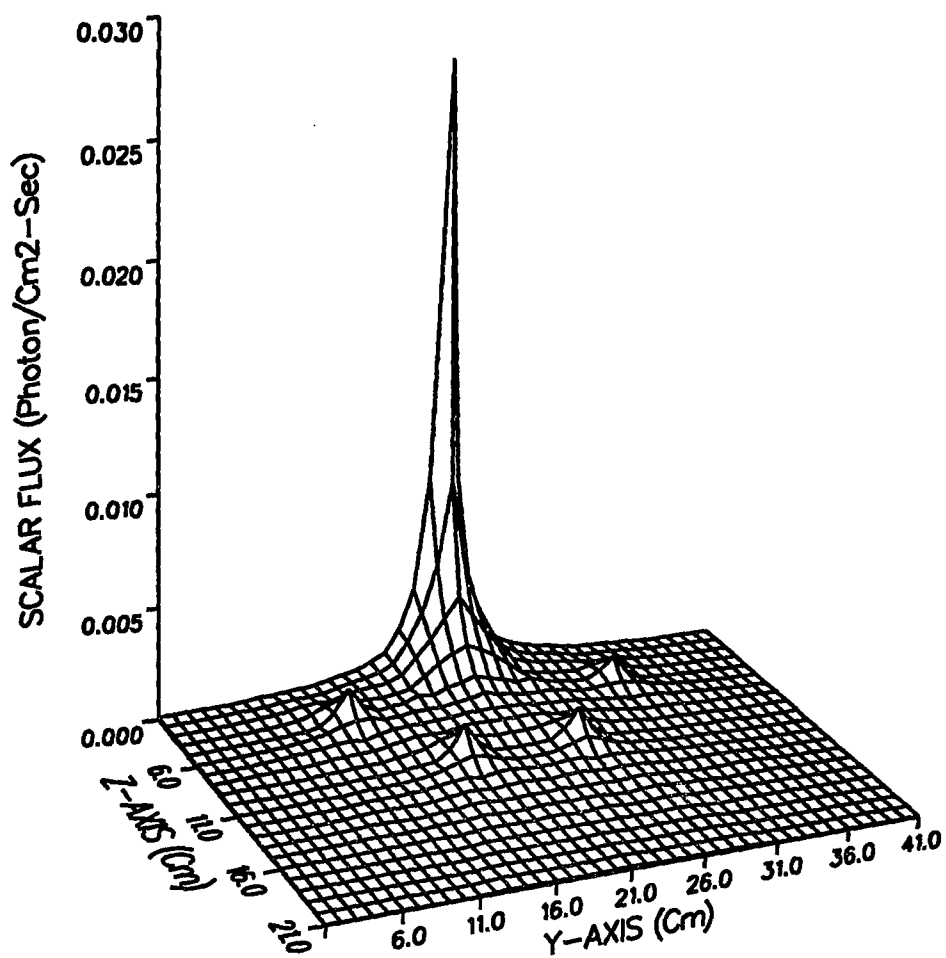


Figure 4.3.2c Flux distribution from SAP₂CS coupled with S₄ when "artificial multiplying" cells are present at the ripples

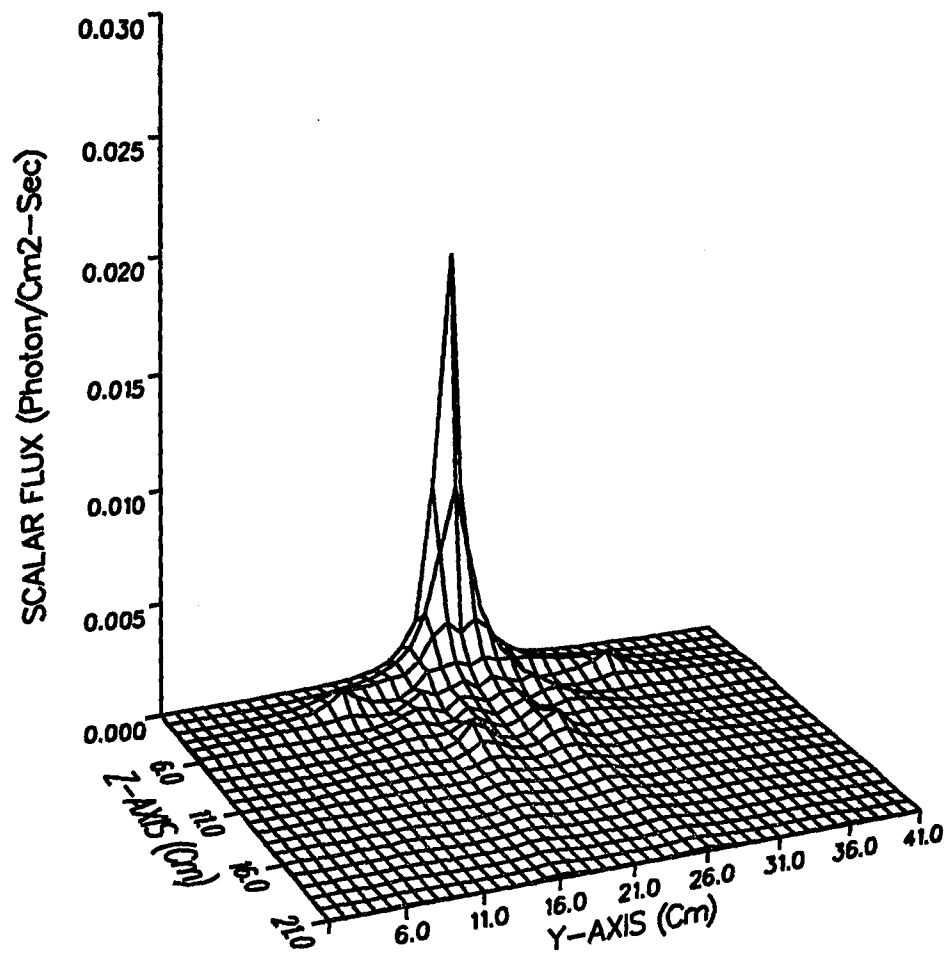


Figure 4.3.3a Flux distribution from S_8 when "artificial multiplying" cells are present at the ripples

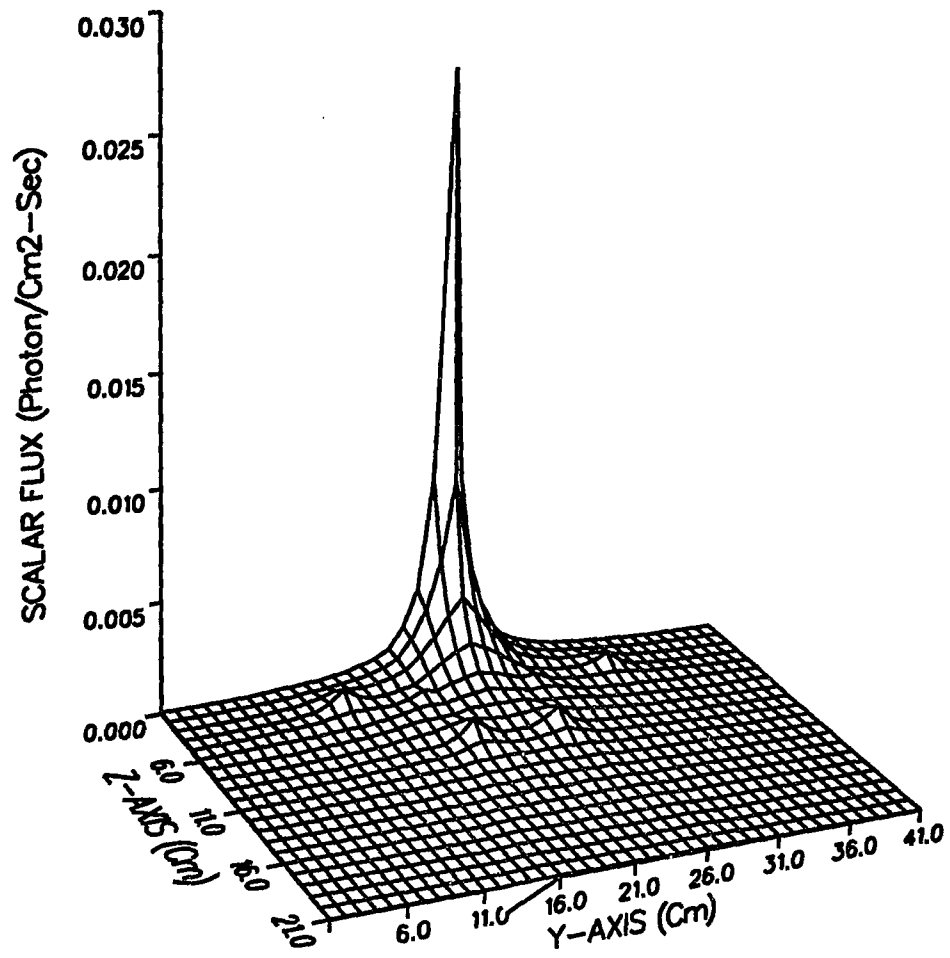


Figure 4.3.3b Flux distribution from SAP₁CS coupled with S₈ when "artificial multiplying" cells are present at the ripples

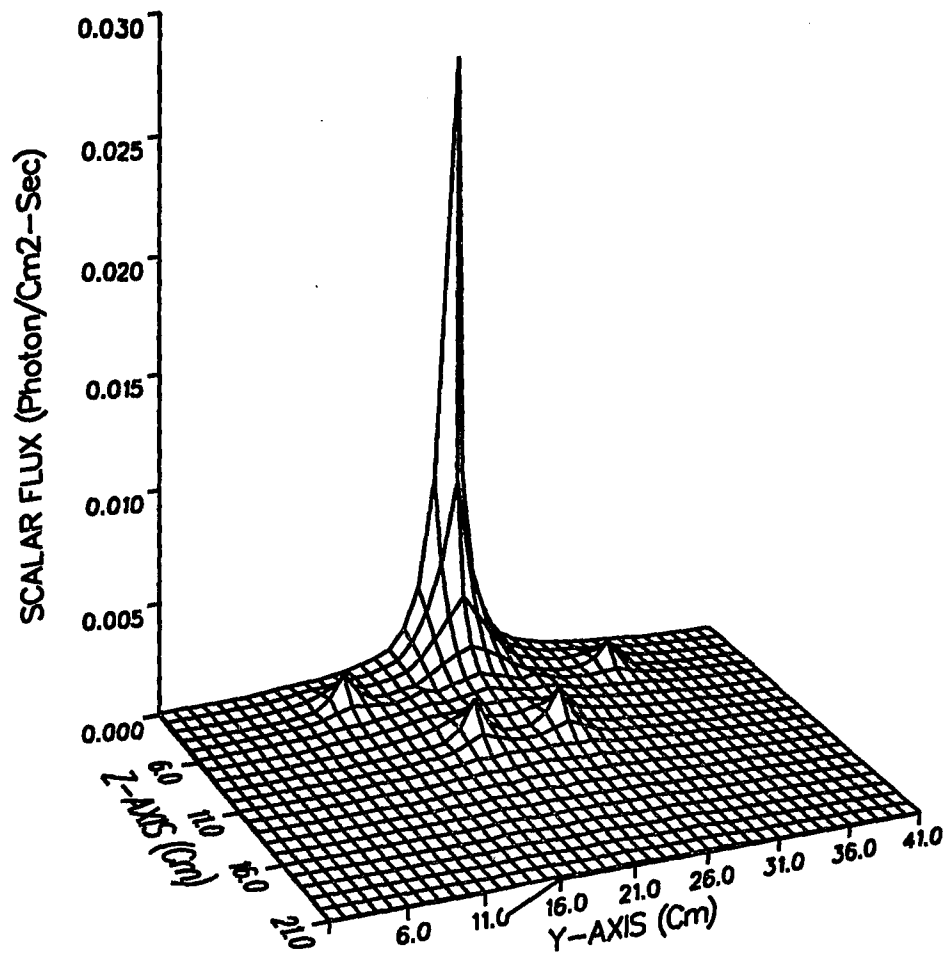


Figure 4.3.3c Flux distribution from SAP₂CS coupled with S₈ when "artificial multiplying" cells are present at the ripples

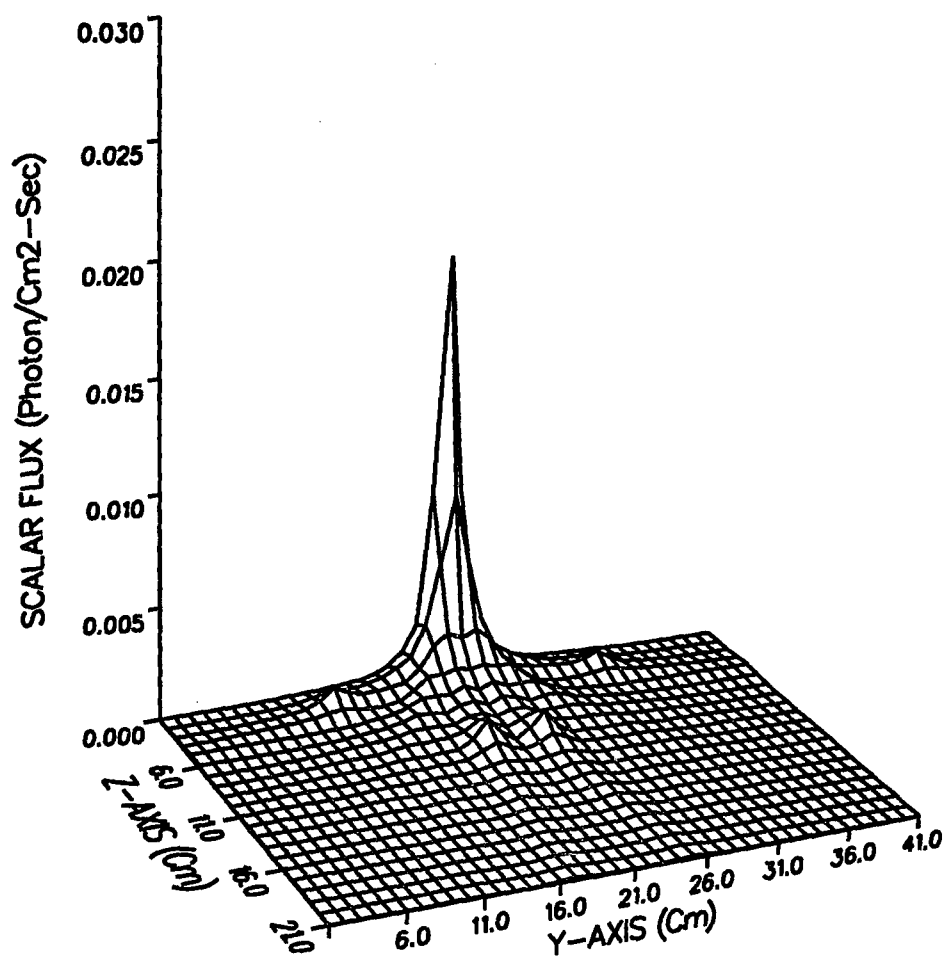


Figure 4.3.4a Flux distribution from S_{12} when "artificial multiplying" cells are present at the ripples

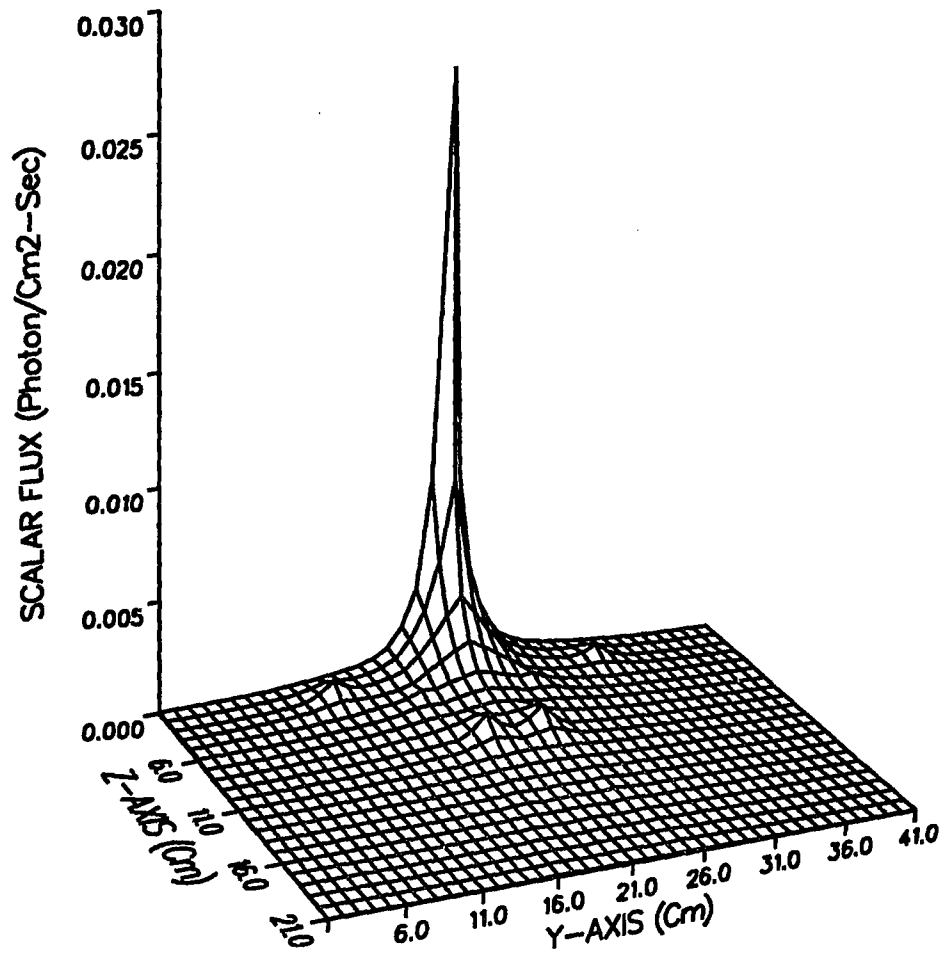


Figure 4.3.4b Flux distribution from SAP_1CS coupled with S_{12} when "artificial multiplying" cells are present at the ripples

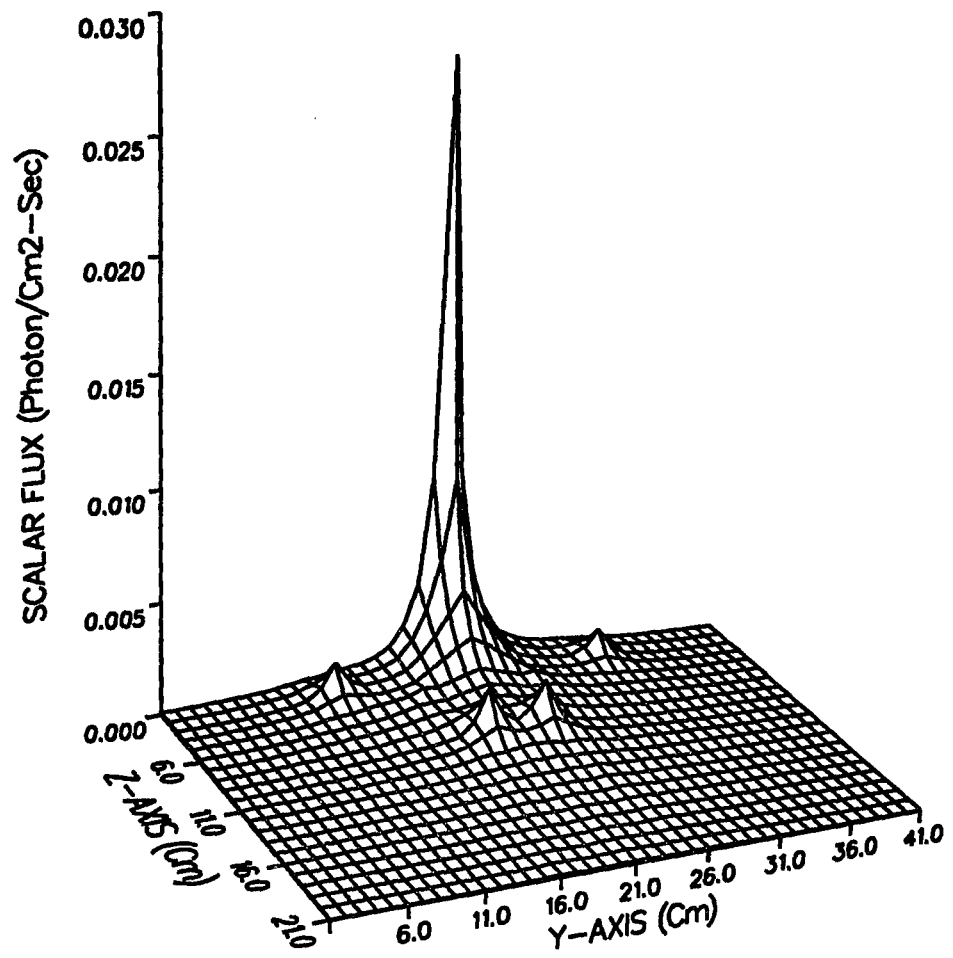


Figure 4.3.4c Flux distribution from SAP_2CS coupled with S_{12} when "artificial multiplying" cells are present at the ripples

4.4 Test Problem Three

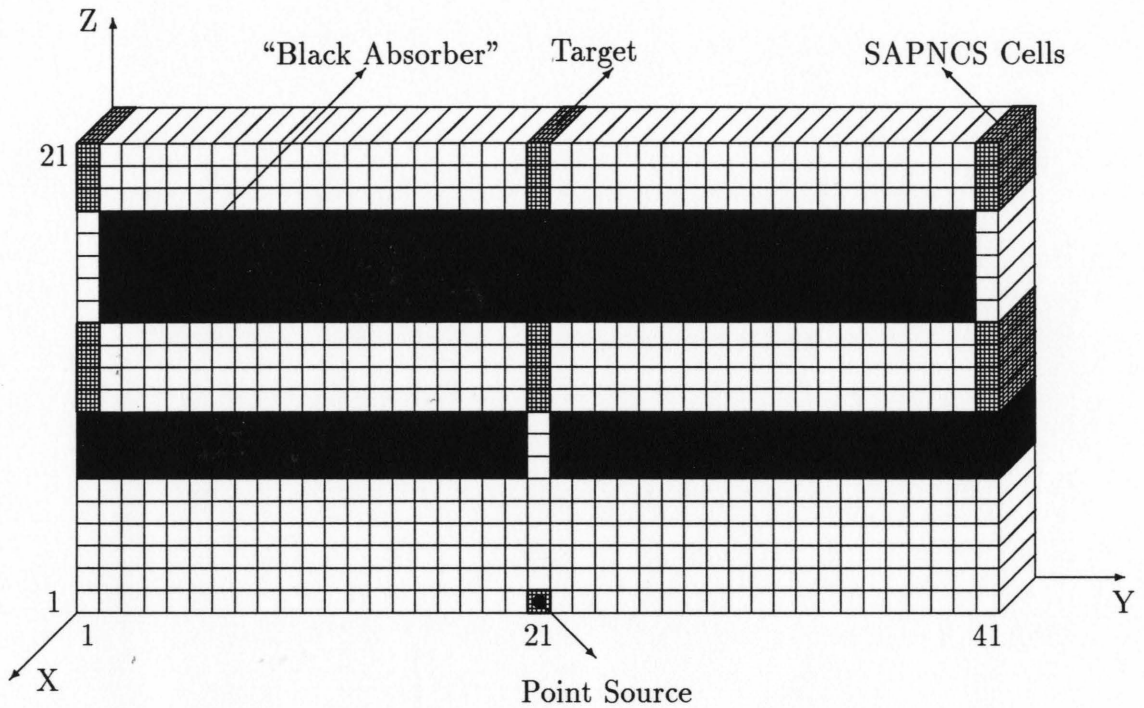


Figure 4.4 Geometric scheme for test problem three

4.4.1 Description of Problem

Figure 4.4 illustrates the geometric scheme for test problem three. The geometric scheme for test problem three involves “black absorber” cells, SAPNCS cells, target cells, and homogeneous mesh cells.

There are three blocks of “black absorber” cells. The “black absorber” cells are the darkest cells in Figure 4.4. The cells have very large absorption cross section. The macroscopic absorption cross section of the “black absorber” cells is one million cm^{-1} and the scattering cross section is zero. The first block of the “black absorber”

cells has x, y, and z coordinates which range from (1,1,7) to (1,20,9) where the first term in the bracket is the x coordinate, the second term is the y coordinate and the third term is the z coordinate. The second block of the “black absorber” cells ranges from (1,22,7) to (1,41,9). The third block is located higher on the z-axis with coordinates which range from (1,2,14) to (2,40,18).

In the geometric scheme for test problem three, there are six blocks of the SAPNCS cells present. The first block of the SAPNCS cells is located at cell (1,21,1) where the source is located. The second block of SAPNCS cells is placed at the center of the y-axis and extends from (1,21,10) to (1,21,13). The third and fourth blocks of SAPNCS cells are located at the first and the last cells along the y-axis and form set one. Block three extends from (1,1,10) to (1,1,13). The fourth extends from (1,41,10) to (1,41,13). The fifth and sixth blocks of SAPNCS cells are also located at the first and the last cells along the y-axis. Their z-axis coordinates extend from 19 to 21. The fifth and sixth blocks also form a set (second set).

The target cells range from (1,21,19) to (1,21,21) and have the same cross sections as the SAPNCS cells. The homogeneous cells have a macroscopic total and scattering cross sections of 0.06 cm^{-1} and zero, respectively.

4.4.2 Objective

The objective of this test problem is to demonstrate the capability of the SAPNCS technique to solve a very hard transport problem, as compared to the conventional discrete ordinates (S_N) method. Three groups of tests have been conducted.

The first group of tests used S_N in which N ranges from two to sixteen. The second group applied S_2 coupled with SAPNCS and the last group adopted S_4 coupled with SAPNCS.

4.4.3 Discrete Ordinates (S_N) Method

This problem could not be solved easily by the ordinary discrete ordinates (S_N) method. Particles coming out from the source could not go directly to the target cells, since "black absorber" was present between the source and the target. All particles reaching the absorber cells will be absorbed. Only those particles which travelled around the absorbing blocks and remained within the geometric scheme reached the target cells. The ordinary discrete ordinates (S_N) method requires large N and many iterations.

4.4.4 SAPNCS Method

Some particles emanating from the source went directly into first block and second block of the SAPNCS cells. A small percentage of the particles which entered the first and second blocks of the SAPNCS cells will be scattered. As a result, the first and second blocks of the SAPNCS cells became first scattering sources. Some of the scattered particles which leave the second block of the SAPNCS cells reach block three and four of the SAPNCS cells and which leave the first block reach the second block only. The third and fourth blocks of the SAPNCS cells become secondary scattering sources for particles leaving these two SAPNCS blocks. Particles coming

out from the third block go to the fifth block, and outgoing particles from the fourth block go to the sixth block. The fifth and sixth blocks then became third scattering sources and spread out the scattered particles. Finally the particles coming out from the third scattering sources reached the target. Only a very small fraction of the total particles transmitted could reach the target.

4.4.5 Test Group One

A group of tests were conducted using S_2 , S_4 , S_8 , S_{12} , and S_{16} . The first test was performed using S_2 . The ray effects as result of the conventional S_N calculation were blocked by the “black absorber” as shown in Figure 4.4.1a. No particles could even pass through a channel located between the first and second “black absorber” blocks.

When S_4 was then applied, particles coming out from the source were able to reach the fifth and sixth blocks of SAPNCS cells as seen in Figure 4.4.1b. Yet they could not go further to the target.

When S_8 was used. the particles were barely able to go further to the target as shown at Figure 4.4.1c. Yet the number of particles reaching the target was very limited and was almost unnoticed.

A larger angular quadrature S_{12} was utilized and the particles were expected to reach the target. However, only a small fraction of particles was able to do so as illustrated in Figure 4.4.1d.

Finally, S_{16} was tested. A larger fraction of particles could reach the target as illustrated in Figure 4.4.1e.

4.4.6 Test Group Two

Two other groups of tests were conducted under the same conditions as above. The first group of tests used S_2 and SAPNCS with the number of collisions from one to five.

When SAP_1C was applied, particles coming out from the source only reached the first and second blocks of SAPNCS cells. No first scattering source was created. Distributed source was created in the cells below the first and second blocks of "black absorber", between the first and second blocks of "black absorber" and the second block of SAPNCS cells. When S_2 was used, the contribution of flux from S_2 was very limited. Total flux was also dominated by SAPNCS cells as shown in Figure 4.4.2a1.

SAP_2C was then applied and the first scattering sources were created at the first and second blocks of SAPNCS. This scattering sources contributed fluxes, included the fluxes along the paths between the first and third blocks of "black absorber" and between the second and third blocks of "black absorber". Therefore the particles were able to reach the third and fourth blocks of SAPNCS cells but they stopped there. The distributed source was created further up to the third and fourth blocks of SAPNCS cells. S_2 was then applied. The total flux was significant up to the third and fourth blocks of SAPNCS cells and was zero beyond those blocks as illustrated in Figure 4.4.2a2.

In order to get the particles go further, one higher step of SAPNCS, SAP₃CS, was used. The second scattering sources were also created at the third and fourth blocks of SAPNCS cells. The particles could go to the fifth and sixth blocks of SAPNCS cells. The distributed source was available up to the fifth and sixth blocks of SAPNCS cells. When S₂ was used, the total flux could not reach the target as shown in Figure 4.4.2a3.

Scattering sources were created at the fifth and sixth blocks of SAPNCS cells when SAP₄CS was used. Consequently, the scattering sources could release particles that have the ability to reach the target. The distributed source was created in the target cells. Finally, the cells which have the same z coordinate as the target were fully occupied by particles as illustrated in Figure 4.4.2a4.

When one higher step of SAPNCS, SAP₅CS, was taken, the result was no different from the previous test as seen in Figure 4.4.2a5. The use of SAP₅CS was unnecessary. The convergence in this problem was obtained by SAP₄CS.

4.4.7 Test Group Three

The second group of tests was using S₄ and SAPNCS with the number of collisions from one to five.

First, SAP₁CS combined with S₄ was used. At large z-axis, the flux from S₄ was greater than the flux from S₂. This combination was able to spread the particles out to the fifth and sixth blocks of SAPNCS and a little farther beyond that areas. Yet those particles could not reach the target as shown in Figure 4.4.3a1.

One higher step for SAPNCS, SAP₂CS, was applied. This SAP₂CS could provide distributed sources for S₄ up to the third blocks of SAPNCS cells. The S₄ had the ability to spread a small fraction of particles out to the target as shown in Figure 4.4.3a2. The fraction of particles that reached the target was so small that it was almost unnoticed.

SAP₃CS was then used. The distributed source was available one block farther up to the fourth and fifth blocks of SAPNCS. From those areas the S₄ was capable of distributing the particles to the target as demonstrated in Figure 4.4.3a3.

When the SAP₄CS combined with S₄ was used, the result was quite the same as the result obtained from the SAP₃CS combined with S₄ as demonstrated in Figures 4.4.3a4 and 4.5.3a5. Additional collisions higher than three did not give any different result. Therefore, the SAP₃CS combined with S₄ provided an adequate result for this problem.

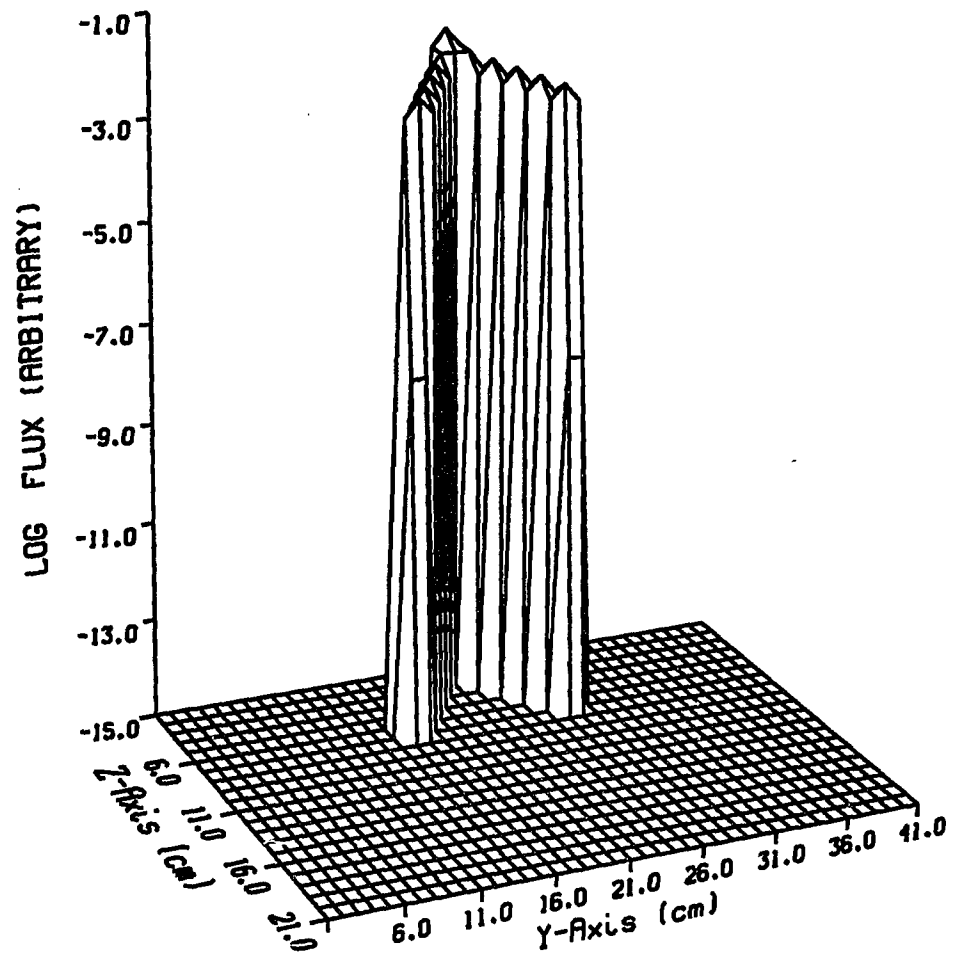


Figure 4.4.1a Flux distribution from S_2 for a very hard transport problem.

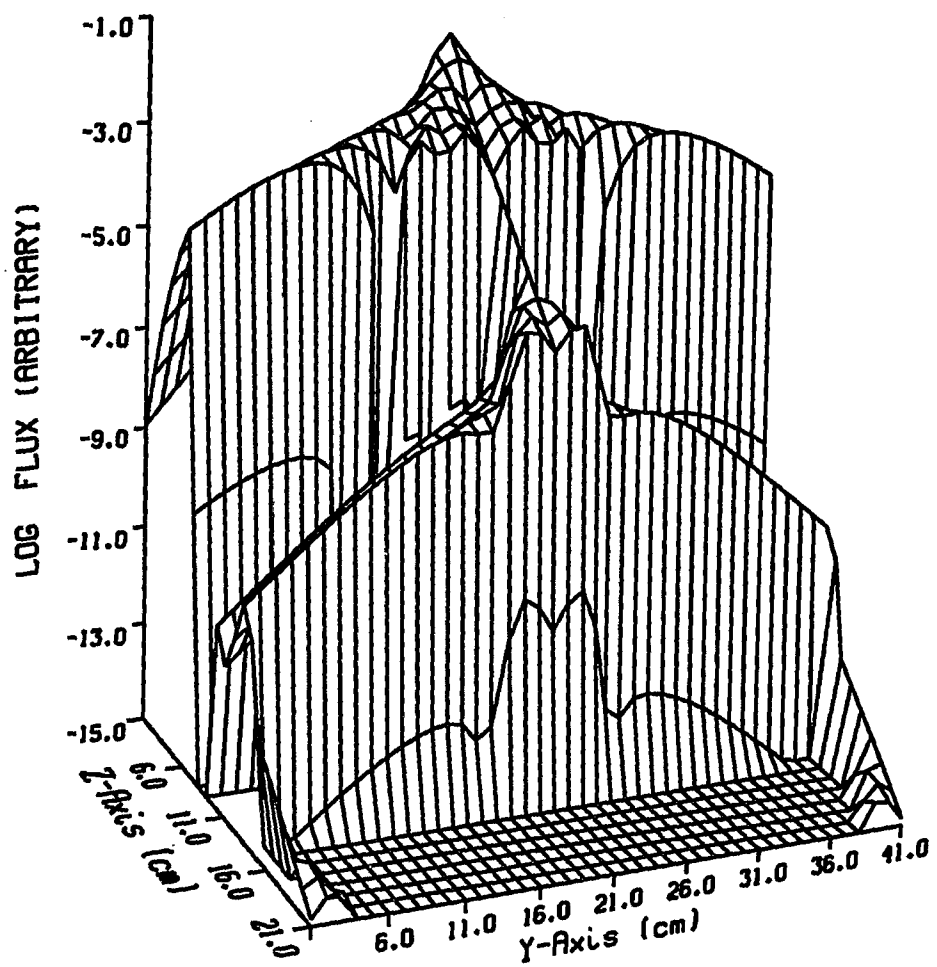


Figure 4.4.1b Flux distribution from S_4 for a very hard transport problem.

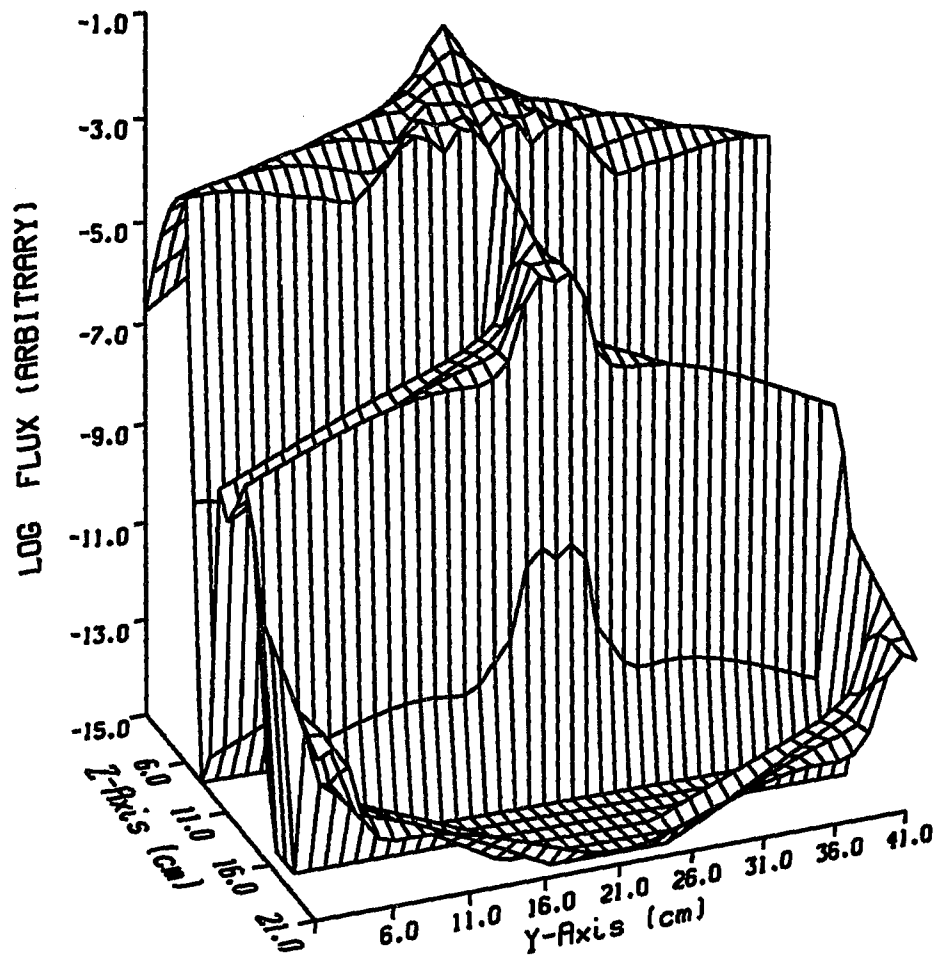


Figure 4.4.1c Flux distribution from S_8 for a very hard transport problem.

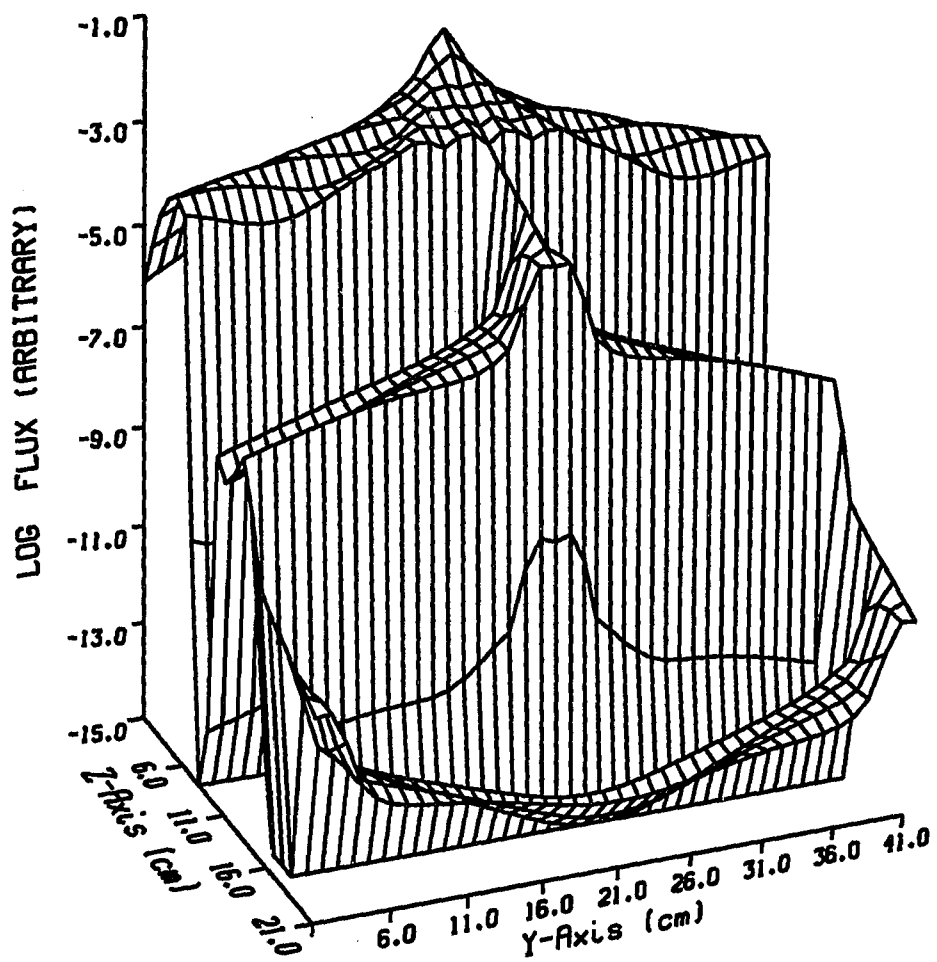


Figure 4.4.1d Flux distribution from S_{12} for a very hard transport problem.

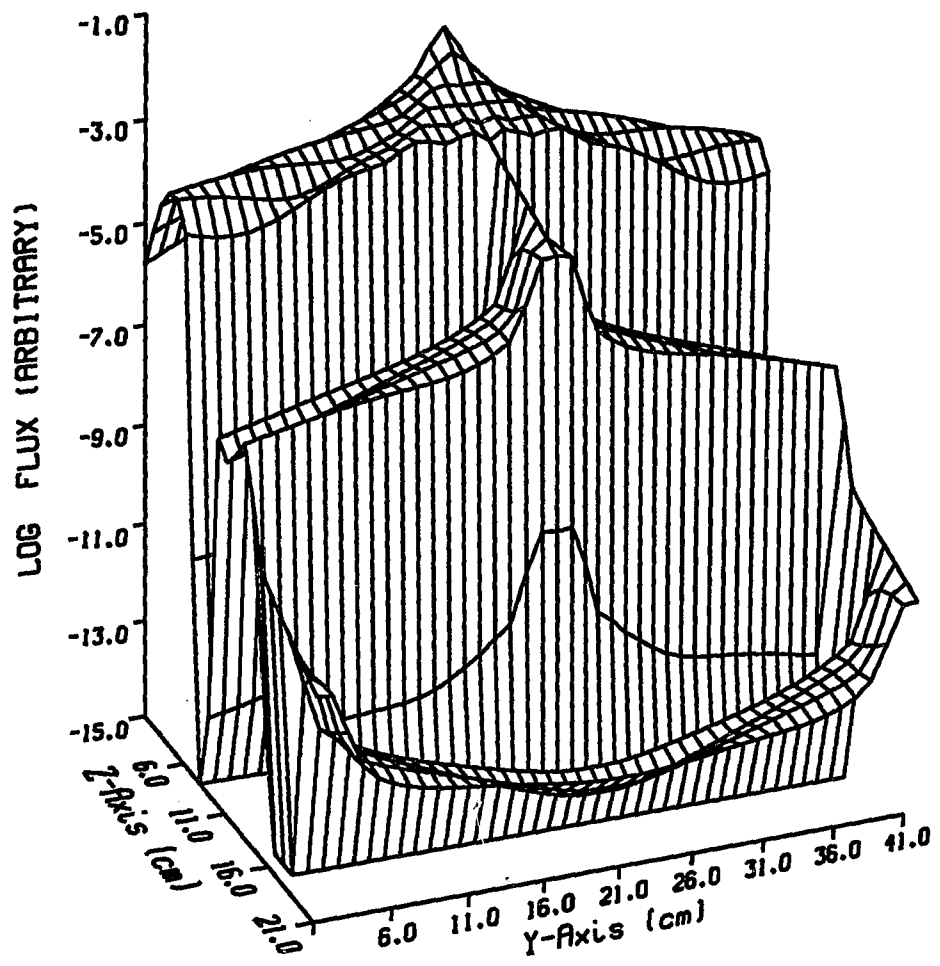


Figure 4.4.1e Flux distribution from S_{16} for a very hard transport problem.

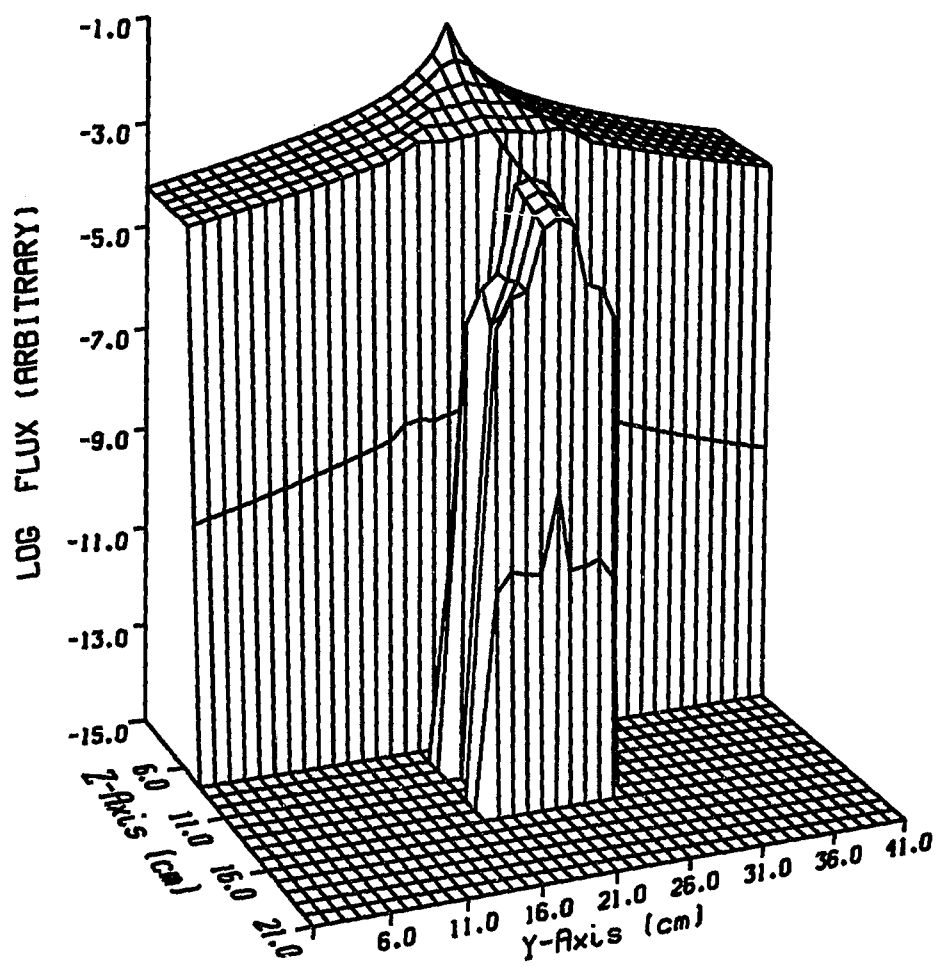


Figure 4.4.2a1 Flux distribution from SAP_1CS coupled with S_2 for a very hard transport problem.

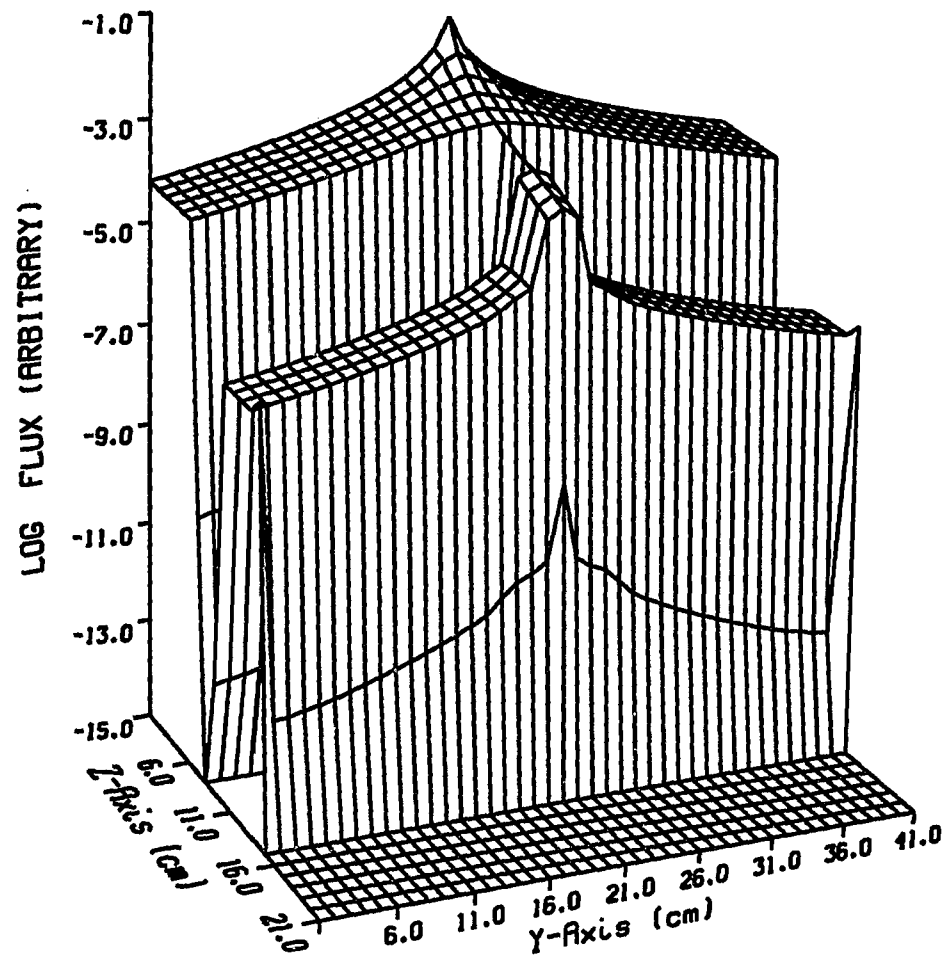


Figure 4.4.2a2 Flux distribution from SAP₂CS coupled with S₂ for a very hard transport problem.

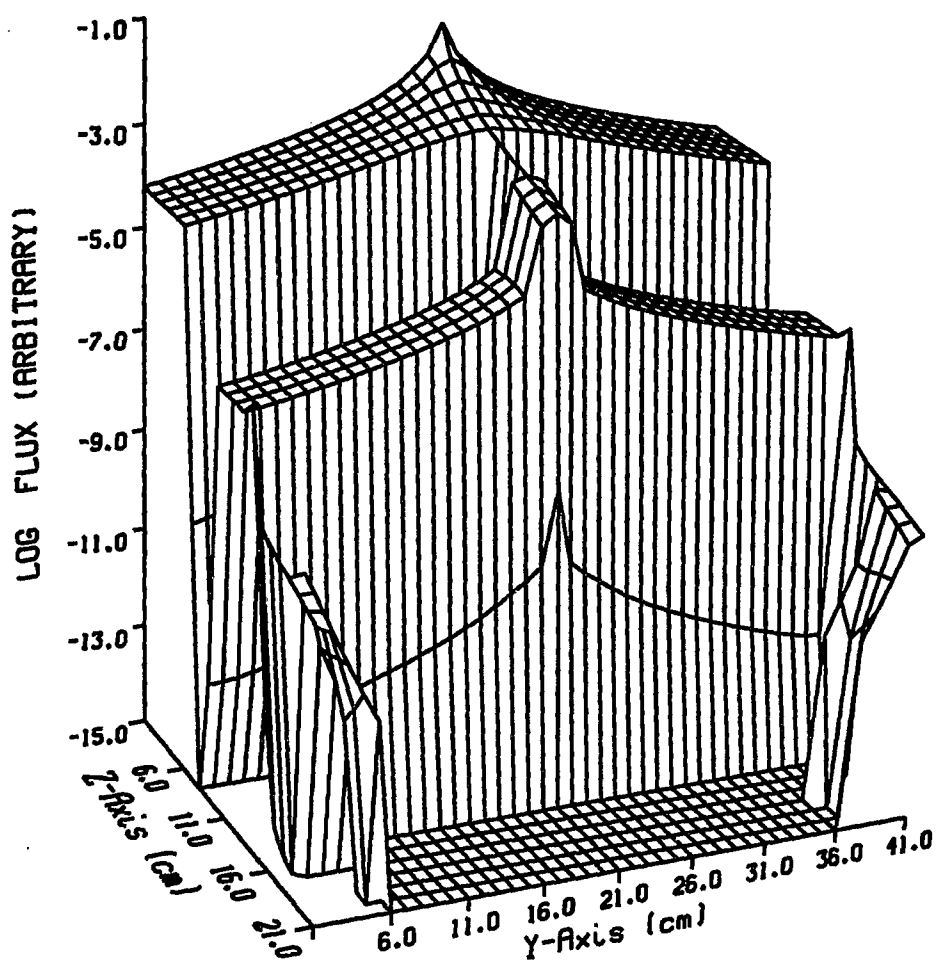


Figure 4.4.2a3 Flux distribution from SAP₃CS coupled with S₂ for a very hard transport problem.

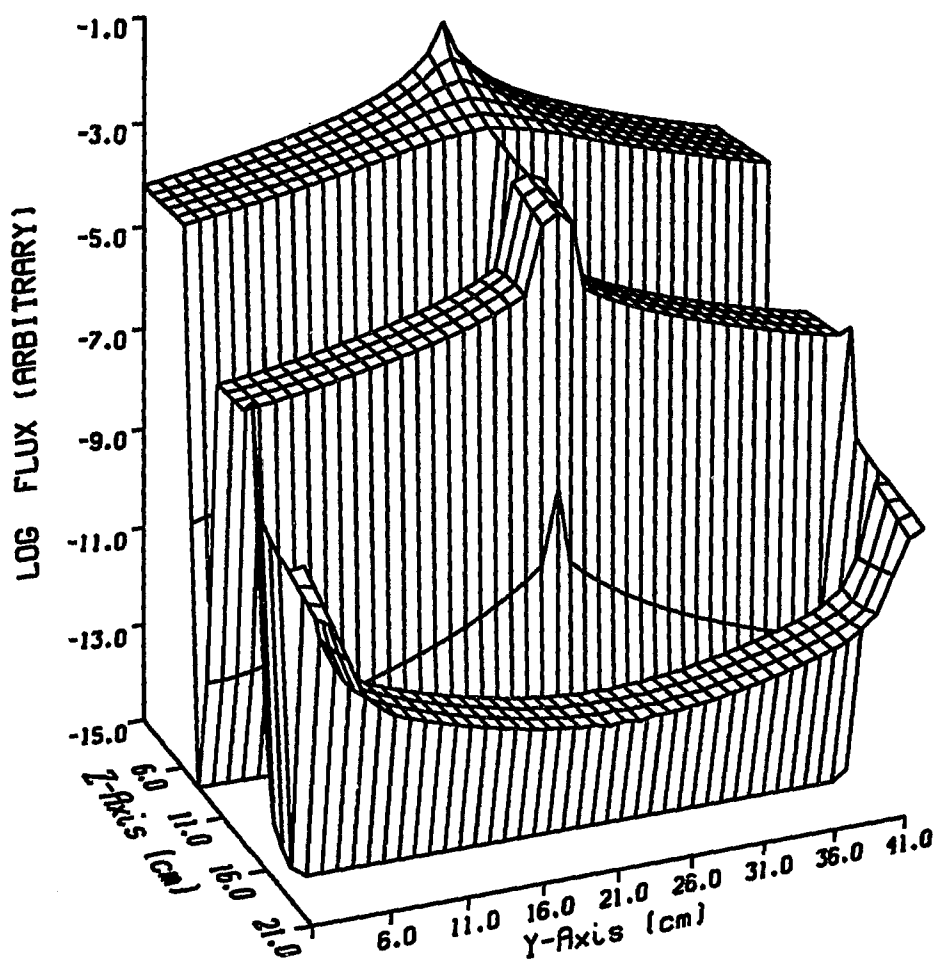


Figure 4.4.2a4 Flux distribution from SAP₄CS coupled with S₂ for a very hard transport problem.

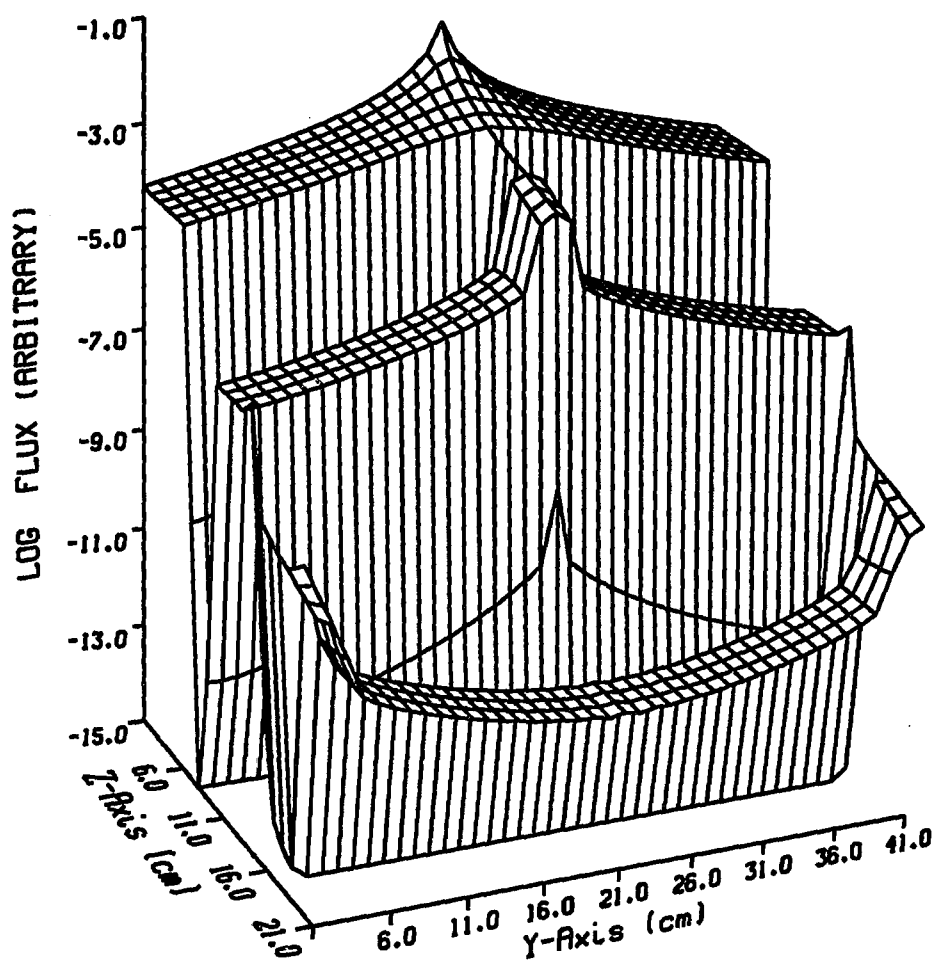


Figure 4.4.2a5 Flux distribution from SAP_5CS coupled with S_2 for a very hard transport problem.

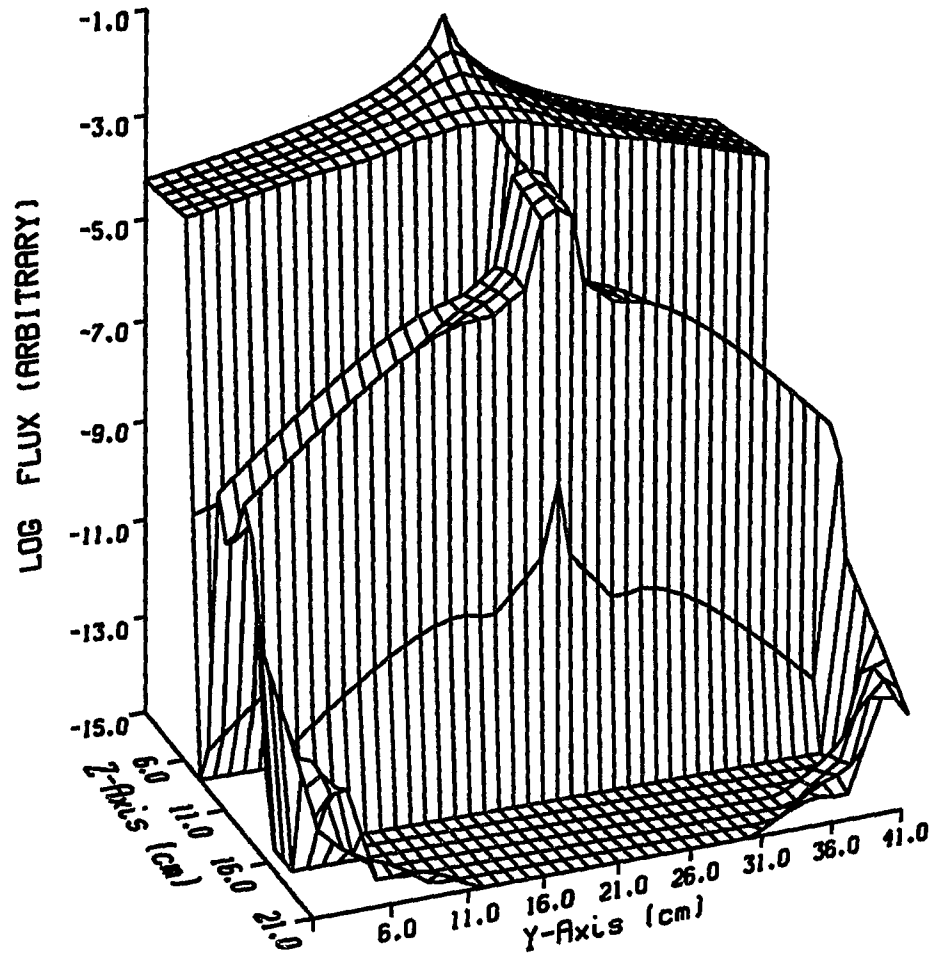


Figure 4.4.3a1 Flux distribution from SAP₁CS coupled with S₄ for a very hard transport problem.

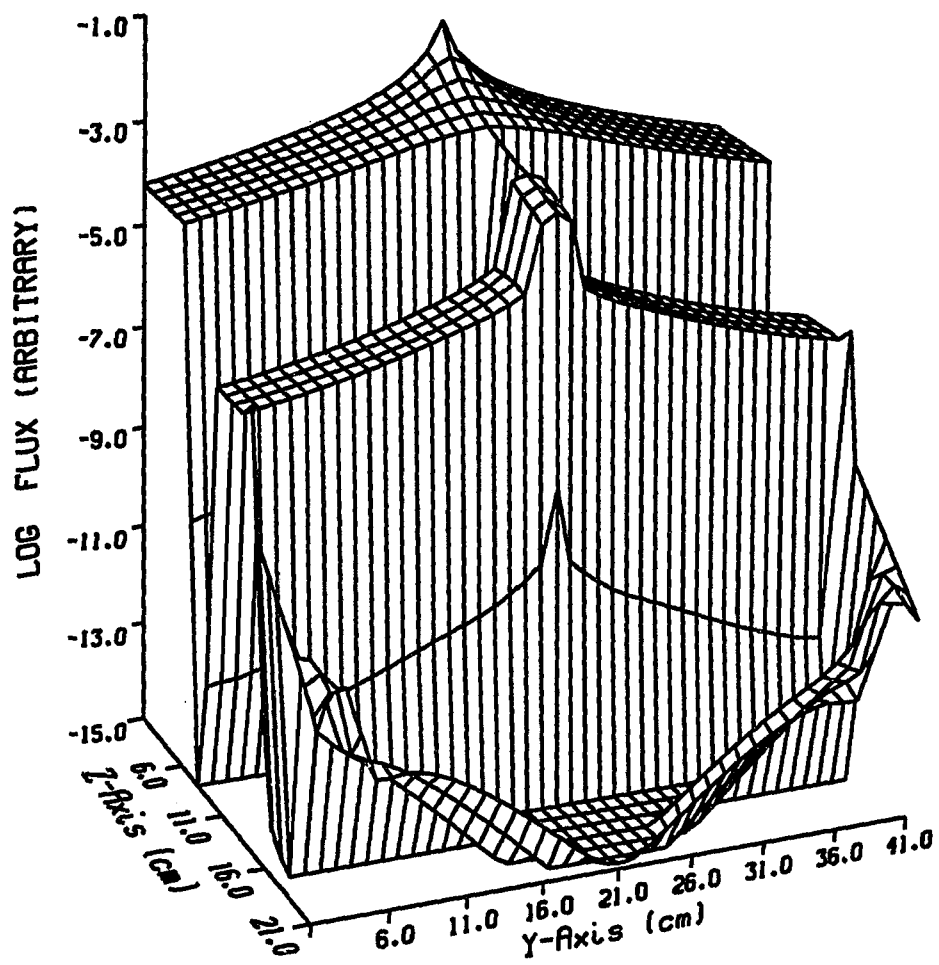


Figure 4.4.3a2 Flux distribution from SAP_2CS coupled with S_4 for a very hard transport problem.

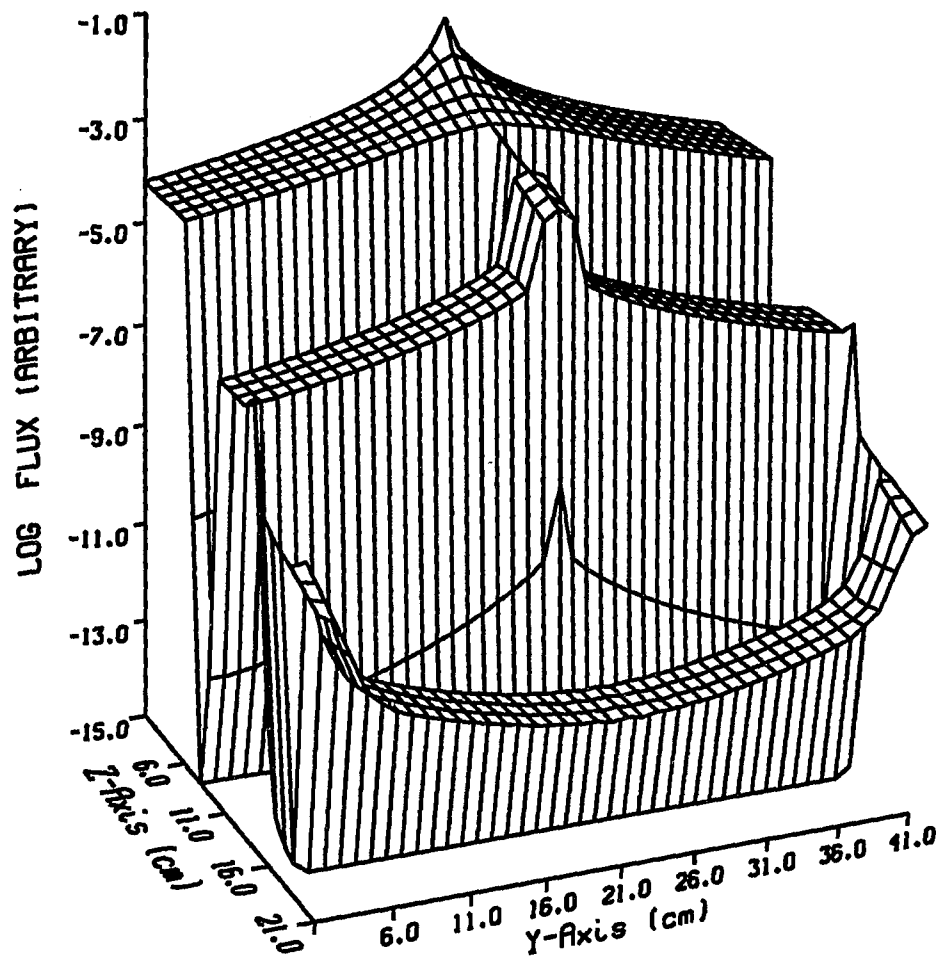


Figure 4.4.3a3 Flux distribution from SAP_3CS coupled with S_4 for a very hard transport problem.

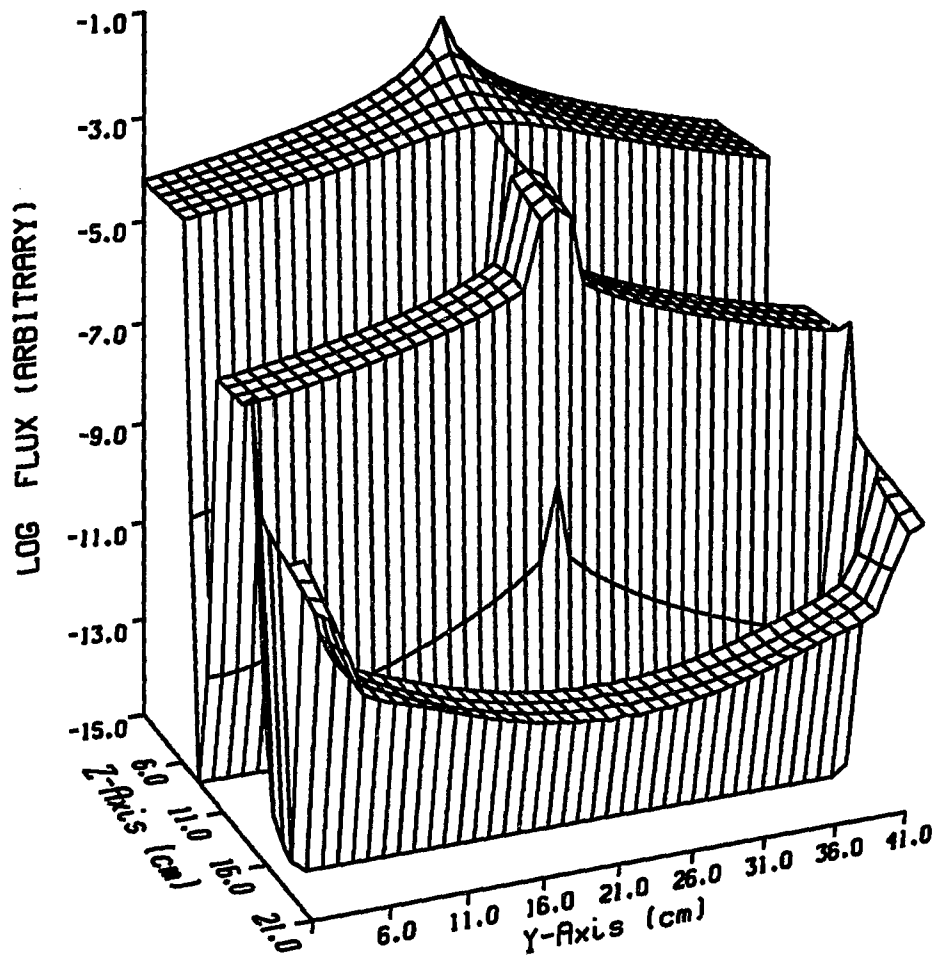


Figure 4.4.3a4 Flux distribution from SAP_4CS coupled with S_4 for a very hard transport problem.

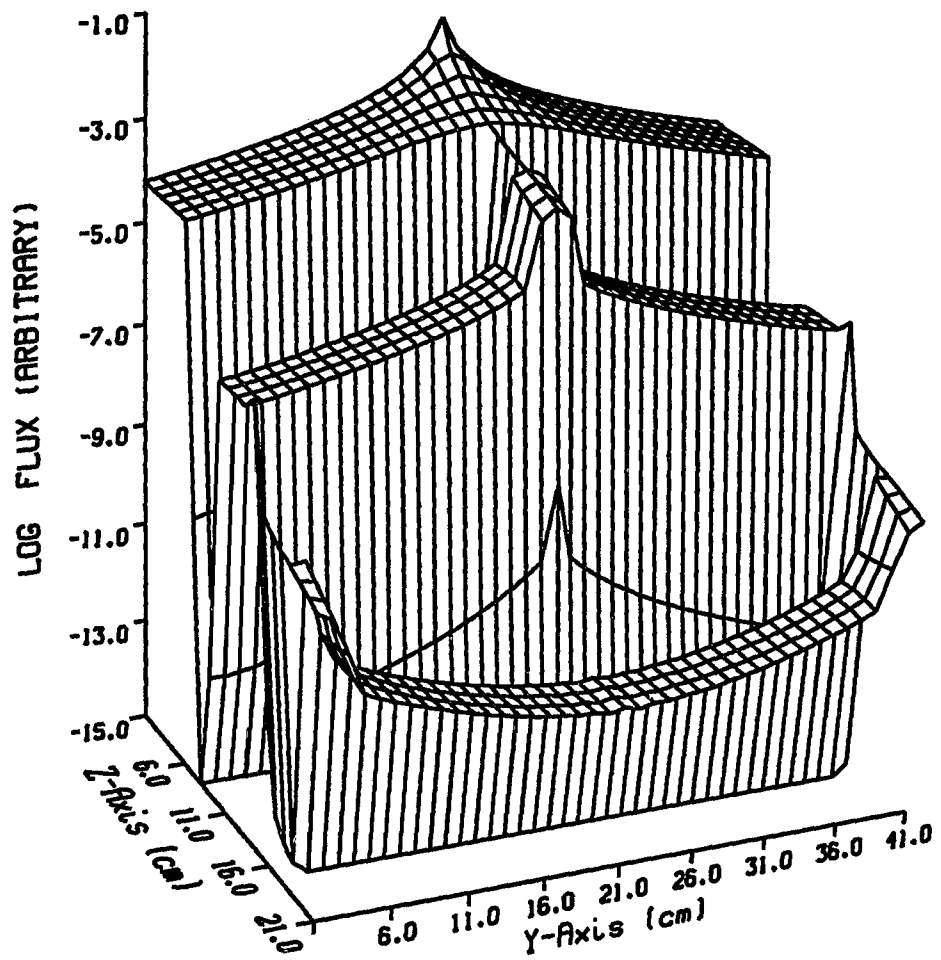


Figure 4.4.3a5 Flux distribution from SAP_5CS coupled with S_4 for a very hard transport problem.

4.5 Test Problem Four

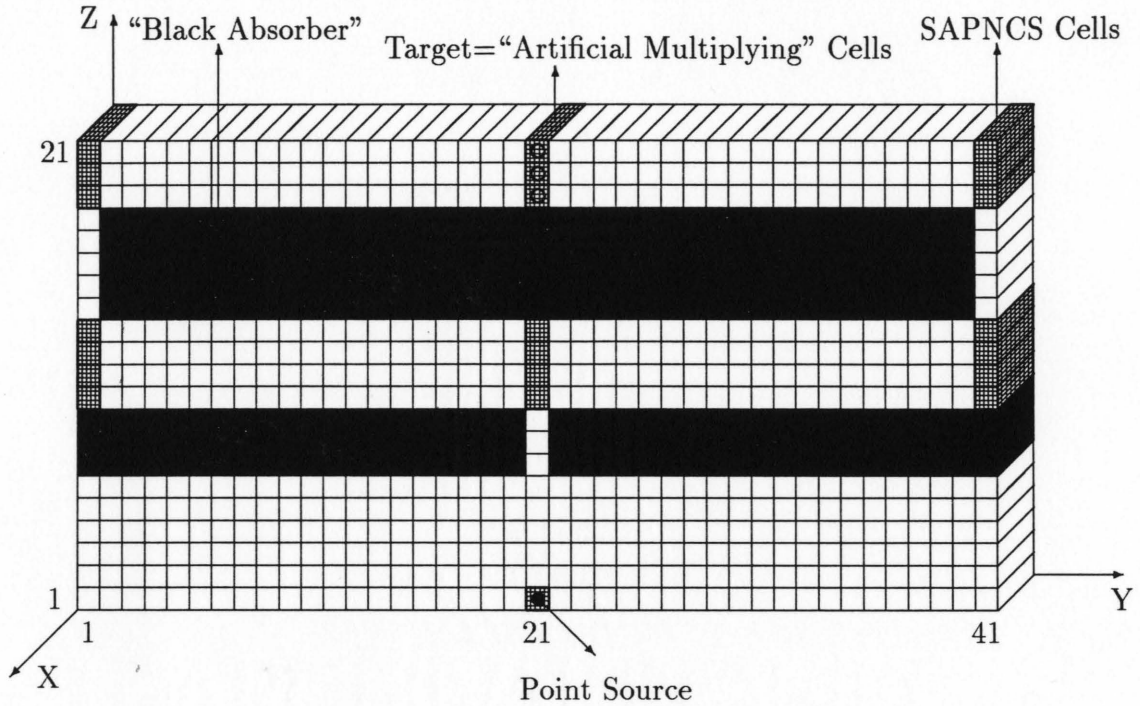


Figure 4.5 Geometric scheme for test problem four

4.5.1 Description of Problem

The geometric scheme for test four is primarily based on the geometric scheme for test three with the exception of the target cells. “Artificial multiplying” material that has a macroscopic scattering cross section thirteen time larger than SAPNCS scattering cross section was inserted into those cells.

4.5.2 Objective

The main objective of this test problem is to demonstrate the effect of the presence of “artificial multiplying” material on the target cells to the flux distribution.

Three groups of tests were conducted. The first group used the S_N method for angular quadratures of 8, 12, and 16. The second group applied S_2 combined with SAP_4CS and SAP_5CS . The last group was performed by using S_4 combined with SAP_3CS and SAP_4CS .

4.5.3 Test Group One

The first group began with S_8 . The S_8 was able to deliver a small fraction of particles to the target. The particles then initiated a scattering process in the target that eventually became a scattering source. Consequently, flux in the target cell was slightly higher than in the surrounding area as shown in Figure 4.5.1a. When we compare Figures 4.5.1a and 4.5.1c, there was almost no effect for the flux in surrounding cells by putting “artificial multiplying” material in the target cells for this test.

When S_{12} was applied, the effect of “artificial multiplying” material was noticeable as shown in Figure 4.5.1b. The fraction of particles reaching the target was big so that the scattering source was also more powerful. Consequently, the scattering source was able to distribute flux in the surrounding area. In fact, the flux in the surrounding area was larger than the flux without the “artificial multiplying” material.

When S_{16} was used, the number of particles coming to the target was much bigger and the scattering source was also much stronger as illustrated in Figure 4.5.1c. Therefore the effect for the surrounding area was very significant.

4.5.4 Test Group Two

The combination of S_2 and SAP_4CS started the test for the second group. Flux in the target and surrounding area was slightly higher than the flux obtained without “artificial multiplying” material inside the target cells as shown in Figure 4.5.2b for S_2 and SAP_4CS . Compared to the result of S_{16} as seen in Figure 4.5.1c, the flux in the target or surrounding area was slightly higher too.

SAP_5CS combined with S_2 was then used. The flux in the target and surrounding cells was much higher than the flux obtained from S_{16} or the combination of S_2 and SAP_4CS as demonstrated in Figure 4.5.2c.

4.5.5 Test Group Three

When S_4 combined with SAP_3CS was used, the effect of using “artificial multiplying” material in the target cells was noticeable as demonstrated in Figure 4.5.3a. The flux inside the target or at surrounding cells was very much higher than the flux obtained from the same combination but without “artificial multiplying” material inside the target cells.

S_4 combined with SAP_4CS was then used. The flux inside the target and surrounding cells was slightly higher than the flux obtained from S_{16} or the combination of S_4 and SAP_3CS as demonstrated in Figure 4.5.3b.

When SAP_5CS combined with S_4 was used, the flux in the target and surrounding cells was very much higher than the flux obtained from S_{16} . It was also slightly higher than the flux obtained from the combination of S_2 and SAP_5CS .

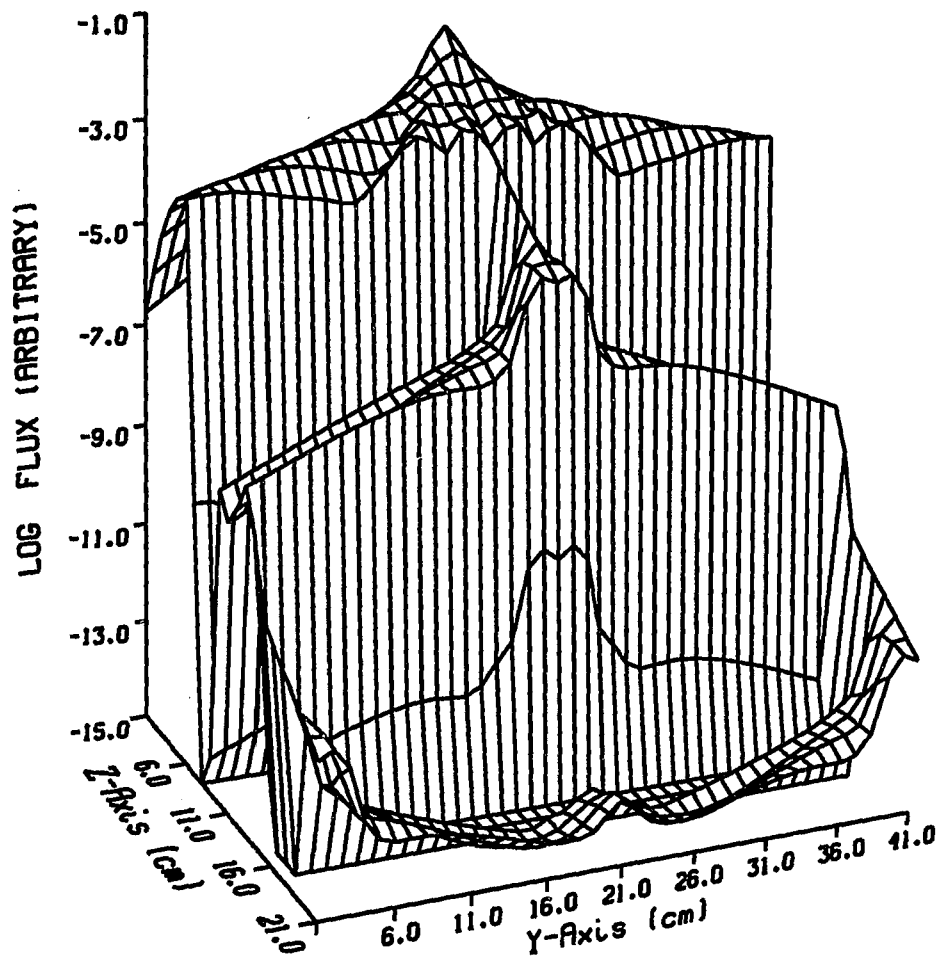


Figure 4.5.1a Flux Distribution from S_8 for a very hard transport problem with "artificial multiplying" material in target cells.

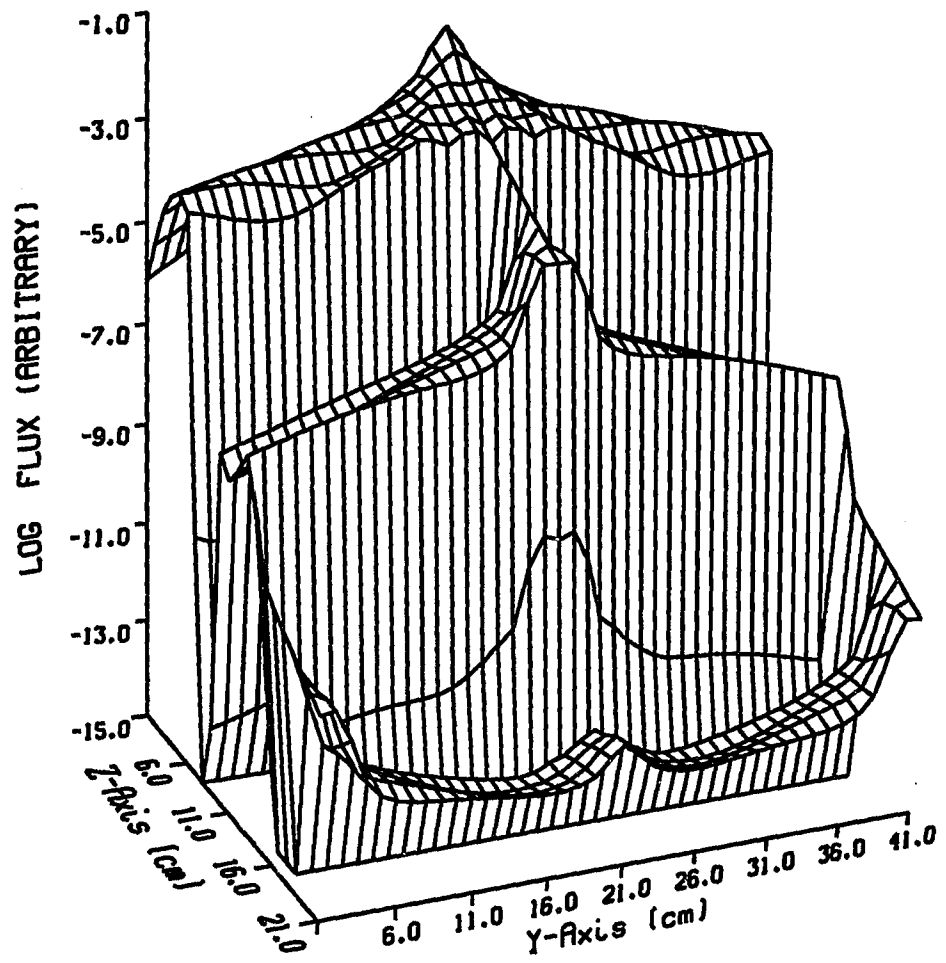


Figure 4.5.1b Flux Distribution from S_{12} for a very hard transport problem with "artificial multiplying" material in target cells.

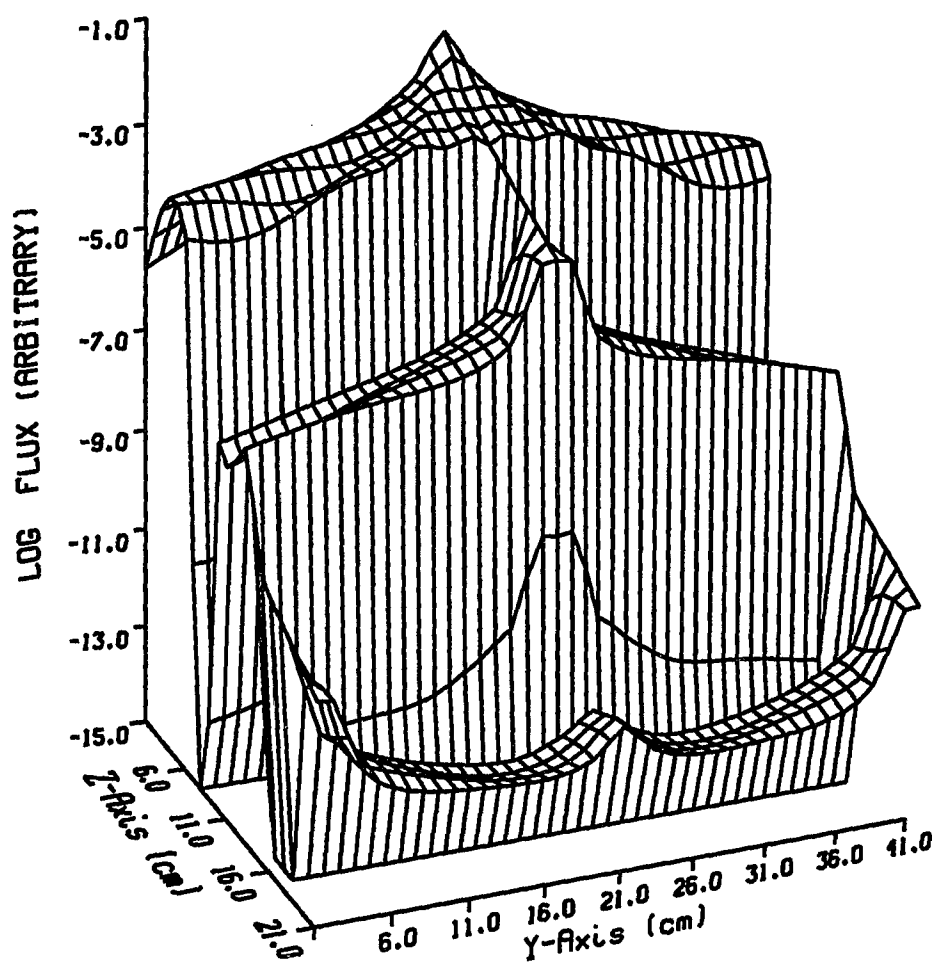


Figure 4.5.1c Flux Distribution from S_{16} for a very hard transport problem with "artificial multiplying" material in target cells.

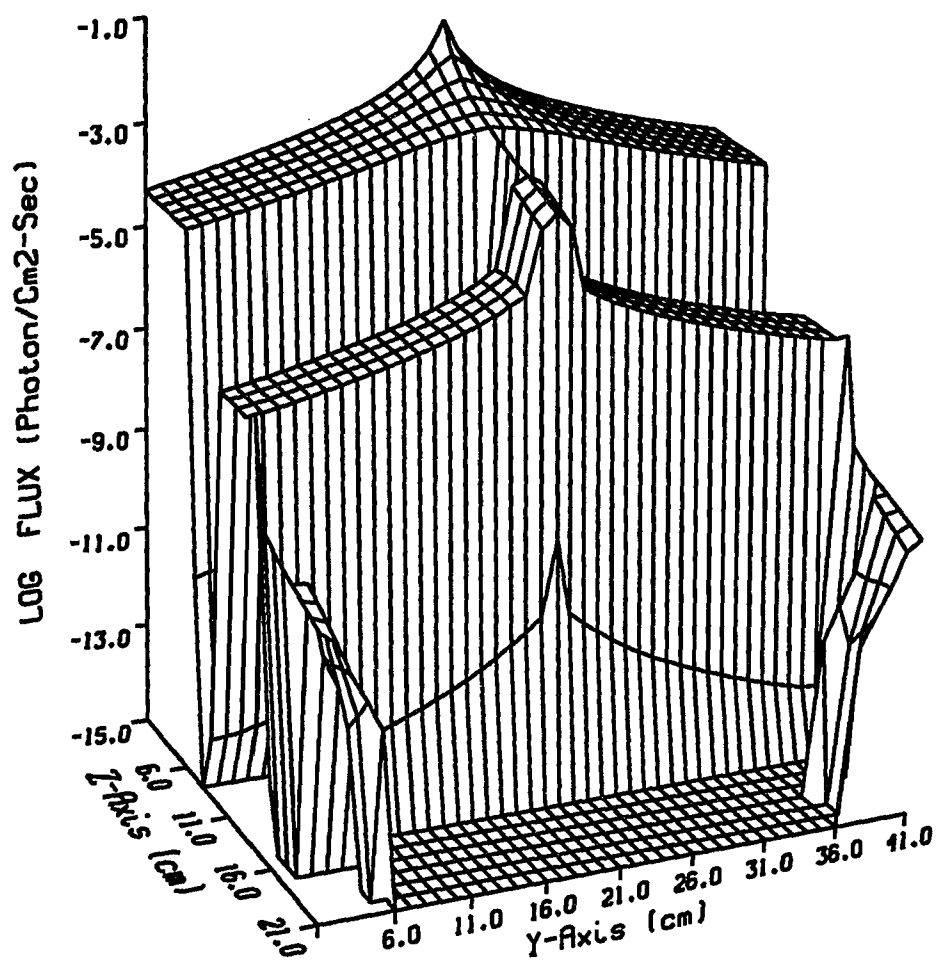


Figure 4.5.2a Flux Distribution from SAP_3CS coupled with S_2 for a very hard transport problem, with “artificial multiplying” material in target cells.

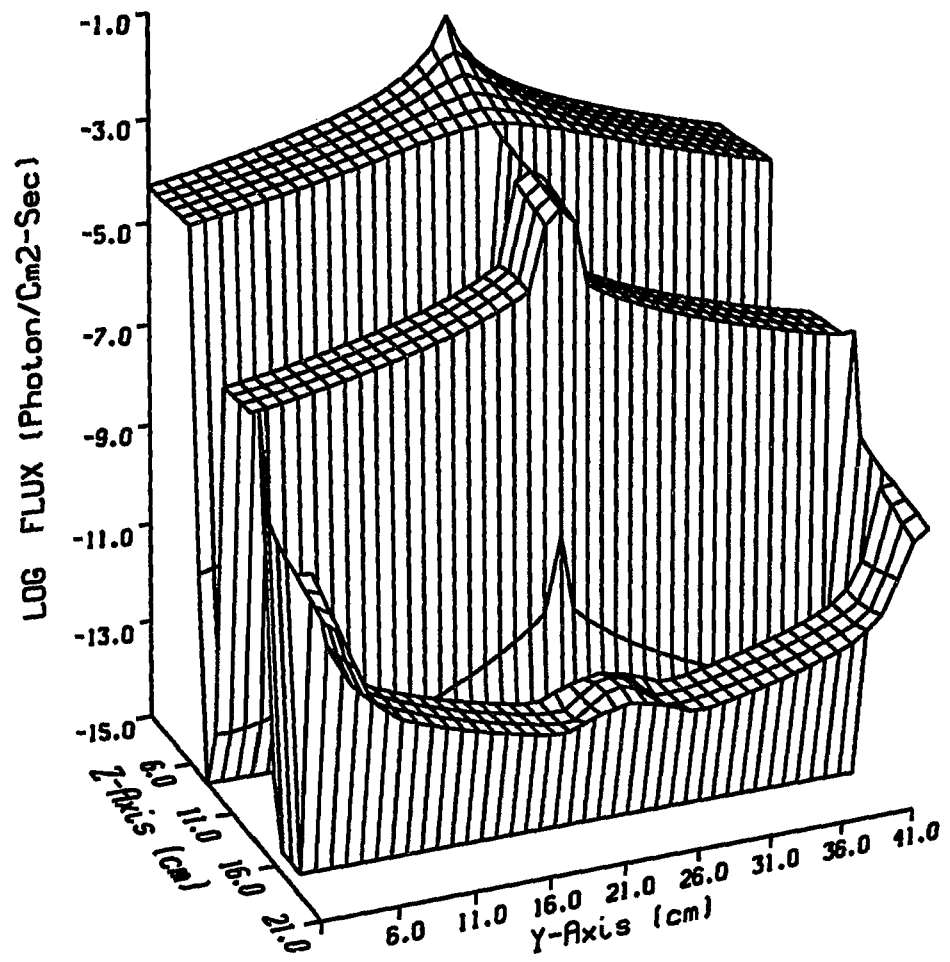


Figure 4.5.2b Flux Distribution from SAP₄CS coupled with S₂ for a very hard transport problem, with "artificial multiplying" material in target cells.

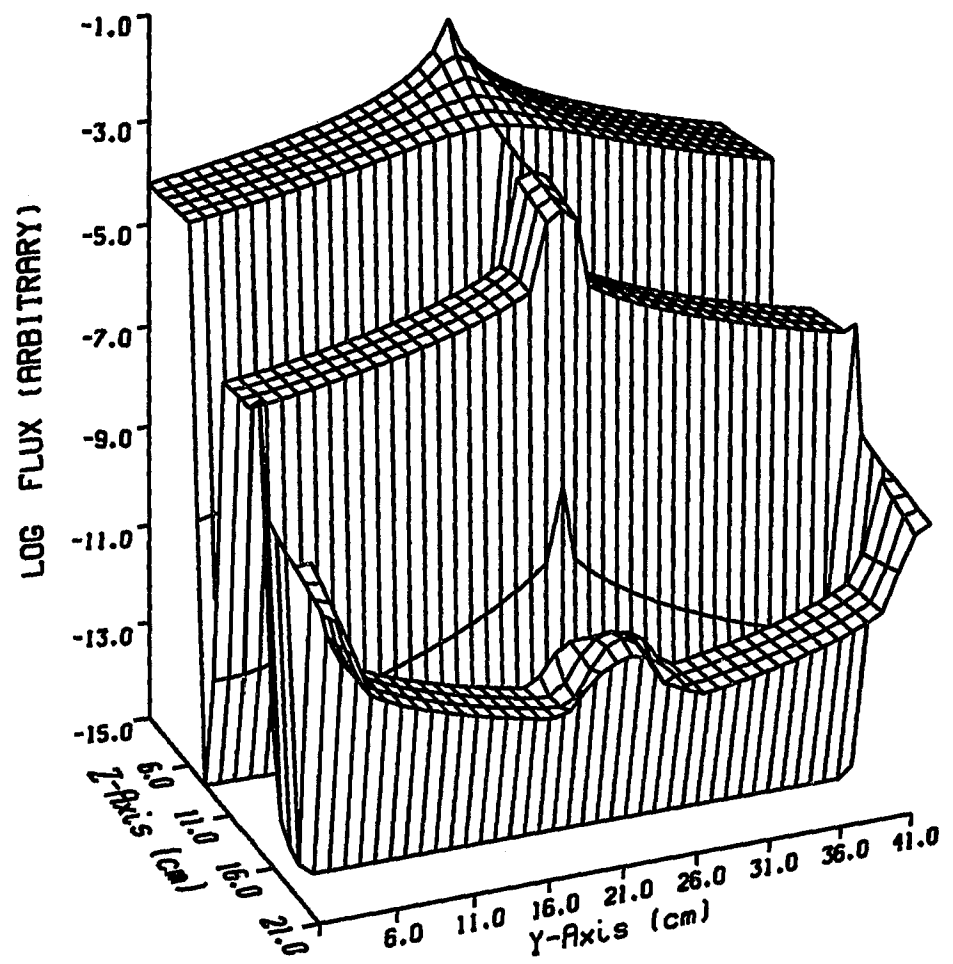


Figure 4.5.2c Flux Distribution from SAP₅CS coupled with S₂ for a very hard transport problem, with “artificial multiplying” material in target cells.

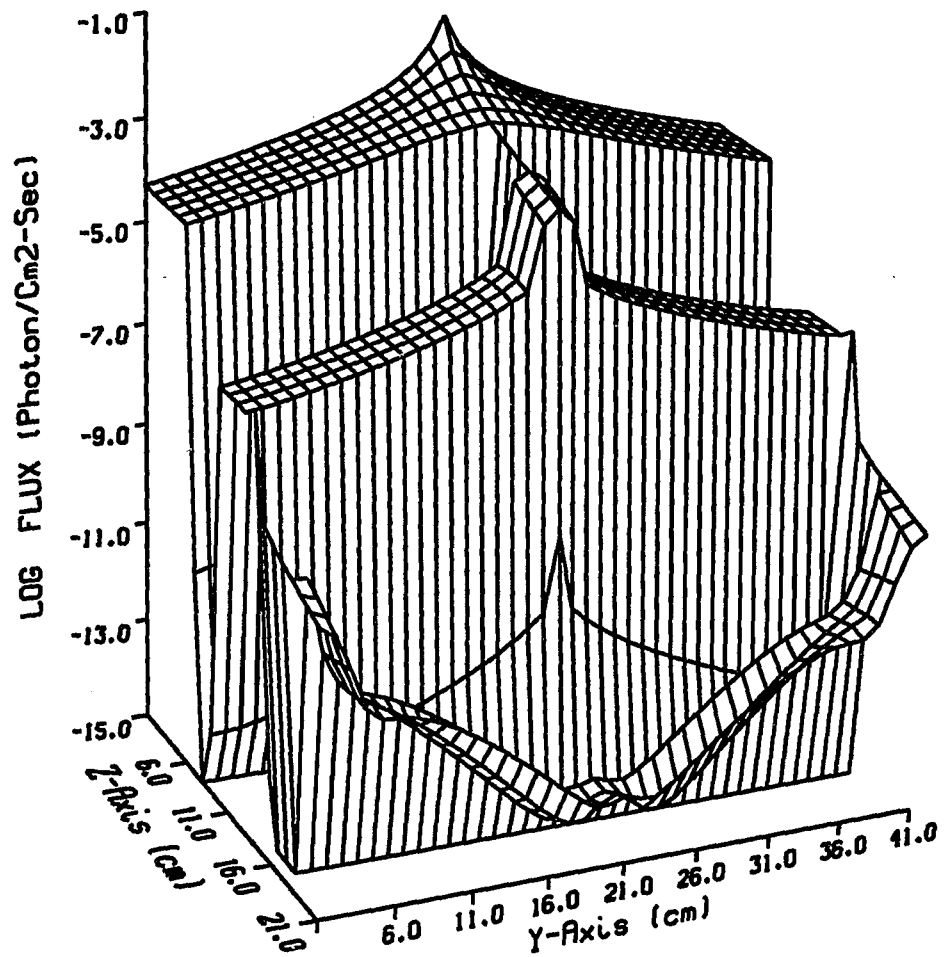


Figure 4.5.3a Flux Distribution from SAP_3CS coupled with S_4 for a very hard transport problem, with "artificial multiplying" material in target cells.

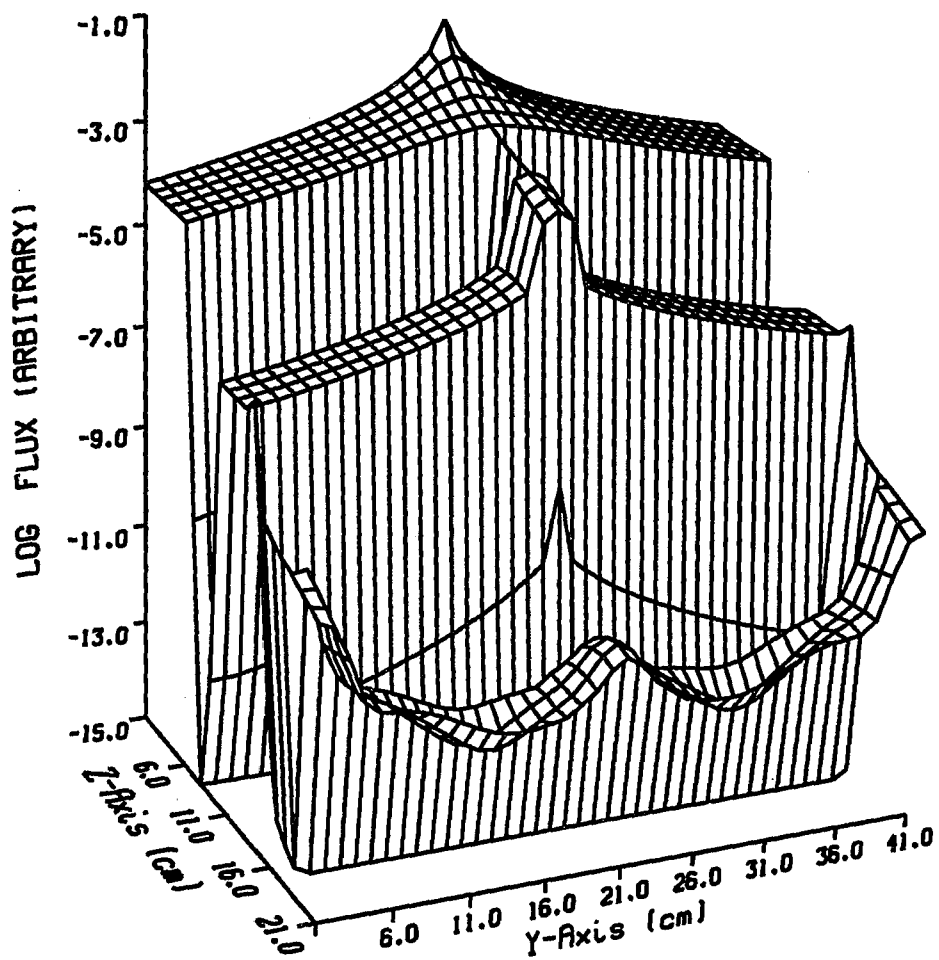


Figure 4.5.3b Flux Distribution from SAP_4CS coupled with S_4 for a very hard transport problem, with "artificial multiplying" material in target cells.

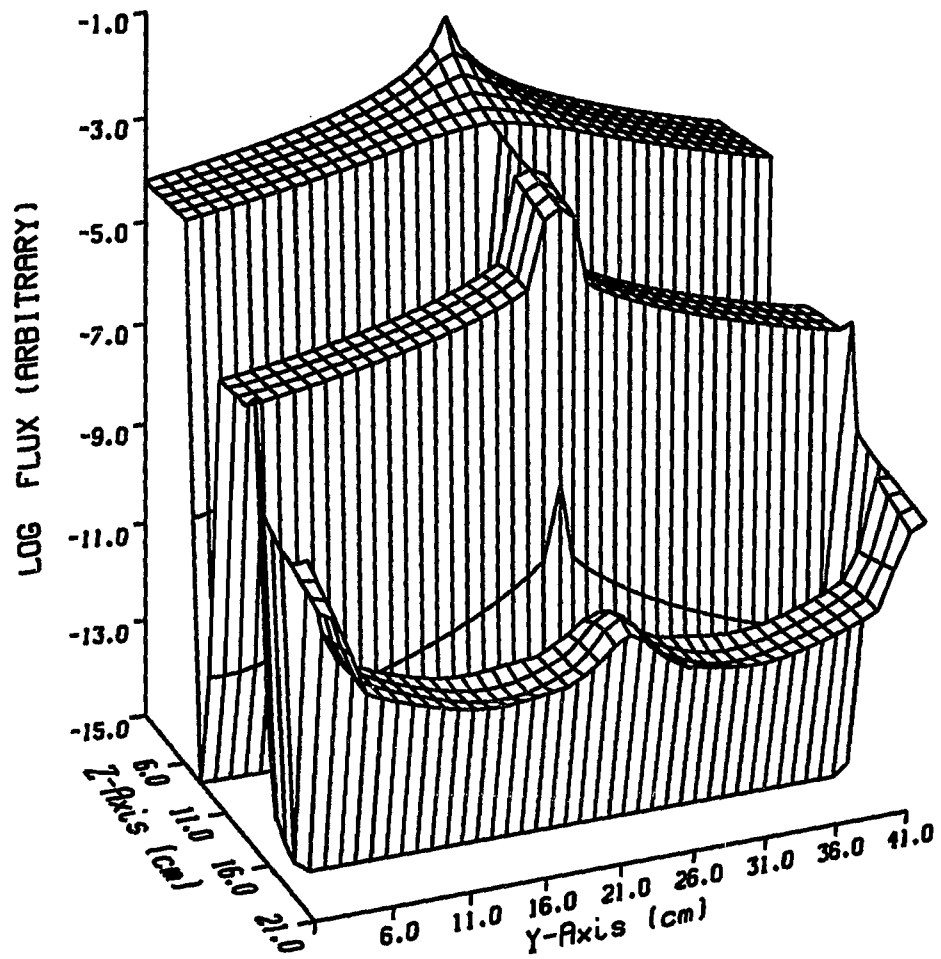


Figure 4.5.3c Flux Distribution from SAP_5CS coupled with S_4 for a very hard transport problem, with "artificial multiplying" material in target cells.

4.6 Test Problem Five

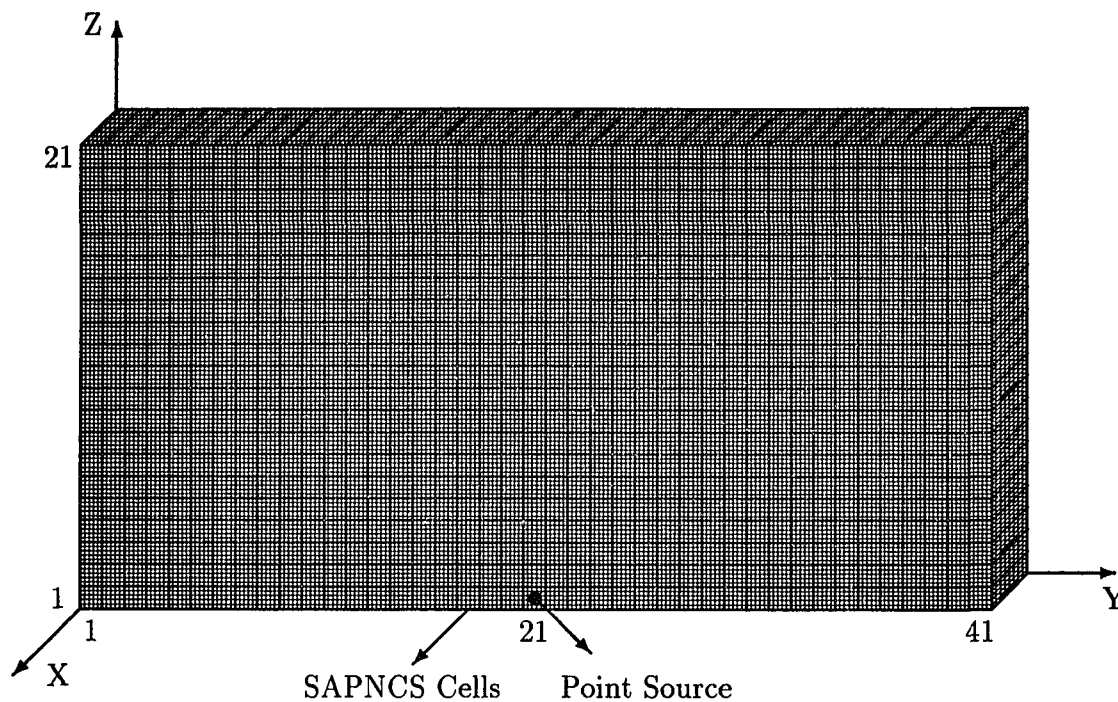


Figure 4.6 Geometric scheme of test problem five

4.6.1 Description of Problem

The geometric scheme for test problem five is primarily based on the general geometric scheme for all tests, however all cells in the geometric scheme are SAPNCS cells.

4.6.2 Objective

The purpose of this test is to show that the flux distribution from the SAPNCS technique are highly comparable to the flux distribution from a Monte Carlo-like technique. The flux distribution from the S_N technique is also compared. There were

two groups for test problem five. The difference between the two groups is based on macroscopic total and scattering cross sections.

4.6.3 Test Group One

Test group one used a macroscopic total and scattering cross sections of 0.1 and 0.09 cm^{-1} respectively.

The first test for test group one used a Monte Carlo-like technique. Ten million histories were used. Figure 4.6.1a demonstrates a flux distribution from the Monte Carlo-like technique. A smooth flux distribution was generated.

Figure 4.6.1b shows the flux distribution for test two using S_{16} . The peak of the flux is lower than the peak obtained from the Monte Carlo-like technique. Despite the use of S_{16} and a higher scattering cross section, ray effects are still present.

The third test used SAP_1CS coupled with S_2 , identified as SAP_1CS-S_2 . The peak of the flux distribution is slightly higher than the peak from the Monte Carlo-like test as shown in Figure 4.6.1c. The ray effects are slightly noticeable.

The fourth test used SAP_1CS coupled with S_4 , identified as SAP_1CS-S_4 . The flux distribution is almost identical to the flux distribution for test three. However, the ray effects are no longer visible.

4.6.4 Test Group Two

Test group two used a macroscopic total and scattering cross sections of 0.0001 and 0.00009 cm^{-1} respectively.

The first test for test group two also uses ten million histories for the Monte Carlo-like technique. Figure 4.6.2a shows the flux distribution using the Monte Carlo-like technique. Irregular fluctuations occur on the flux distribution.

Figure 4.6.2b shows the flux distribution for test two using S_{16} . The flux distribution peak from this test is the smallest peak obtained from all four tests in test group two. The ray effects are also present.

On the other hand, the SAP_1CS-S_2 technique does not produce the ray effects as illustrated in Figure 4.6.2c. The flux distribution is very smooth. The flux distribution peak is slightly higher than the peak from the Monte Carlo-like technique.

Figure 4.6.2d shows the flux distribution obtained from $SAP_1CS - S_4$ technique. The flux distribution is again very smooth. In addition, the flux distribution peak is very close to the peak from both the Monte Carlo-like technique and the SAP_1CS-S_2 technique.

4.6.5 Comparison Between the Two Groups

Overall, the flux distribution peaks from test group two are lower than the flux distribution peaks from test group one.

The flux distribution from the Monte Carlo-like technique for test group two (Figure 4.6.2a) is quite different than the flux distribution from the Monte Carlo-like technique for test group one (Figure 4.6.1a). The irregular fluctuations in Figure 4.6.2a are caused by inadequate histories. In order to get a smooth distribution, as many as 30 million histories would be required.

The ray effects on the flux distribution from S_{16} for test group two are more prominent (Figure 4.6.2b) than those for test group one as shown in Figure 4.6.1b. The much lower scattering cross section is a major contribution to this.

The flux distribution from the SAP_1CS-S_2 test for test group two (Figure 4.6.2c) is much smoother than the flux distribution from the same test for test group one (Figure 4.6.1c). The ray effect is not present in Figure 4.6.2c.

The flux distributions from the SAP_1CS-S_4 test for both test group one and test group two are almost identical as shown in Figure 4.6.1d and Figure 4.6.2d, respectively. Both flux distributions are very smooth and without ray effects.

The flux distribution from the Monte Carlo-like technique and the flux distribution from the SAP_1CS-S_4 technique are similar. The similarity between those two flux distributions is reasonable enough to confirm the validity of the SAPNCS technique.

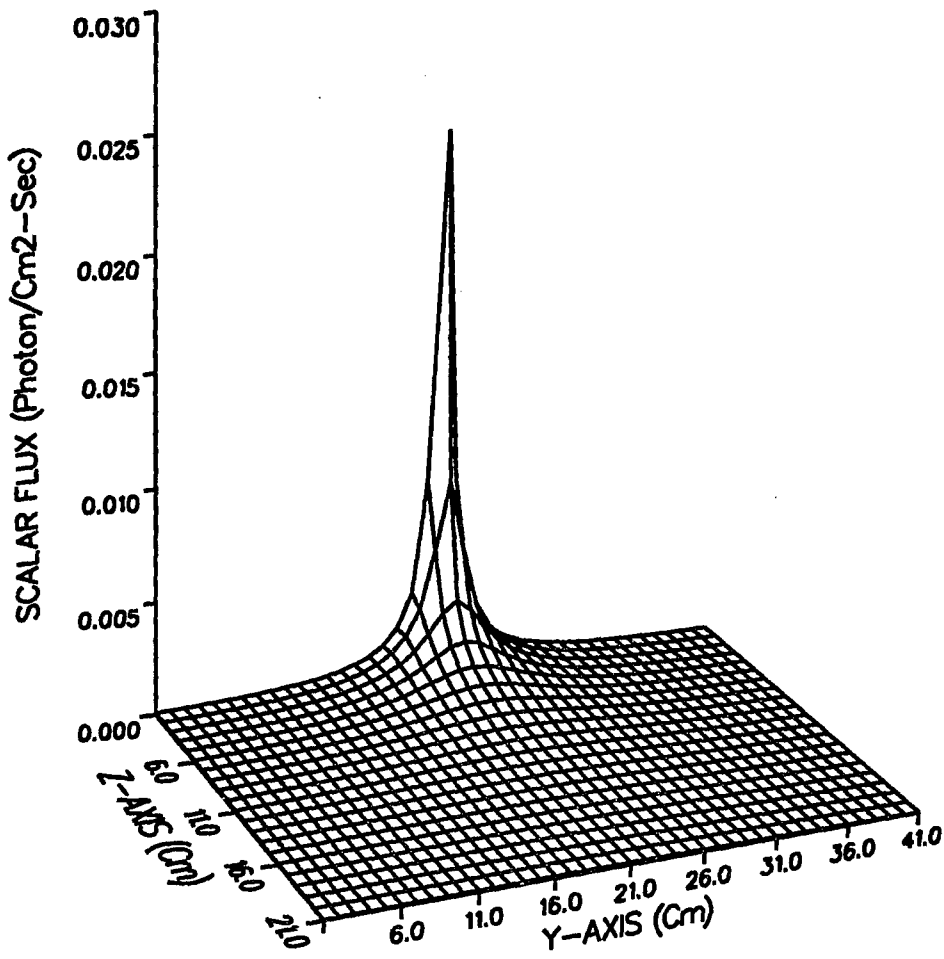


Figure 4.6.1a Flux distribution from Monte Carlo-like technique on homogeneous cells for total cross section = 0.1 cm^{-1} .

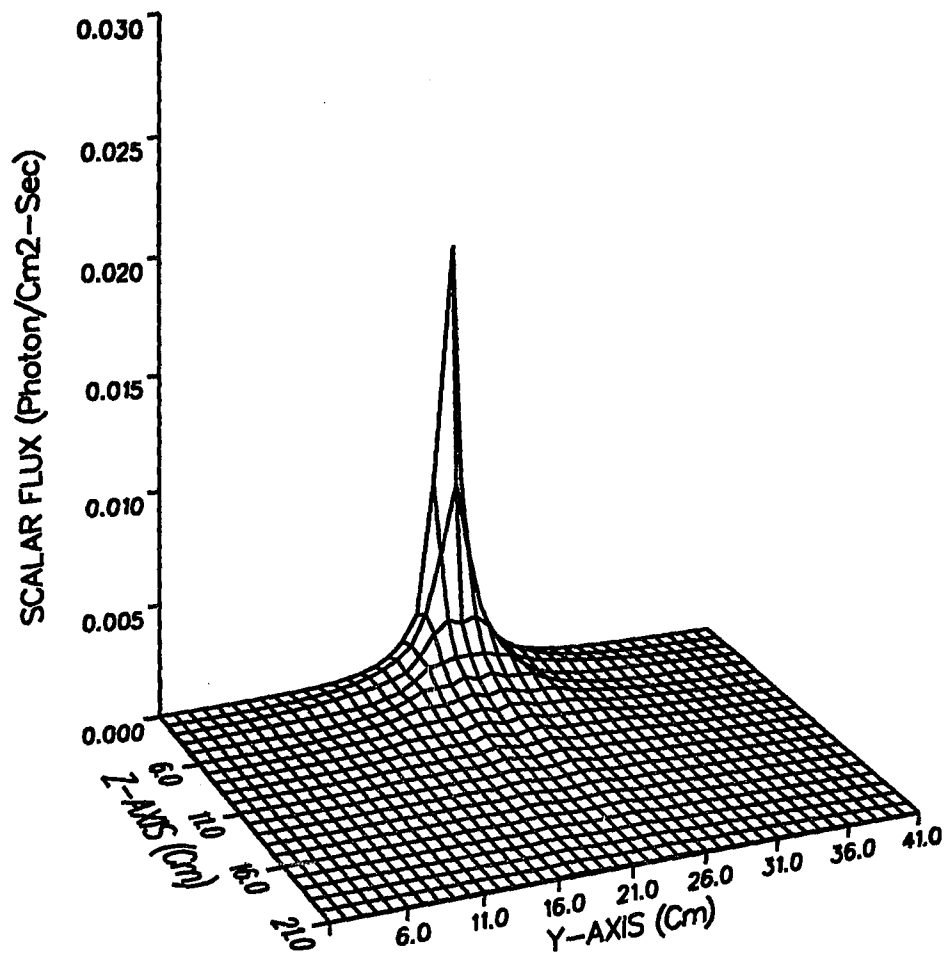


Figure 4.6.1b Flux distribution from S_{16} on homogeneous cells for total cross section = 0.1 cm^{-1} .

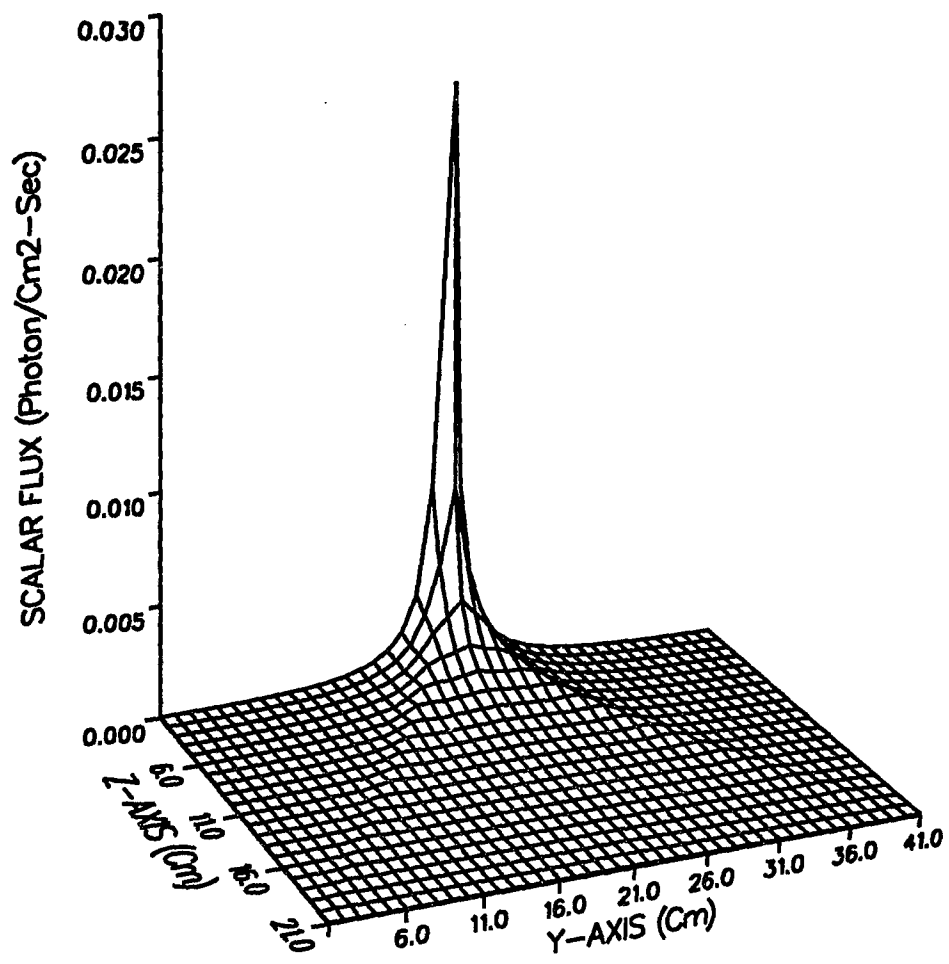


Figure 4.6.1c Flux distribution from SAP_1CS coupled with S_2 on homogeneous cells for total cross section = 0.1 cm^{-1} .

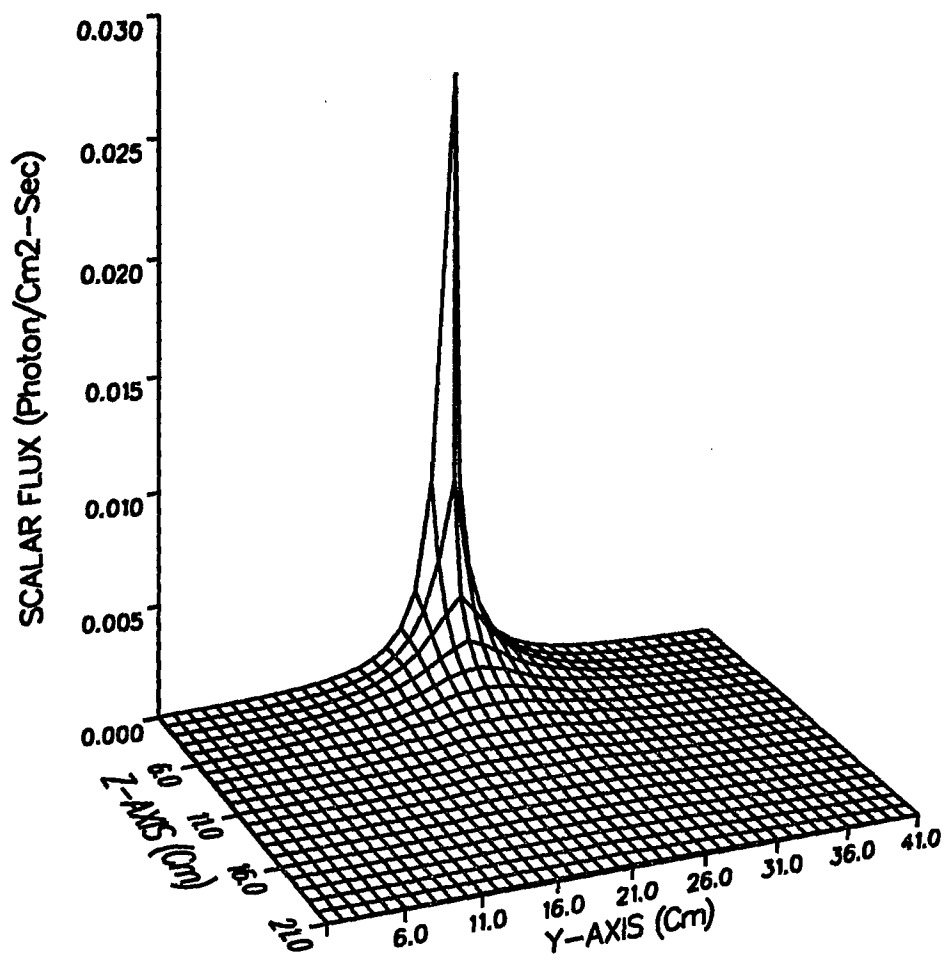


Figure 4.6.1d Flux distribution from SAP_1CS coupled with S_4 on homogeneous cells for total cross section = 0.1 cm^{-1} .

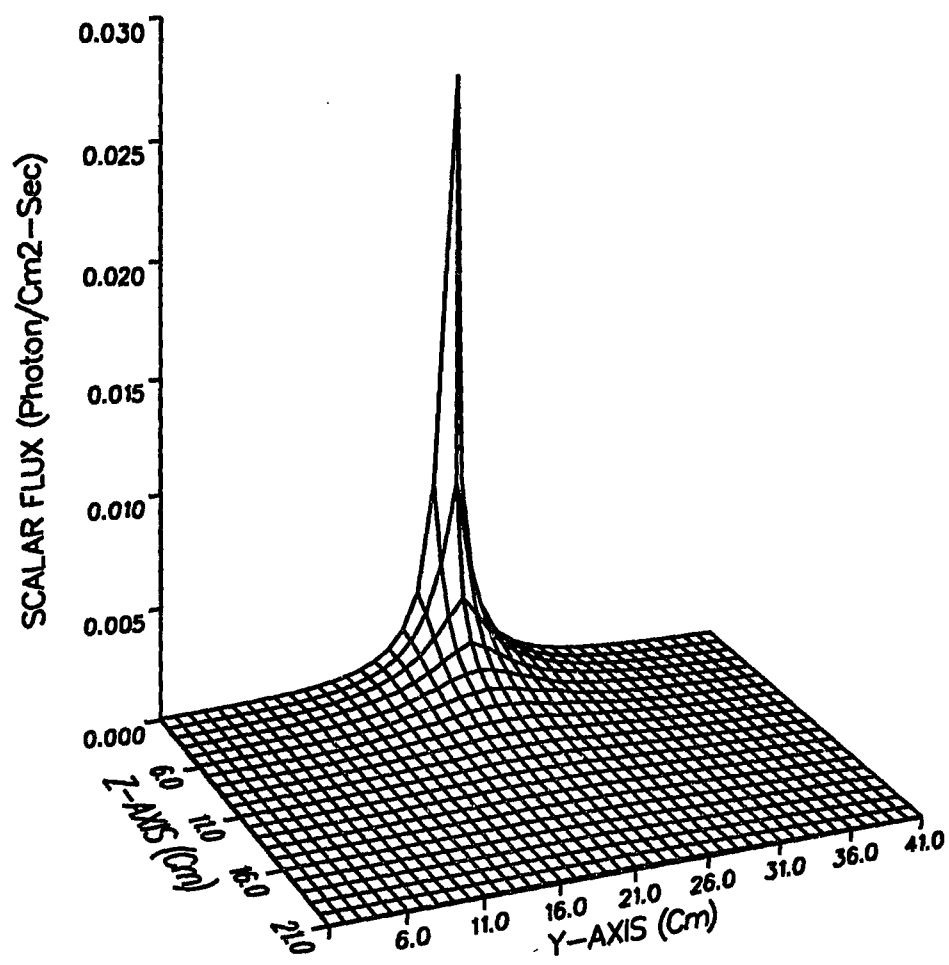


Figure 4.6.1e Flux distribution from SAP_1CS coupled with S_8 on homogeneous cells for total cross section = 0.1 cm^{-1} .

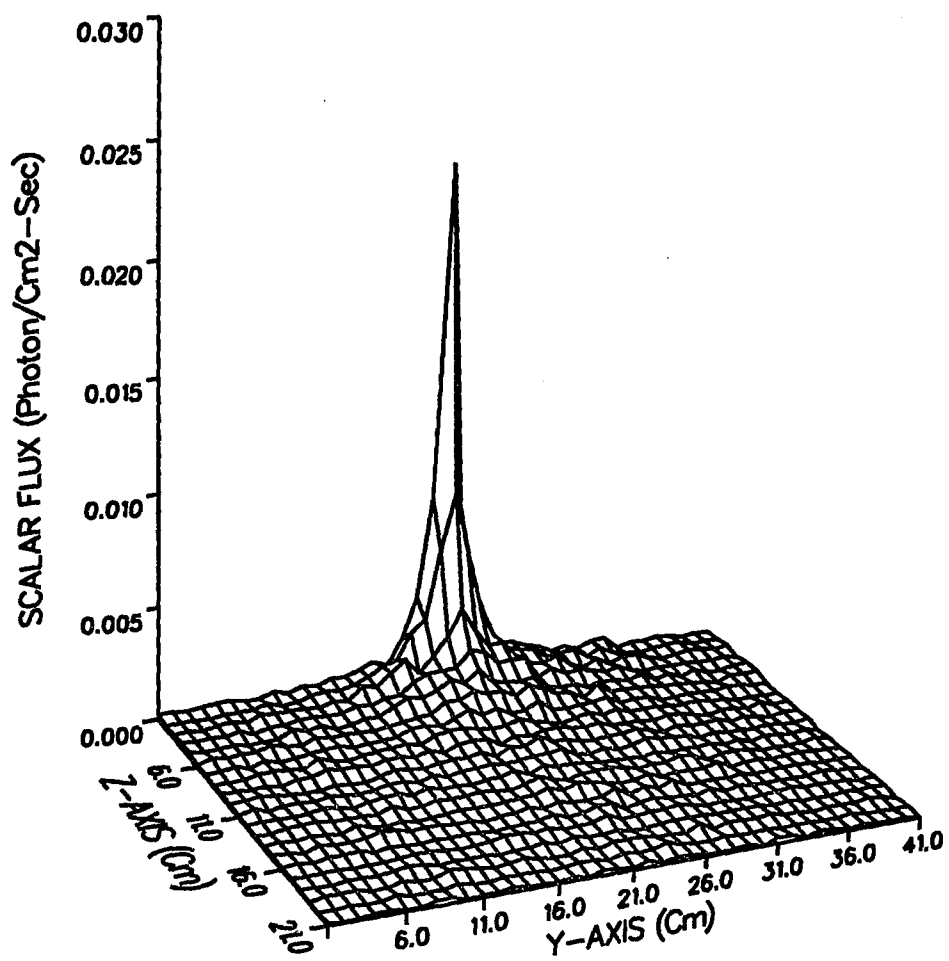


Figure 4.6.2a Flux distribution from Monte Carlo-like technique on homogeneous cells for total cross section = 0.0001 cm^{-1} .

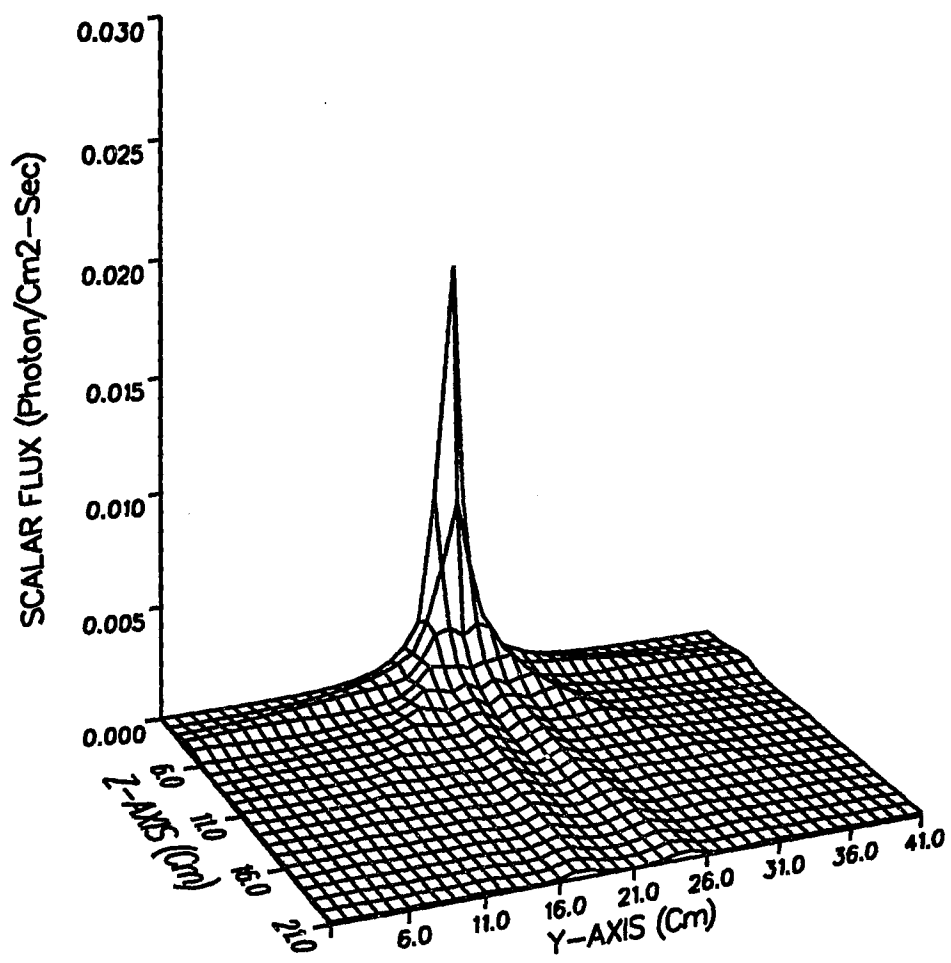


Figure 4.6.2b Flux distribution from S_{16} on homogeneous cells for total cross section = 0.0001 cm^{-1} .

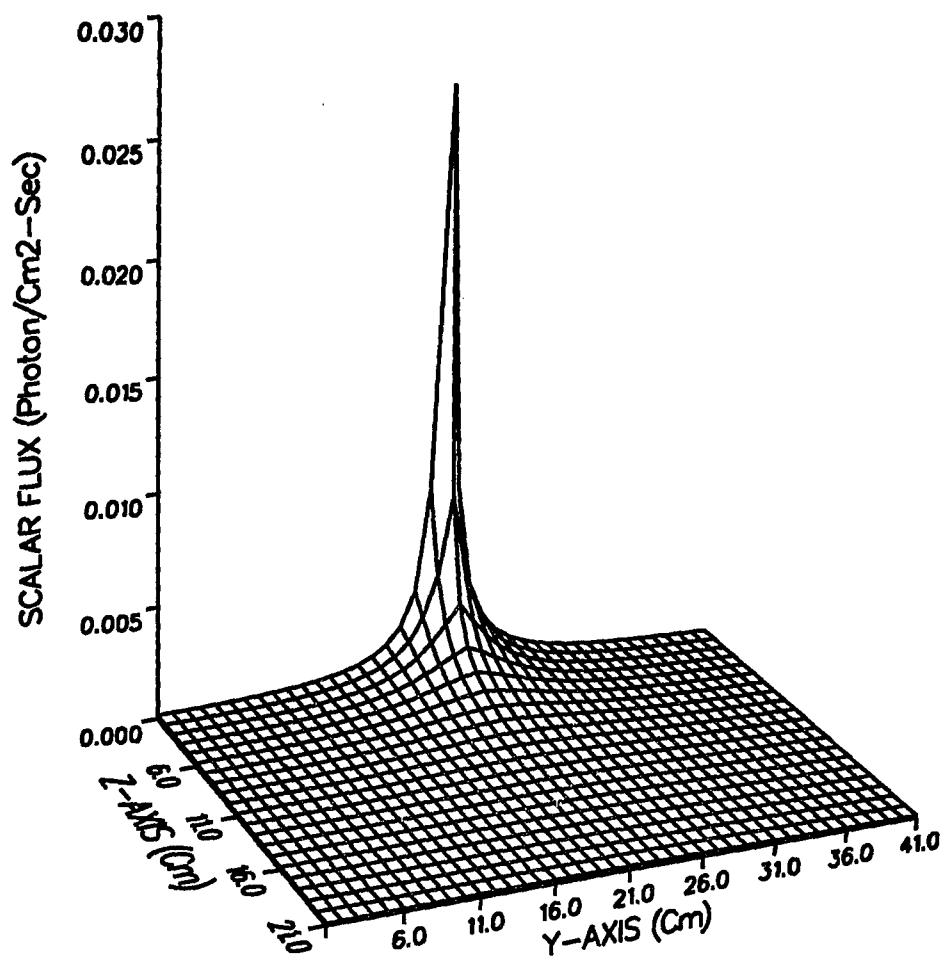


Figure 4.6.2c Flux distribution from SAP_1CS coupled with S_2 on homogeneous cells for total cross section = 0.0001 cm^{-1} .

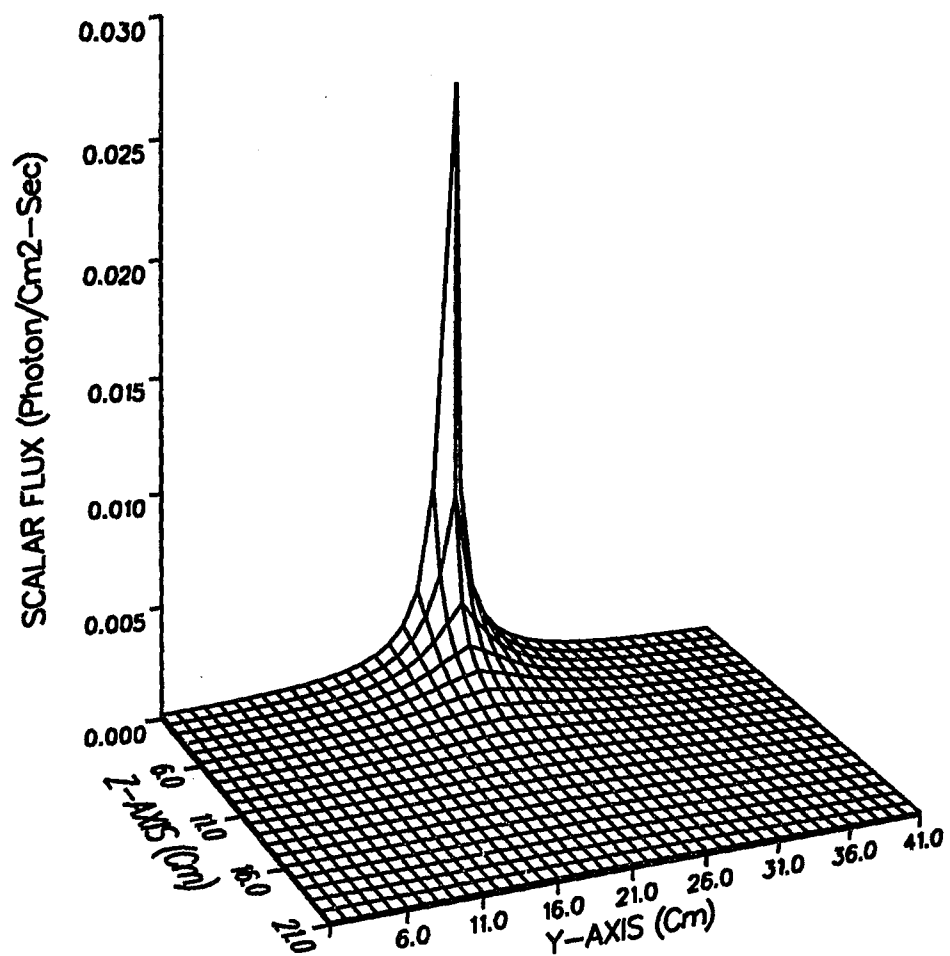


Figure 4.6.2d Flux distribution from SAP_1CS coupled with S_4 on homogeneous cells for total cross section = 0.0001 cm^{-1} .

CHAPTER 5

CONCLUSION

The SAPNCS method is definitely capable of solving the ray effect problem. This method can eliminate the ray effects that rise from S_{16} and even S_2 . The ray effects rising from the fewest directions of S_N , S_2 , are much more persistent than those rising from the higher directions. The higher directions of S_N need only the first collision source in order to eliminate the ray effects. However, the fewest directions of S_N , S_2 , used the second collision source to get the same result from higher directions. We therefore conclude that the SAPNCS method is able to eliminate the ray effect while keeping the calculation total number of directions on discrete ordinates, N , relatively small.

The capability of the SAPNCS method to mitigate or eliminate the ray effect has widened into secondary ray effects. The secondary effects arising from secondary sources are very severe and persistent. They can not be eliminated by using the first collision source alone. Second or higher collision sources have been used to solve this problem. In fact, this method is able to mitigate, and even to eliminate, the secondary ray effects.

This SAPNCS technique is also able to handle a very hard transport problem. The use of Monte Carlo technique is unlikely to solve this problem, unless very many histories are used. The conventional discrete ordinates technique also needs high

number of discrete directions and iteration processes to deal with this problem. Both techniques require enormous computational time. These are technically inefficient and economically expensive. On the other hand, the SAPNCS technique solves the problem with moderate consumption of computational time and yields better results.

The agreement between Monte Carlo-like technique and SAPNCS method is reasonable enough to confirm the validity of the SAPNCS method. Established codes are needed for further confirmation of the validity of the SAPNCS method.

This SAPNCS method can be carried out without a single modification of present day S_N codes. The distributed source generated by the SAPNCS method is perfectly suitable to the S_N . Moreover, this method is easily implemented in three-dimensional S_N codes. For these reasons, this SAPNCS method is a very promising method for solving three-dimensional transport problem.

This promising method has a lot of room for improvement. The first step of improvement is to extend the method to anisotropic scattering. It requires moderate modification of the SAPNCS code. The next step is either to put multi-group energy models into the code or to apply the SAPNCS technique to curved geometries. The latter suggestion would be difficult to implement, but for many applications the SAPNCS method is very promising.

The symmetry of the test problems suggests the possibility of dividing the test regions in two, and using reflection boundary conditions at the mid-plane. This is another recommendation for future research.

REFERENCES

1. W. L. Filippone, S. Woolf, and R. Lavigne, "Particle Transport Calculations with the method of Streaming Rays", Nucl. Sci. Eng., 77, 119 (1981).
2. W. L. Filippone and S. Woolf, "Application of the Method of Streaming Rays to Particle Transport in Complex Geometries", Proc. International Topical Meeting on Advances in Mathematical Methods for the Solution of Nuclear Engineering Problems, Munich, 1, 69 (1981).
3. K. D. Lathrop, "Ray Effects in Discrete Ordinate Equation", Nucl. Sci. Eng., 32, 357 (1968).
4. K. D. Lathrop, "Remedies of Ray Effects", Nucl. Sci. Eng., 45, 255, (1971).
5. S. Kaplan, "A New Derivation of Discrete Ordinate Approximations", Nucl. Sci. Eng., 34, 76 (1968).
6. M. Natelson, "Variational Derivation of Discrete Ordinate Like Approximations", Nucl. Sci. Eng., 43, 131 (1971).
7. W. F. Miller, Jr., E. E. Lewis, and E. C. Rossow, "The Application of Phase-Space Finite Elements to the Two-Dimensional Neutron Transport Equation in X-Y Geometry", Nucl. Sci. Eng., 52, 12 (1973).
8. L. L. Briggs, W. F. Miller, Jr., and E. E. Lewis, "Ray-Effect Mitigation in Discrete Ordinate-Like Angular Finite Element Approximations in Neutron Transport", Nucl. Sci. Eng., 57, 205 (1975).
9. Wm. H. Reed, "Spherical Harmonic Solutions of the Neutron Transport Equation from Discrete Ordinate Codes", Nucl. Sci. Eng., 49, 10 (1972).
10. J. Jung, H. Chijiwa, K. Kobayashi, and H. Nishihara, "Discrete Ordinate Neutron Transport Equation Equivalent to P_L Approximation", Nucl. Sci. Eng., 49, 1 (1972).
11. W. F. Miller, Jr. and Wm. H. Reed, "Ray-Effect Mitigation Methods for Two-Dimensional Neutron Transport Theory", Nucl. Sci. Eng., 62, 391, (1977).
12. W. L. Filippone and B. D. Ganapol, "An S_N -Monte Carlo Hybrid Transport Method", Trans. Am. Soc., 41, 487 (1982).
13. R. E. Alcouffe, R. D. O'Dell, and F. W. Brinkley, Jr., "A First Collision Source Method that Satisfies Discrete S_N Transport Balance", Nucl. Sci. Eng., 105, 198 (1990).

14. W. L. Filippone and S. Woolf, "An Extended First Collision Source Method for Electron Beam Source Problems", Nucl. Sci. Eng., 112, 1 (1992).
15. Shean P. Monahan and W. L. Filippone, "Super Computer S_N Calculations without Observable Ray Effects or Numerical Diffusion", Trans. Am. Nucl. Soc., 56, 306 (1988).
16. Shean P. Monahan and W. L. Filippone, "An Integral S_N Method for Large Memory Super Computer", Nucl. Sci. Eng., 107, 201 (1991).
17. E. E. Lewis and W. F. Miller, Jr, "Computational Methods of Neutron Transport", John Wiley & Sons, New York (1984).